1-1-2017

Role Of Alström Syndrome 1 (alms1) In Nkcc2 Endocytosis, Thick Ascending Limb Function, Blood Pressure Regulation And Metabolic Function

Ankita Bachhawat Jaykumar
Wayne State University,

ROLE OF ALSTRÖM SYNDROME 1 (ALMS1) IN NKCC2 ENDOCYTOSIS, THICK ASCENDING LIMB FUNCTION, BLOOD PRESSURE REGULATION AND METABOLIC FUNCTION

by

ANKITA BACHHAWAT JAYKUMAR

DISSERTATION

Submitted to the Graduate School

Wayne State University School of Medicine,

Detroit, Michigan

in partial fulfillment of the requirements

for the degree of

DOCTOR OF PHILOSOPHY

2017

MAJOR: PHYSIOLOGY

Approved By:

_____

Advisor Date

_____

_____

_____

_____

DEDICATION

To the loving memory of my Grandpa 'Dadu', an undying essence of intelligence.

To my parents, Sarita Bachhawat and Jaykumar Bachhawat for their unconditional love, trust, and encouragement. Their unfailing examples of determination, courage, and wisdom inspire me to be better with every passing day.

To my husband, Krushal Shah for his love, patience and understanding my challenges of graduate life. His persistent support and motivation has given me immense strength to make this dream a reality.

ACKNOWLEDGEMENTS

I would like to thank my mentor Dr. Pablo A. Ortiz for his guidance, encouragement and support. His valuable advice and his commitment in my formation instilled in me a sense of immense gratitude towards him. I couldn't have been more fortunate to find a mentor with such enthusiasm and passion for science.

I would like to thank the members of my dissertation committee, Dr. Noreen F. Rossi, Dr. William H. Beierwaltes, Dr. Douglas R. Yingst and Dr. Stanley Terlecky for their constructive feedback.

I would like to thank our collaborators Bakhos A. Tannous for providing ssBirA lentivirus vector, Dr. Jürgen Naggert for generous gift of ALMS1 antibody and carboxyl-terminus ALMS1 constructs, Gene Editing Rat Resource Center (GEERC) at Medical College of Wisconsin for providing *ALMS1* knockout (KO) rats and Dr. William H. Beierwaltes and Dr. Nour-Eddine Rhaleb for their expertise and contribution towards expanding our understanding of the *ALMS1* KO rat model.

I am very grateful to Dr. Paulo S. Caceres for his technical, intellectual input and his friendship, to Ms. Christine Cupps for her motherly perspective, and for excellent predisposition with administrative matters, to my professors, classmates and colleagues at Hypertension and Vascular Research division- Henry Ford Hospital and Wayne State University- Department of Physiology.

I am very thankful to Emily L. Henson and D'Anna Potter for help with blood pressure measurements, to Dr. Tang-Dong Liao for help with immunohistochemistry, to Gulser Gurocak for help with enzyme immuno assays and to Indrani Datta for help with Ingenuity Pathway analysis. I am also very thankful to Cheryl Pickering for her excellent assistance with *ALMS1* KO rat animal colony maintenance.

I would like to acknowledge all the living beings whose lives have been sacrificed for the advancement of medical research and the pursuit of scientific knowledge. To them, humankind owes immense gratitude.

Sources of Funding: This research was supported by the Interdisciplinary Biomedical Science Program from the Graduate School- Wayne State University, pre-doctoral fellowship 16PRE27510032 from the American Heart Association and Graduate School tuition coverage award to Ankita B. Jaykumar. Research funding was provided by the National Institutes of Health from grants 1P01HL090550-01A1 and 1R01DK107263-01A1, by an American Heart Association Grant-in-Aid and by internal funds from the Henry Ford Health System to Dr. Pablo A. Ortiz.

TABLE OF CONTENTS

LIST OF TABLES

LIST OF FIGURES

PREFACE

The dissertation that follows is the result of my training as a graduate student in the laboratory of Dr. Pablo A. Ortiz at Hypertension and Vascular Research Division, Henry Ford Hospital, Detroit. Since I had some prior research experience with total internal reflection fluorescence (TIRF) microscopy, during the first 1.5 years, we developed a method for real-time monitoring of $Na^+/K^+/2Cl^-$ co-transporter (NKCC2) endocytosis by TIRF microscopy in Mardin Darby Canine Kidney (MDCK) cells and in thick ascending limb (TAL) primary cultured cells. However, the focus of research in the lab at the time was to elucidate novel protein-protein interactions of NKCC2 that regulate NKCC2 apical trafficking. Thus, while I was preparing to submit the above-mentioned work for publication to *American Journal of Physiology* as the first author, I had started working on my main dissertation project to determine the role of ALMS1 in NKCC2 endocytosis, NaCl reabsorption and blood pressure. The work that led to this dissertation was performed by a previous colleague in the lab who had identified ALMS1 as one of the interacting partners with the carboxyl-terminus of NKCC2, a domain important for NKCC2 endocytosis. NKCC2 endocytosis is a critical mechanism to regulate NaCl reabsorption by the kidney, which plays a vital role in the regulation of arterial pressure.

In the years preceding the preparation of this dissertation, I completed another manuscript as first author corresponding to my main project which I submitted to my mentor for ultimate publication in *Journal of Clinical Investigation*. While performing my main research, I became interested in characterizing the *ALMS1* rat knockout (KO) model for metabolic, cardiovascular and renal function which became the focus of my

third first author manuscript to be submitted to *American Journal of Physiology*. In this dissertation, I demonstrate that ALMS1 interacts with NKCC2 and stimulates NKCC2 endocytosis and maintains normal NKCC2 surface expression and NKCC2-mediated NaCl reabsorption by the TAL, thereby maintaining normal blood pressure. Further, I show that deletion of *ALMS1* in rats leads to the development of age-dependent metabolic syndrome. All data used in this thesis are either already published or are in the process of being published.

Data such as characterization of endothelial, cardiovascular function in *ALMS1* knockout rats will be included in a separate manuscript where I am a contributing author. I performed GST-pull down assays with carboxyl-terminus ALMS1 in rat TAL lysates and pulled down a number of proteins which if pursued in the future per Dr. Ortiz, will guarantee my name as a contributing author in the respective manuscript/s. I was also involved in providing scientific input and maintaining an *ALMS1* KO rat colony for a graduate student in the lab: Keyona N. King-Medina for three years and hence will be a contributing author in both her ALMS1-related manuscripts. I maintained *ALMS1* mutant and floxed mice colonies for three years and hence will be a contributing author in the corresponding manuscripts. In summary, my work as a graduate student in Dr. Ortiz's lab has contributed to several manuscripts published, submitted or awaiting submission to peer-reviewed journals for publication.

CHAPTER 1 - BACKGROUND AND GENERAL HYPOTHESIS

Anatomy of the kidney

Nephrons are the structural and functional building blocks of the kidney (Figure1). Each nephron consists of a glomerulus through which blood is filtered into the tubular space called the Bowman's capsule. The filtrate then passes along the various segments of the tubule, where it is modified in composition and ultimately excreted as urine. Various segments of the nephron have different absorptive and

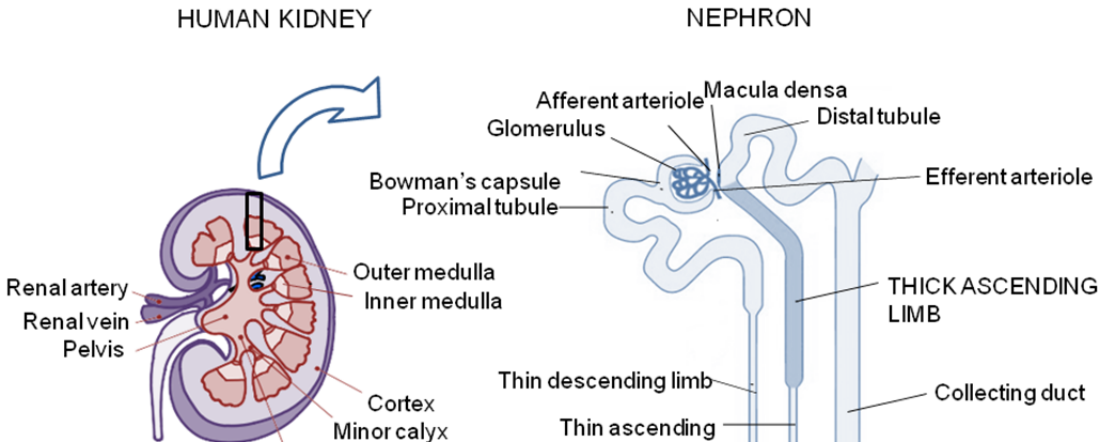

Figure 1: Diagrammatic representation of anatomy of the kidney and the nephron

secretory properties. Excretion of waste metabolites, ions and osmolytes are regulated by the kidneys and thus is an important determinant of blood pH, osmolality, ion and water composition. Additionally, renal tubular segments secrete several vasoactive substances and therefore allow a coordinated regulation of fluid volume in the extracellular compartments, a determinant of blood pressure.

One of the segments is the loop of Henle, which extends deep into the renal medulla. The most distal part of the loop of Henle is the thick ascending limb (TAL), which is divided into medullary and cortical regions.

Role of NKCC2 in NaCl reabsorption by the thick ascending limb

The TAL reabsorbs about 25 - 30% of the NaCl load filtered by the glomerulus. TAL reabsorbs Na^+, Cl^-, Mg^{2+}, Ca^{2+} ions while remaining impermeable to the movement of water. This results in a hyperosmotic interstitium *via* a counter current multiplier mechanism that generates osmotic force for water reabsorption at the collecting duct. Thus TAL plays a vital role in regulating water and ion reabsorption in the kidney thereby influencing, urine concentration and the regulation of arterial pressure.

Figure 2 shows a currently accepted model for NaCl reabsorption in the TAL. Epithelial cells that line the TAL have apical-basolateral polarity.

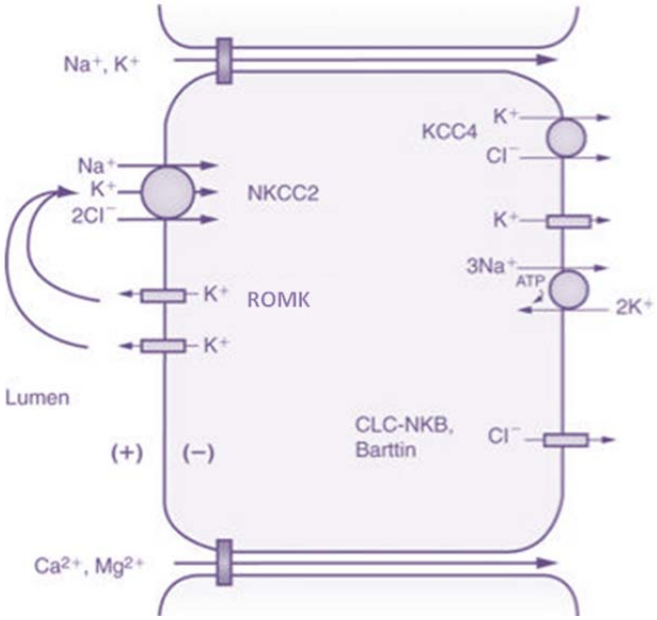

Figure 2: Representation of NaCl reabsorption by the thick ascending limb

On the apical surface, $Na^+/K^+/2Cl^-$ co-transporter (NKCC2) and Na-H exchanger (NHE3) (not shown) [1,2,11,12] reabsorb Na^+, K^+ and Cl^- ions from the lumen by utilizing the electrochemical gradient [3-5] generated by the sodium-potassium pump (Na^+-K^+ ATPase) in the basolateral membrane. Na^+ exits the cell at the basolateral side through the Na^+-K^+ ATPase while the Cl^- leaves through the Cl^- channels and $K^+/2Cl^-$ co-

transporters [5,6,7].

K^+ ions are recycled back into the lumen *via* the renal outer medullary potassium channel (ROMK) [8], thereby creating a positive luminal electric potential that drives Na^+, Ca^{2+}, Mg^{2+} absorption *via* the paracellular pathway [9,10].

Control of blood pressure: Role of NKCC2

Bartter syndrome type I [13-19] is characterized by polyuria, inability to concentrate urine and hypotension [20-22] and is caused by loss of function mutations in NKCC2. Mice models with genetic deletion of NKCC2 recapitulate Bartter syndrome type I phenotype [23], associated with severe volume depletion. Two independent groups [24,25] have shown that mutations in NKCC2 decrease NKCC2-mediated NaCl reabsorption and blood pressure in humans. Conversely, enhanced NKCC2-mediated NaCl reabsorption is associated with salt-sensitive hypertension in animal models [25-29] and in humans [30,31]. NKCC2 activity is inhibited by loop diuretics such as bumetanide and it is used clinically for the treatment of hypertension. Thus, NKCC2-mediated NaCl absorption by the TAL is crucial in regulation of blood pressure [30,32].

Regulation of NKCC2 by protein trafficking

NKCC2-mediated NaCl reabsorption is regulated by 1) phosphorylation at threonine (96/101) by STE20- and SPS1-related proline and alanine-rich kinases (SPAK) and oxidative stress-responsive kinase 1 (OSR1) [49,96-98] and at Ser(126) site by PKA [99], 2) protein-protein interactions [49,100-102] and 3) protein trafficking determining NKCC2 apical abundance [29,33,37,38]. While the regulation of NKCC2 *via* phosphorylation has been well studied, very little is known about mechanisms and protein-protein interactions which regulate NKCC2 apical trafficking. While most NKCC2 is located sub-apically as visualized by electron microscopy [34], our laboratory

previously showed that at a steady-state, only a small fraction (~5%) of the total NKCC2 is targeted to the apical surface of the TAL cells [35]. Steady-state surface NKCC2 levels are maintained by a balance between various protein trafficking modalities such as exocytic delivery [36], endocytosis and recycling [37,38], together determining NKCC2 activity (Figure 3). Our lab previously showed that blocking NKCC2 endocytosis leads to increased NKCC2 levels at the apical surface and increased NKCC2-mediated NaCl absorption in the TAL [37,38]. Additionally, surface NKCC2 was

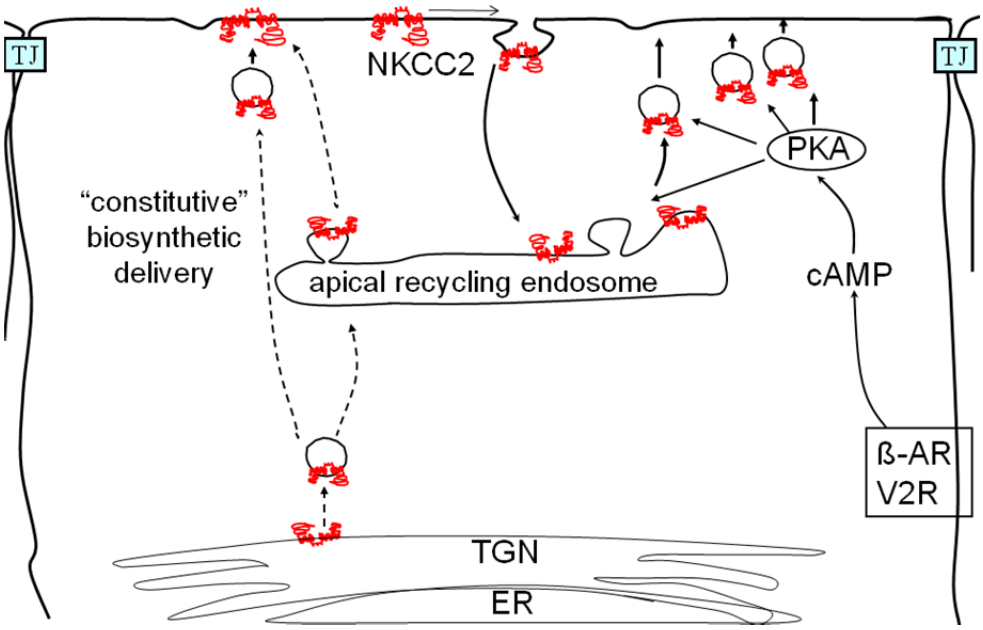

Figure 3: Trafficking pathways of NKCC2 in the thick ascending limb.

found to be significantly higher in a rat model of salt-sensitive hypertension [29]. These observations demonstrate the important relationship between regulation of NKCC2 abundance at the apical membrane by NKCC2 endocytosis and NKCC2-mediated NaCl reabsorption by the TAL. This also highlights the importance of NKCC2 endocytosis as a mechanism to regulate renal function and blood pressure.

Single molecule tagging method to measure NKCC2 endocytosis in real time

Given the significance of NKCC2 endocytosis in regulating NKCC2 activity, the dynamic process of this mechanism is poorly understood partly due to lack of methods to study endocytosis. Biochemical surface biotinylation of apical proteins with NHS-SS biotin [37,38] has been used to measure the rate of NKCC2 endocytosis. However there are several disadvantages in this biochemical technique because it is limited in its time resolution and cannot capture the dynamic process of endocytosis in real time [39]. Optical methods such as total internal reflection fluorescence (TIRF) microscopy have been developed that permit imaging trafficking events at the plasma membrane. TIRF microscopy generates an evanescent field of illumination penetrating to about ~200 nm into the cell thereby allowing direct imaging of fluorescent molecules at or near the plasma membrane, and thus may be well suited for imaging individual endocytic events in real time [40]. TIRF microscopy has been previously used to study trafficking of clathrin-coated vesicles and many membrane proteins in non-polarized cells [41- 43, 45, 46]. In polarized cells, TIRF microscopy has been used to image basolateral membrane trafficking dynamics of several proteins [47]. Imaging trafficking events at the apical membrane has been challenging due to technical limitations of the TIRF configuration, which requires a glass-water interface to generate the evanescent field. However in the recent years, there have been successful attempts to adapt this technique to image proteins in recycling endosomes which are in close proximity to the apical membrane [48,46]. Therefore TIRF imaging with site-specific fluorescent labeling of NKCC2 may allow monitoring of NKCC2 endocytosis with high signal to noise ratio and good time resolution in Mardin Darby Canine Kidney (MDCK) cells and TAL primary cultured cells.

Studying protein-protein interactions that play a role in regulating NKCC2 endocytosis

Despite the importance of NKCC2 endocytic pathway and development of novel methods to study the dynamic process, the molecular mechanisms that regulate NKCC2 endocytosis are not clear. Protein-protein interactions with NKCC2 as in the case of myelin and lymphocyte-associated protein (MAL/VIP17) has been described to regulate NKCC2 endocytosis [49] by interacting with a 71 amino acid domain in the carboxyl-terminus of NKCC2 (C2-NKCC2), shown to be important for apical targeting of NKCC2 [81]. Targeted proteomics using glutathione-S-transferase (GST) fusion protein with C2-NKCC2 as bait in the TAL is a promising method [44] to identify and characterize new C2-NKCC2 interacting partners and will allow characterization of novel proteins that play a role in NKCC2 endocytosis, regulation of blood pressure and renal function. In a GST pull-down assay in rat TAL, we identified (Alström syndrome 1 protein) ALMS1 as a novel interacting partner of C2-NKCC2.

Role of ALMS1 in hypertension, renal and metabolic function

ALMS1 is a protein initially associated to Alström syndrome. This is a human disorder characterized by hypertension, obesity, insulin resistance, kidney dysfunction and chronic kidney disease. Renal impairment in these patients include reduced glomerular filtration rate (GFR) and albuminuria. Renal function deteriorates with age and end-stage renal disease is a common cause of death in these patients [50-53]. Two independent genome-wide association studies discovered single nucleotide polymorphisms in *ALMS1* locus associated with GFR and chronic kidney disease [62-65]. Hypertension is a common risk factor for chronic kidney disease (CKD) [54, 55]. *ALMS1* gene was linked to hypertension status in a multipoint linkage analysis in

primary sibling samples of African American, Caucasian and Mexican population. In this population analysis, seven single nucleotide polymorphisms in *ALMS1* were associated with hypertension and increased pulse pressure [56]. Quantitative trait loci (QTL) associated with blood pressure and salt-sensitive hypertension were mapped to *ALMS1* locus [57-61]. However, the mechanism involved in regulation of Na^+ handling in the kidney and salt-sensitive hypertension by ALMS1 is unknown.

Role of ALMS1 in protein trafficking

ALMS1 was originally shown to be present in the basal body of the cilia, yet fibroblasts from human Alström syndrome patients have normal cilia but had defects in trafficking of transferrin [66]. Therefore, the pathology observed in these patients may be due to defects in intracellular trafficking [51,67,68]. In *ALMS1* mutant mice, the apical protein rhodopsin in the retina is mislocalized, suggesting a role for ALMS1 in intracellular trafficking in the retina [67]. Loss of ALMS1 caused accumulation of notch receptors in the late endosomes but did not affect recycling [68], suggesting a role in endosome trafficking. *ALMS1* mutant mice displayed altered intracellular localization of glucose transporter-4 (GLUT4) and decreased insulin-stimulated trafficking of GLUT4 to the plasma membrane in adipocytes [69]. Proteins such as alpha-actinin1/4 (ACTN1/4), Myosin Vb (MYO5B), Rad50 interactor 1 (RINT1) play a role in endocytosis [66,70-73] and interact with ALMS1. We hypothesize that ALMS1 acts as a scaffolding protein between the cytoskeleton and membrane proteins during endocytosis.

Protein-protein interaction as a possible mechanism for ALMS1-mediated endocytosis of NKCC2

The genetic association of obesity, salt-sensitive hypertension with *ALMS1*, its cellular role in trafficking of membrane protein [69] and its interaction with proteins in the

endocytic pathway [66] are well described. In this dissertation, we tested whether ALMS1 interacts with NKCC2 as a possible mechanism that stimulates NKCC2 endocytosis and decreases surface NKCC2 abundance, NKCC2-mediated NaCl reabsorption by the TAL, thereby maintaining normal blood pressure. We also tested the effect of deletion of *ALMS1* in the development of metabolic dysfunction in rats.

General hypothesis and project aims

In this work *we developed a method to measure NKCC2 endocytosis in real time by TIRF microscopy* and tested the general hypothesis that *ALMS1 interacts with NKCC2 in the thick ascending limb to stimulate NKCC2 endocytosis, decrease NaCl reabsorption, and thereby maintains normal blood pressure. We also tested the role of ALMS1 in maintaining normal metabolic function in rats.* We addressed this hypothesis in five aims that follow.

Aim 1: Hypothesis: Site-specific labeling allows visualization of apical NKCC2 by Total internal reflection fluorescence (TIRF) microscopy in polarized MDCK and TAL cells

We will transduce biotin acceptor domain (BAD) tagged NKCC2 to perform site specific biotinylation of surface NKCC2 mediated by *Escherichia coli* biotin ligase (BirA). Fluorescent labeling of biotinylated NKCC2 will be performed for imaging surface NKCC2 by total internal reflection fluorescence (TIRF) microscopy.

Aim 2: Hypothesis: Total internal reflection fluorescence (TIRF) microscopy allows monitoring of NKCC2 endocytosis in polarized MDCK and TAL cells in real time

We will measure intensities of surface NKCC2 puncta for monitoring endocytic events signified by exponential decrease in the intensity of an individual punctum. The rate of NKCC2 endocytosis will be calculated by measuring the rate of disappearance of surface NKCC2 puncta on the TIRF field.

Aim 3: ALMS1 interacts with NKCC2 and stimulates NKCC2 endocytosis thereby decreasing steady-state surface NKCC2 expression

First, we will confirm that ALMS1 is a part of a complex with NKCC2 in TALs. Then we will define the region of ALMS1 that interacts with NKCC2. We will inhibit ALMS1 expression *in vivo* in rat TALs by a) gene silencing *via* short hairpin RNA (shRNA), b) *ALMS1* genetic deletion in rats. We will then measure steady-state surface NKCC2 and rate of NKCC2 endocytosis in TALs.

Aim 4: ALMS1 decreases NKCC2-mediated NaCl reabsorption by the TAL, thereby plays a role in salt sensitive hypertension

We will inhibit ALMS1 expression *in vivo* by genetic deletion of *ALMS1* in rats. We will then measure bumetanide-induced water and NaCl excretion and systolic blood pressure on normal salt and water diet. We will measure salt sensitivity by measuring systolic blood pressure response to increasing salt in drinking water.

Aim 5: Deletion of ALMS1 causes sex-based differences in development of age-dependent metabolic syndrome in rats

We will inhibit ALMS1 expression by genetic deletion of *ALMS1* in rats. We will measure body weight, abdominal fat pad weight, average daily food intake, random blood glucose, fasting blood glucose, plasma insulin and leptin, serum triglyceride, cholesterol, low density lipoprotein (LDL) and high density lipoprotein (HDL) levels and systolic blood pressures in 6-12 week and 16-18 week old male and female rats.

CHAPTER 2 - REAL TIME MONITORING OF NKCC2 ENDOCYTOSIS BY TOTAL INTERNAL REFLECTION FLUORESCENCE MICROSCOPY

(This chapter contains previously published material. See Appendix C)

Introduction

The abundance of NKCC2 at the apical membrane of TAL cells is determined by a balance between exocytic delivery, recycling, and endocytosis. Biochemical surface biotinylation allows measurement of these trafficking modalities such as NKCC2 endocytosis. However, this method has low time resolution and does not allow imaging of the dynamic process of endocytosis [39,40]. In this chapter we tested whether total internal reflection fluorescence (TIRF) microscopy imaging of labeled NKCC2 would allow monitoring of NKCC2 endocytosis in polarized Mardin Darby Canine Kidney (MDCK) and TAL primary cultured cells. We tested this in two aims by transducing a NKCC2 construct containing a biotin acceptor domain (BAD) sequence between the 5th and 6th trans-membrane domains in MDCK and TAL cells. This would allow biochemical and/or metabolic NKCC2-specific biotinylation. Subsequent labeling with a fluorophore was performed for TIRF live cell imaging and visualizing individual endocytic events in real-time.

Aim 1: Hypothesis: Site-specific labeling allows visualization of apical NKCC2 by Total internal reflection fluorescence (TIRF) microscopy in polarized MDCK and TAL cells

Rationale

Site-specific biotinylation of cell surface proteins is achieved by tagging proteins with a biotin acceptor domain (BAD) sequence, catalyzed by *Escherichia coli* biotin ligase (BirA) to add biotin moieties to the lysine residue of the sequence [74-77]. This is an efficient method to tag and image apical proteins in mammalian cells [78,79]. Optical

methods such as total internal reflection fluorescence (TIRF) microscopy which generate an evanescent field of illumination, allow direct imaging of fluorescent molecules at or near the plasma membrane with high signal-to-noise ratio [40]. Here we tested whether NKCC2- specific biotinylation at the apical surface by exogenously added or co-expressed BirA allows imaging of surface NKCC2 by TIRF microscopy.

Results

Heterologous NKCC2 can be expressed in polarized MDCK cells

Full-length NKCC2 has been successfully expressed in non-polarized cells such as opossum kidney cells [80] while only a few investigators have succeeded in expressing it in polarized cells [81]. We expressed full-length NKCC2 construct in polarized epithelial cells, and tested whether N-terminus eGFP-tagged NKCC2 is expressed and targeted to apical membrane in polarized MDCK cells. For this, MDCK cells grown to confluence on collagen-coated permeable support transwells were transduced with eGFP-NKCC2 adenoviruses and then co-labeled for NKCC2 and tight junction protein zonula occludens-1 (ZO-1).

Figure 4A shows a representative image of MDCK cells in which eGFP-NKCC2 (in green) was observed in the same plane as ZO-1 (in red). In order to verify lack of basolateral targeting of eGFP-NKCC2, eGFP-NKCC2 transduced MDCK cells were labeled with antibodies that bind surface NKCC2 (directed to the extracellular loop between TM5-TM6) on both the apical and basolateral compartment of the transwell in addition to apical tight junction protein ZO1. X-Y and Y-Z confocal reconstruction of polarized MDCK cells show that NKCC2 was only located in the apical surface in the same plane as ZO-1, while no labeling was observed in the lateral or basolateral

membranes (Figure 4B).

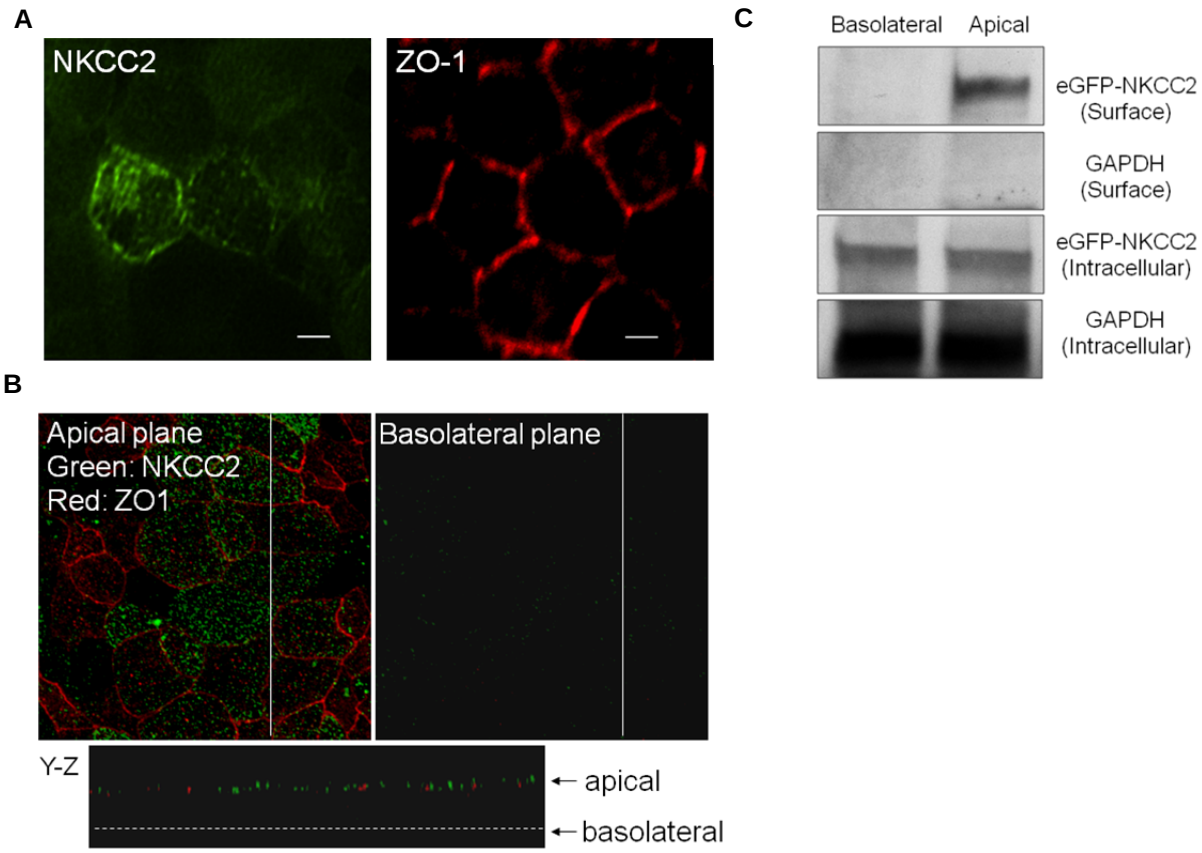

Figure 4: Apical targeting of eGFP-NKCC2 in polarized MDCK cells. A) Immunofluorescence labeling of ZO-1 (red) and eGFP-NKCC2 (green). Scale bar = 5 µm, n = 3. B) X-Y and Y-Z confocal reconstruction of MDCK cell monolayer immuno-labeled with surface eGFP-NKCC2 (green) and ZO-1 (red), n = 3. C) Representative Western blot indicating presence of eGFP-NKCC2 in the apical surface protein fraction of MDCK cells subjected to surface biotinylation, n = 4.

To confirm that eGFP-NKCC2 reached the apical surface in MDCK cells, biotinylation of apical or basolateral surface proteins of eGFP-NKCC2 transduced MDCK cells was performed. This was done by masking biotinylation sites either in the apical or basolateral membranes of MDCK cells growing on trans-wells by NHS-acetate to facilitate biotinylation of basolateral or apical proteins respectively. Expression of eGFP-NKCC2 was observed only in the apical surface fraction but not in the basolateral surface fraction (Figure 4C). Taken together, these data indicate correct targeting of eGFP-NKCC2 to the apical membrane but not to the basolateral membrane in polarized

MDCK cells.

Site-specific NKCC2 biotinylation and apical labeling for TIRF microscopy imaging

After confirming apical targeting of NKCC2 construct in polarized MDCK cells, we developed a method to selectively label NKCC2 at the apical surface. To selectively tag NKCC2, a NKCC2 construct containing a Biotin Acceptor Domain (BAD) in the extracellular loop between trans-membrane domains 5 and 6 (NKCC2-BAD) was generated. MDCK cells were transduced with NKCC2-BAD adenoviral construct (Figure 5) and biochemical surface biotinylation was achieved by exogenous addition of

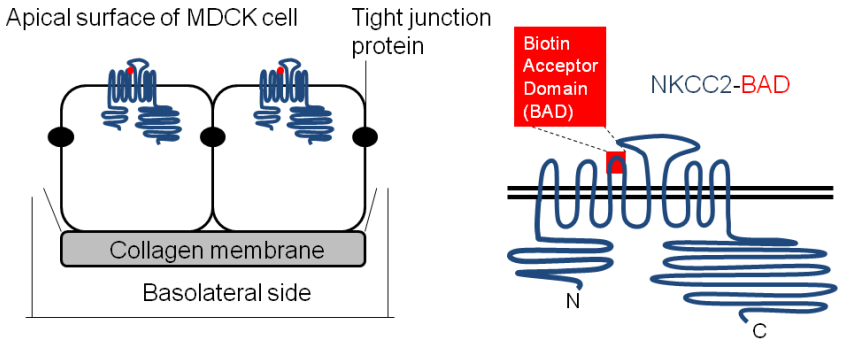

Figure 5: Expression of NKCC2-BAD on apical surface of MDCK cells. Schematic representation of expression of NKCC2-BAD on the apical membranes of MDCK cells. The Biotin Acceptor Domain (BAD) inserted in the extracellular loop between the 5th and 6th trans-membrane domain of NKCC2.

bacterial biotin ligase BirA, biotin and ATP for 15 minutes to the apical side of the transwell [78]. Fluorescent labeling of biotinylated apical NKCC2 was achieved by incubating the apical surface with Alexa Fluor 488- conjugated streptavidin (Figure 6).

Figure 6: Step-wise selective biotinylation of surface NKCC2-BAD and labeling with Streptavidin Alexa Fluor 488.

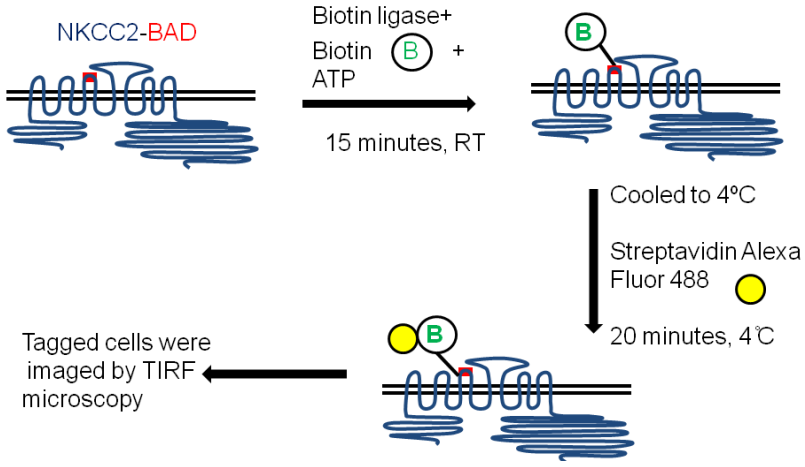

Apical membranes were then imaged by TIRF microscopy in a temperature-controlled chamber as shown in Figure 7. TIRF microscopy is based on the principle of generation of an evanescent field upon laser excitation to allow fluorescence of molecules only in the immediate vicinity (100-200 nm) of the glass coverslip [82,83]. To maximize the apical membrane area in proximity to the glass coverslip to be visualized, the collagen-coated membrane was gently pushed with a glass pipette.

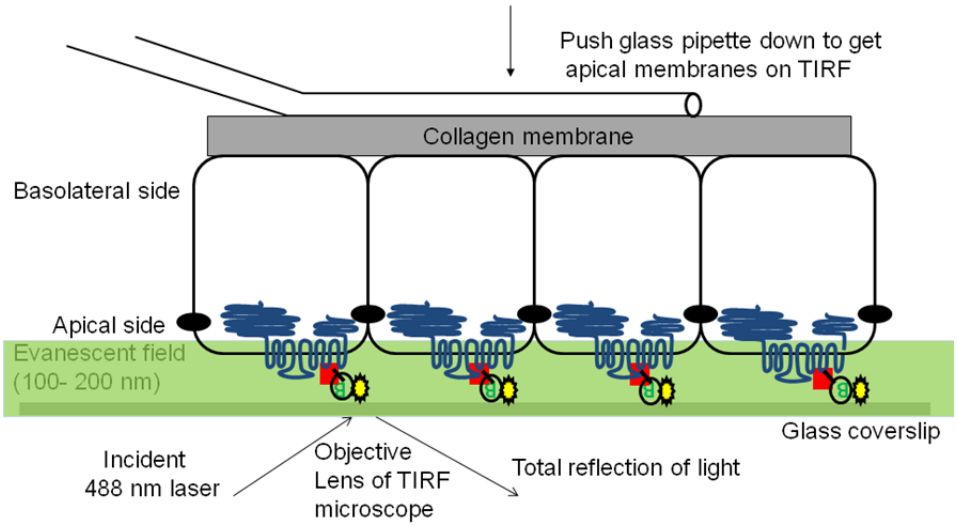

Figure 7: Diagrammatic representation of temperature controlled chamber set up for live cell imaging of apical membranes by TIRF microscopy.

As shown in Figure 8A, NKCC2 was observed at the apical surface of MDCK cells. Heterogeneous pattern of distribution of apical surface NKCC2 restricted to discrete domains referred here as puncta (singular- punctum) was observed which

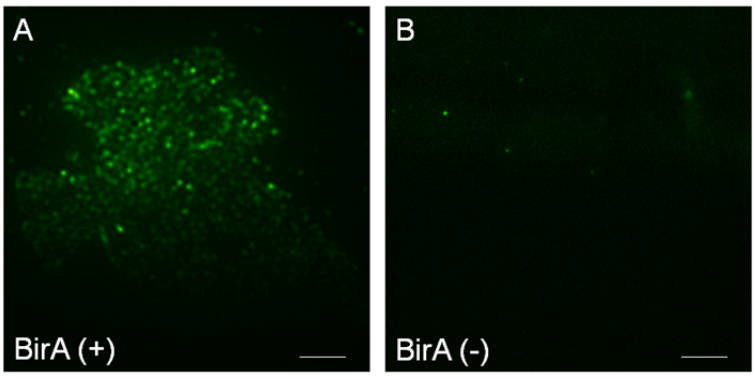

Figure 8: TIRF images of apical membranes of MDCK cells expressing NKCC2-BAD subject to biochemical biotinylation. Biotinylation performed A) with or B) without biotin ligase (BirA) followed by labeling with streptavidin Alexa Fluor 488, n = 3. Scale bar = 10 µm.

appeared to be clustered (Figure 9). Clustering was demonstrated by measuring area of individual surface NKCC2 punctum while area of individual immobilized fluorescent biotin beads on a glass slide served as a control. To assure that only NKCC2 was

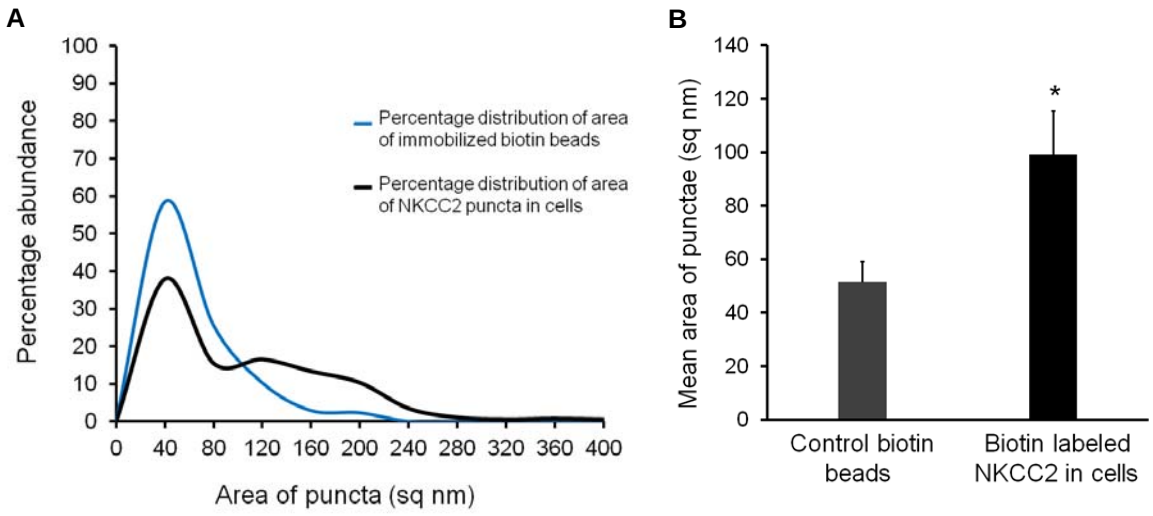

Figure 9: Clustering of NKCC2 puncta. A) Distribution of NKCC2 surface puncta area and abundance. B) Mean area of surface NKCC2 puncta measured with Metamorph® software. Immobilized fluorescent biotin beads on a glass slide serve as control, n = 3 (~50 puncta per slide), * $p < 0.05$ vs. control.

biotinylated, negative controls were performed in parallel to every experiment. MDCK cells transduced with NKCC2-BAD were incubated in the absence of BirA but in the presence of biotin followed by streptavidin labeling. Negative controls showed absence of non-specific labeling in MDCK cells (Figure 8B). These data indicate that genetic incorporation of the BAD domain to NKCC2 results in specific biotinylation of NKCC2 by BirA at the apical surface of polarized MDCK cells for TIRF imaging.

Metabolic biotinylation yields specific labeling of NKCC2-BAD in MDCK cells

Our data indicate that surface NKCC2-BAD can be successfully biotinylated biochemically by exogenous addition of BirA to the apical bath of the transwells. However this method may be associated with experimental variability in tagging NKCC2 with biotin due to numerous steps involved. In addition, ATP in the reaction mixture can

potentially cause purinoceptor activation [84,85]. In order to improve our previous biotinylation method, we performed metabolic biotinylation of NKCC2-BAD *via* co-transduction of MDCK cells with a secretory form of the enzyme (ssBirA) [74,75,86,87]. The presence of the secretory signal (ss) in the BirA ensures that expressed biotin ligase will be in contact with proteins in the trans-Golgi and the secretory pathway to allow biotinylation of proteins with endogenous biotin eliminating the need of exogenous addition of BirA and biotin. 24 hrs after co-transduction, cells were then cooled to 4ºC and directly labeled with Alexa Fluor 488- conjugated streptavidin. To assure that NKCC2 biotinylation and labeling was specific, a negative control was included in parallel to every experiment in which MDCK cells were transduced with only NKCC2-BAD but not with ssBirA followed by streptavidin labeling. We observed apical surface NKCC2-BAD biotinylation as indicated by surface puncta obtained by TIRF imaging (Figure 10A). No signal was observed in the negative control which indicated specific biotinylation and labeling of NKCC2-BAD by co-expressed ssBirA (Figure 10B). These data indicate that metabolic biotinylation can be used as a more convenient alternative to biochemical biotinylation for imaging apical NKCC2 by TIRF microscopy.

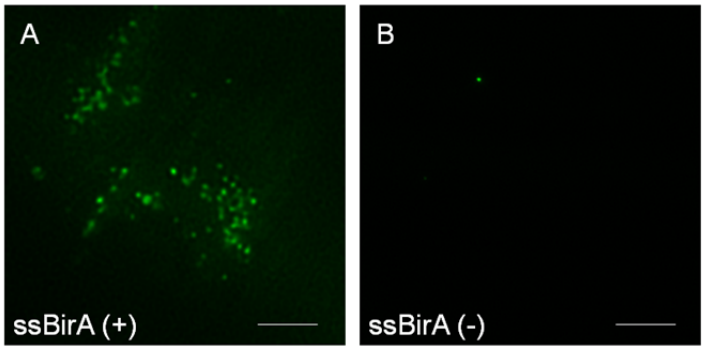

Figure 10: TIRF images of apical membranes of MDCK cells expressing NKCC2-BAD subject to metabolic biotinylation. Biotinylated performed A) with or B) without secretory signal biotin ligase (ssBirA) followed by labeling with streptavidin Alexa Fluor 488, n = 3. Scale bars = 10 μm.

Metabolic biotinylation yields specific labeling of NKCC2-BAD in TAL cells

To test whether apical NKCC2 can be specifically tagged and imaged by TIRF

microscopy in native TALs, we generated primary cultures of rat TALs as described [88]. Primary cultures of rat TAL cells were co-transduced with adenoviral NKCC2-BAD and ssBirA constructs to induce metabolic biotinylation. Figure 11A shows a representative image of NKCC2 puncta observed at the apical surface of rat TAL primary cultured cells after labeling with streptavidin.

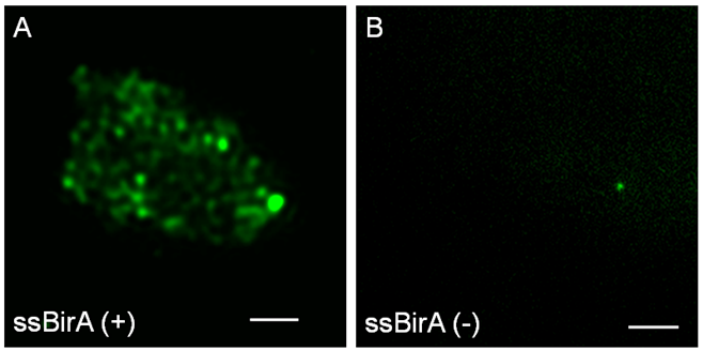

Figure 11: TIRF images of apical membrane of rat TAL cells expressing NKCC2-BAD subject to metabolic biotinylation. Biotinylation performed A) with or B) without secretory signal biotin ligase (ssBirA) followed by labeling with streptavidin Alexa Fluor 488, n = 3. Scale bar = 10 µm.

In parallel to every experiment, negative controls were performed in which TAL cells were transduced with only NKCC2-BAD but not with ssBirA to ensure NKCC2-specific biotinylation was performed followed by labeling with Alexa Fluor 488-conjugated streptavidin. As shown in Figure 11B, no labeling was observed in negative control cells. These data indicate that NKCC2-BAD can be specifically labeled at the apical surface of rat TAL primary cultures for imaging by TIRF microscopy.

Conclusion

We observed that transduction of NKCC2 construct containing a biotin acceptor domain (BAD) sequence between the 5^{th} and 6^{th} trans-membrane domains in MDCK and TAL cells allowed NKCC2-specific biotinylation by exogenous biotin ligase (BirA). We also demonstrate that expression of a secretory form of BirA in TAL cells induced metabolic biotinylation of NKCC2. Subsequent labeling with a fluorophore allowed live cell imaging by TIRF microscopy. On the TIRF field, we observed that most apical

NKCC2 was located within small discrete domains or clusters referred to as 'puncta'. Therefore we conclude that site-specific labeling of NKCC2 allows visualization of apical NKCC2 by Total Internal Reflection Fluorescence (TIRF) microscopy in polarized MDCK and TAL cells. The significance and in depth interpretation of all these observations will be addressed in the discussion in Chapter 5.

Aim 2: Hypothesis: Total internal reflection fluorescence (TIRF) microscopy allows monitoring of NKCC2 endocytosis in polarized MDCK and TAL cells in real time

Rationale

The thick ascending limb (TAL) of the loop of Henle reabsorbs about 25 - 30% of the NaCl filtered by the glomerulus *via* the apical Na^+-K^+-$2Cl^-$ co-transporter (NKCC2) [37,38]. Under steady-state conditions, only a small fraction of NKCC2 (4-5%) is present at the apical surface while the rest of the NKCC2 pool is located sub-apically [11,34,35]. Recent studies indicate a direct relationship between the amount of NKCC2 at the apical surface with NKCC2 activity and the reabsorptive capacity of the TAL [36,35]. The steady-state levels of NKCC2 at the apical surface are maintained by a dynamic balance between endocytosis, exocytic delivery, and recycling [36-38,88]. However, the underlying molecular mechanisms of NKCC2 trafficking and the proteins involved are poorly understood. This is in part due to a lack of methods to study NKCC2 trafficking.

Surface biotinylation of apical proteins with NHS-SS biotin [37,38] is used to study NKCC2 endocytosis. However, this technique has several limitations because it cannot capture the dynamics of endocytosis in real time [39,40]. Optical methods such as TIRF microscopy have been developed that allow imaging of trafficking events at the plasma membrane. For example, TIRF microscopy has been used to study the

dynamic process of trafficking of clathrin-coated vesicles along with many membrane proteins in non-polarized cells [41-46]. In polarized cells, TIRF microscopy has been used to image basolateral membrane dynamics of trafficking of several proteins [47]. Very recently, TIRF imaging has been applied to visualize apical and sub-apical trafficking events in polarized epithelial cells [48,49]. We hypothesized that TIRF imaging of apical NKCC2 would allow monitoring of NKCC2 endocytosis with good time resolution.

Results

Visualization of individual NKCC2 endocytic events on apical surface of MDCK cells in real time.

After apical NKCC2-specific tagging and imaging by TIRF microscopy in MDCK cells, we monitored the disappearance of an individual NKCC2 punctum in real time which is an indication of an endocytic event. Cells were placed at 37ºC to allow endocytosis, and images were acquired every second by TIRF microscopy. Individual surface NKCC2 punctum was tracked by defining a region of interest as shown in Figure 12A and its fluorescence intensity was quantified. A rapid decrease in

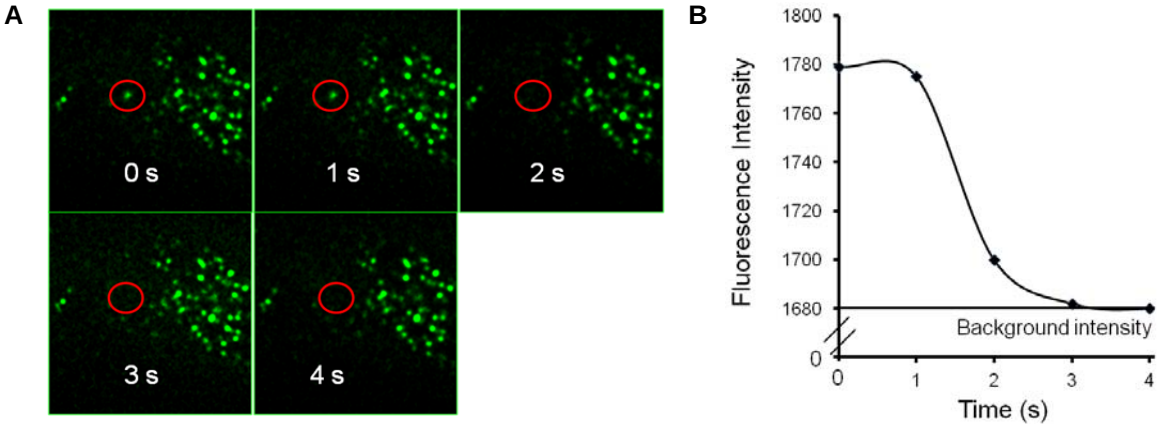

Figure 12: Single NKCC2 endocytic event at the apical membrane of MDCK cells captured by TIRF microscopy. A) Snapshots of TIRF images taken every 1 second. Individual NKCC2 punctum are encircled in red. B) Graphical representation of fluorescence intensity of a NKCC2 punctum undergoing internalization.

fluorescence reaching background fluorescence intensity within a second was observed (Figure 12B), representing a single endocytic event. Occurrence of several endocytic events resulted in a decrease in the total number of surface NKCC2 puncta on the TIRF field over time which was quantified with the Granularity module of Metamorph®. The number of surface puncta was analyzed over a period of 20 minutes and 23.5 ± 6.1% of the initial number of NKCC2 punctum were observed to disappear from the cell surface (Figure 13). This is representative of an endocytic rate of 1.18 ± 0.16 % per minute

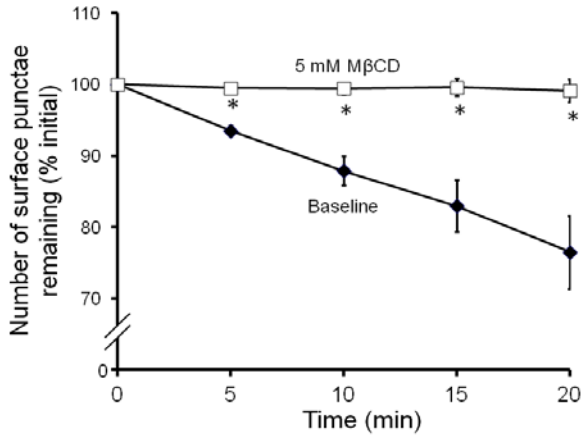

Figure 13: Graphical representation of change in number of NKCC2 surface puncta over time in MDCK cells. Under conditions of with or without 5 mM Methyl β cyclodextrin (MβCD) n = 5, * p < 0.01 *vs*. baseline.

under baseline conditions. To assure that the disappearance of NKCC2 puncta from the surface was due to NKCC2 endocytosis, cells were pre-treated with 5 mM Methyl-β-cyclodextrin (MβCD), a cholesterol chelating agent previously shown to completely block NKCC2 endocytosis [38]. Treatment of MβCD completely prevented the decrease of NKCC2 puncta from the TIRF field of view and consequently the number of surface puncta did not change significantly over 20 minutes. The rate of NKCC2 endocytosis in the presence of MβCD was 0.14 ± 0.06 % per minute ($p < 0.01$ MβCD treated *vs*. untreated) (Figure 13). These data indicate that the decrease in the number of surface NKCC2 puncta observed under baseline conditions was indeed due to NKCC2 endocytosis.

Studying NKCC2 endocytosis in rat TAL cells

To test whether apical surface TIRF imaging can be used to study endocytosis in native TALs, we generated primary cultures of rat TALs as described [88]. NKCC2-BAD specific metabolic biotinylation and labeling in rat TAL cells was performed as explained in Aim 1 for imaging by TIRF microscopy. Then, we monitored the disappearance of surface NKCC2 puncta from the apical membrane of rat TAL cells over 20 minutes at 37ºC. We observed that the number of surface NKCC2 puncta gradually decreased over time (Figure 14) at a rate of 1.09 ± 0.08 % per minute, a surrogate of constitutive NKCC2 endocytic rate. Taken together, these data indicated that single-molecule biotinylation of surface NKCC2-BAD and apical TIRF imaging can be used to monitor NKCC2 endocytosis in TAL cells.

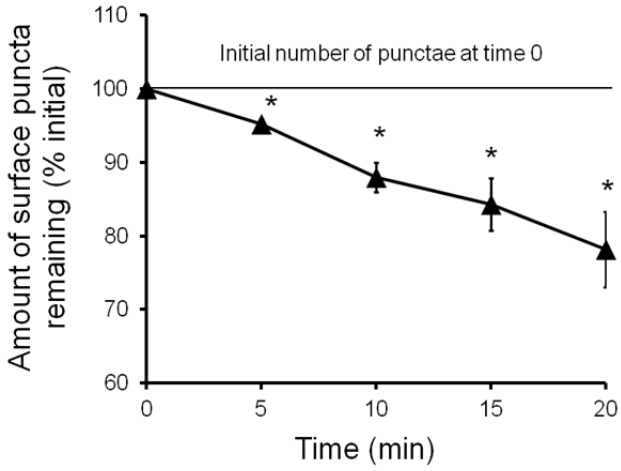

Figure 14: Graphical representation of change in number of NKCC2 surface puncta over time in rat TAL cells. N = 5, * p < 0.01 *vs*. initial number of surface puncta.

Conclusion

We show here that site-specific labeled NKCC2 referred as NKCC2 puncta were observed to disappear from the TIRF field indicating an endocytic event which led to decrease in the number of surface puncta at a rate synonymous with the rate of NKCC2 endocytosis. Treating cells with a cholesterol chelating agent (MβCD) completely blocked NKCC2 endocytosis and disappearance of surface puncta. We conclude that

TIRF microscopy of labeled NKCC2 is appropriate for dynamic and real time imaging of individual endocytic events at the apical membrane of MDCK cells and TAL cells and can be extended to study dynamic internalization events of other proteins.

CHAPTER 3 - ROLE OF ALMS1 IN NKCC2 ENDOCYTOSIS AND THICK ASCENDING LIMB FUNCTION AND BLOOD PRESSURE

Introduction

Increased NKCC2 activity and apical trafficking are associated with salt sensitive hypertension in rodents and humans [25-31]. NKCC2 endocytosis has been shown to be important in maintaining surface NKCC2 levels [37,38]. Despite its importance, the regulation of NKCC2 endocytosis is poorly understood. MAL/VIP17 has been shown to interact with a domain in the carboxyl-terminus of NKCC2 and regulate NKCC2 internalization [49]. To discover novel proteins that interact with this region of NKCC2 and play a role in NKCC2 endocytosis, we followed a targeted proteomics approach. We identified a new protein not known to be previously expressed in the TAL - Alström syndrome 1 (ALMS1). In this chapter we tested whether ALMS1 is involved in NKCC2 endocytosis to maintain surface NKCC2 levels, NKCC2-mediated NaCl reabsorption and therefore in regulating blood pressure and inducing salt sensitivity. We divided this chapter into two additional aims. In Aim 3 we tested whether ALMS1 interacts with the C-terminus region of NKCC2 and mediates endocytosis thereby decreasing steady-state surface NKCC2 expression. In Aim 4 we tested whether inhibition of ALMS1 expression increases NKCC2-mediated NaCl reabsorption in the TAL and therefore elevates blood pressure and induces salt sensitivity.

Aim 3: Hypothesis: ALMS1 binds the C-terminus region of NKCC2 and mediates NKCC2 endocytosis thereby decreasing steady-state surface NKCC2 expression in the TAL.

Rationale

NKCC2 surface levels are maintained by a balance between NKCC2 endocytosis, recycling and exocytosis. We showed that NKCC2 undergoes constitutive

endocytosis and inhibition of endocytosis enhanced surface NKCC2 and NaCl reabsorption by the TALs [33,37,38], indicating a direct relationship between apical NKCC2 abundance and NKCC2 activity. Despite the importance of the endocytic pathway, the molecular mechanisms that regulate NKCC2 endocytosis are not clear. Only one protein has been described to bind and regulate NKCC2 endocytosis (MAL/VIP17) [49]. This protein interacts with a 71-amino acid domain in the carboxyl-terminus of NKCC2 (C2-NKCC2) which has been shown to be important for NKCC2 apical targeting [81]. Thus, we hypothesized that proteins that bind to this domain may play an important role in NKCC2 endocytosis. We performed a proteomic-based identification of glutathione-S-transferase (GST)-C2-NKCC2 interacting proteins in the TAL and identified Alström syndrome 1 (ALMS1) protein as one of the interacting partners. ALMS1 is known to play a role in trafficking of transporters such as glucose transporter 4 (GLUT4) [69] and C-terminus of ALMS1 (C-ALMS1) interacts with several proteins such as Myosin Vb (MYO5B), α-actinin (ACTN), Rad50 interactor 1 (RINT1) that play a role in the endocytic pathway [70-73]. We tested the hypothesis that ALMS1 interacts with NKCC2 and stimulates its endocytosis to maintain NKCC2 surface levels. To specifically address the role of ALMS1, we inhibited its expression by gene silencing *via* short hairpin RNA (shRNA) and genetic deletion in rats.

Results

ALMS1 is expressed in the TAL

First, to study the localization of ALMS1 in the kidney, we performed immuno-fluorescent labeling of ALMS1 in rat kidney transverse section (Figure 15A). We observed that ALMS1 is expressed in TALs indicated by co-immunolabeling for NKCC2.

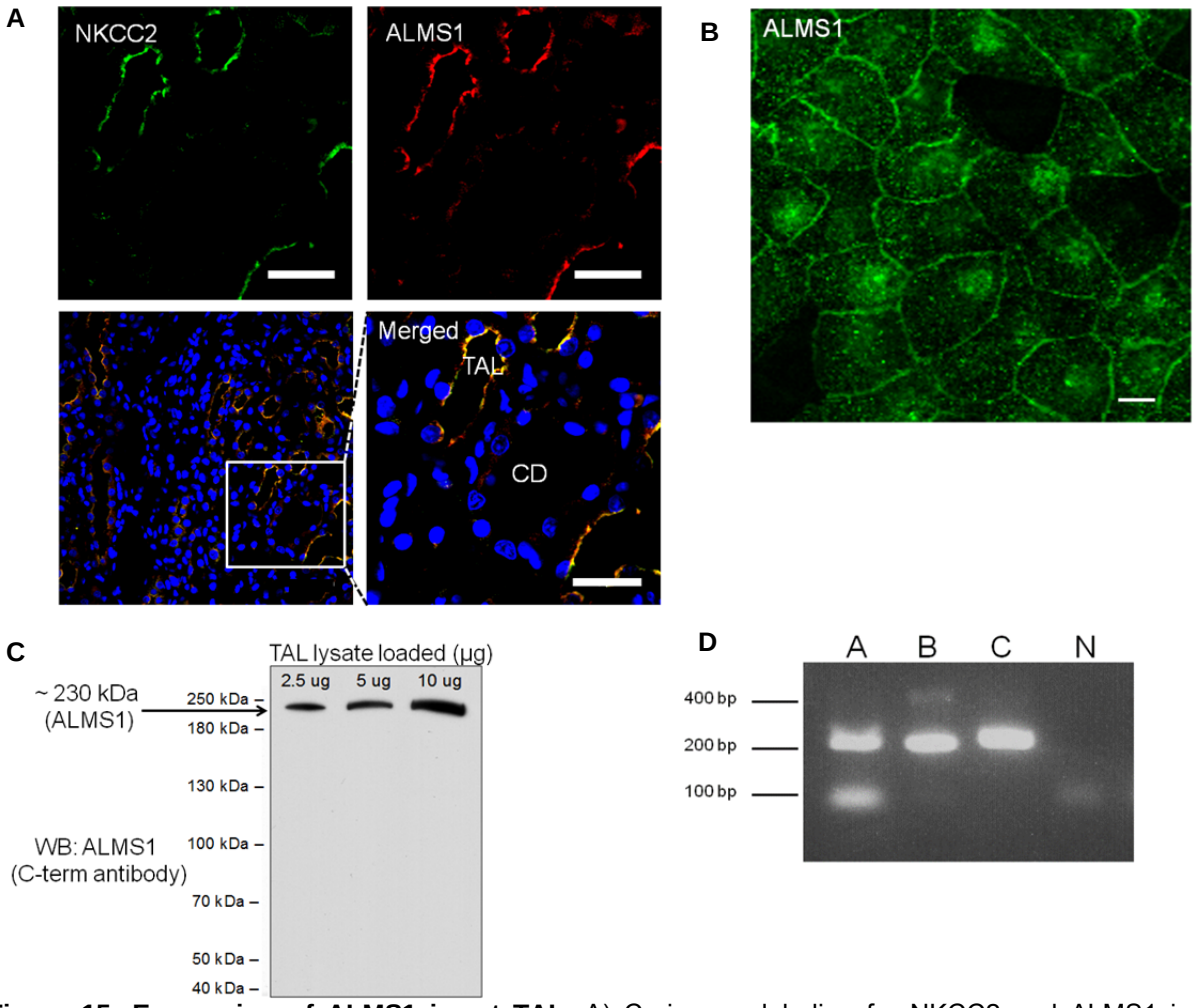

Figure 15: Expression of ALMS1 in rat TAL. A) Co-immunolabeling for NKCC2 and ALMS1 in rat kidney section. TAL: Thick Ascending Limb; CD: Collecting duct, n = 3, scale bars = 20 µm. B) Immuno-labeling of ALMS1 in rat primary cultured cells, n = 3, scale = 5 µm. C) Representative Western blot of ALMS1 (corresponding to ~230 kDa protein band) in rat TAL, n = 3. D) RT-PCR with A, B and C primers for amplification of 3', 5' and middle region of *ALMS1* mRNA in rat TAL, N = negative control.

We cultured primary TAL cells and immuno-labeled for ALMS1 (Figure 15B). We confirmed the expression of ALMS1 in TAL by Western blot as an expected 230 kDa protein band (Figure 15C). We detected *ALMS1* mRNA in rat TAL by RT-PCR (Figure 15D). All these data together indicate and confirm the expression of ALMS1 in rat TAL.

Identification of ALMS1 as an interacting partner of NKCC2 in the TAL

In order to test whether ALMS1 expressed in the TAL interacts with C2-NKCC2, a region important for NKCC2 apical targeting, we followed a targeted proteomics

approach. We designed a GST-fusion protein with C2-NKCC2 (GST-C2-NKCC2) and used it as bait in GST pull-down assays from TAL lysates. We characterized the interacting proteins by liquid chromatography followed by mass spectrometry. Of all the proteins identified, we focused on the proteins most likely to play a role in endocytosis and blood pressure regulation, by applying the following criteria: 1) It is associated with QTL for high blood pressure according to Rat Genome Database (RGD), 2) Has been associated with blood pressure, cardiovascular or renal phenotype in humans in the (NHGRI) genome-wide association studies (GWAS) catalog and the PheGenI database. 3) The known interacting partners according to STRING and EntrezGENE databases are proteins of known relevance in cardiovascular and renal physiology. Of all the proteins identified, ALMS1 was chosen as a candidate for further study (Figure 16).

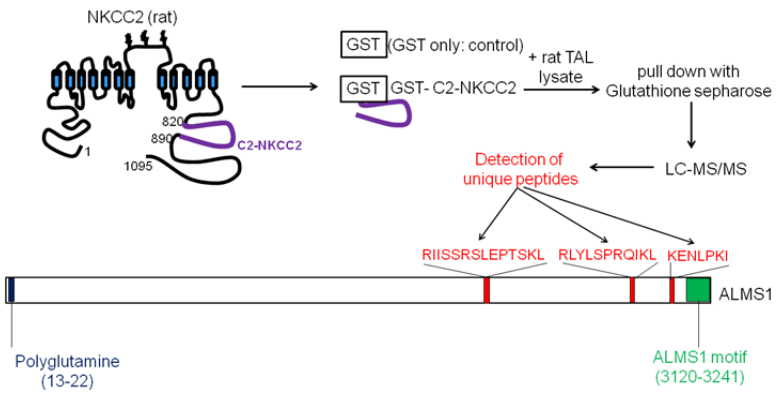

Figure 16: GST pull-down of ALMS1 in TAL lysate with C2-NKCC2. Unique peptides corresponding to ALMS1 picked up by liquid chromatography-mass spectrometry in Glutathione-S-transferase (GST) pull down assay using GST-carboxyl-terminus of NKCC2 fusion protein (GST-C2-NKCC2) or GST alone (control) as baits in rat TAL lysates.

C-ALMS1 interacts with NKCC2 and forms a part of its endocytic network

The carboxyl-terminus of ALMS1 is known to interact with endocytic proteins such as MYO5B, RINT1, ACTN1/4 [70-73]. Therefore, we studied if C-ALMS1 also interacts with NKCC2. To test this, we used truncated portions of ALMS1 C-terminus (C-ALMS1 A/B) fused to GST (GST-C-ALMS1 A/B) as a bait in GST pull-down assay in TAL lysates. GST alone was used as a negative control. We identified a region in

ALMS1 that is able to pull down full length NKCC2 by Western blot (Figure 17A). Someof the proteins identified by mass spectrometric analysis of C-ALMS1 A/B and C2-

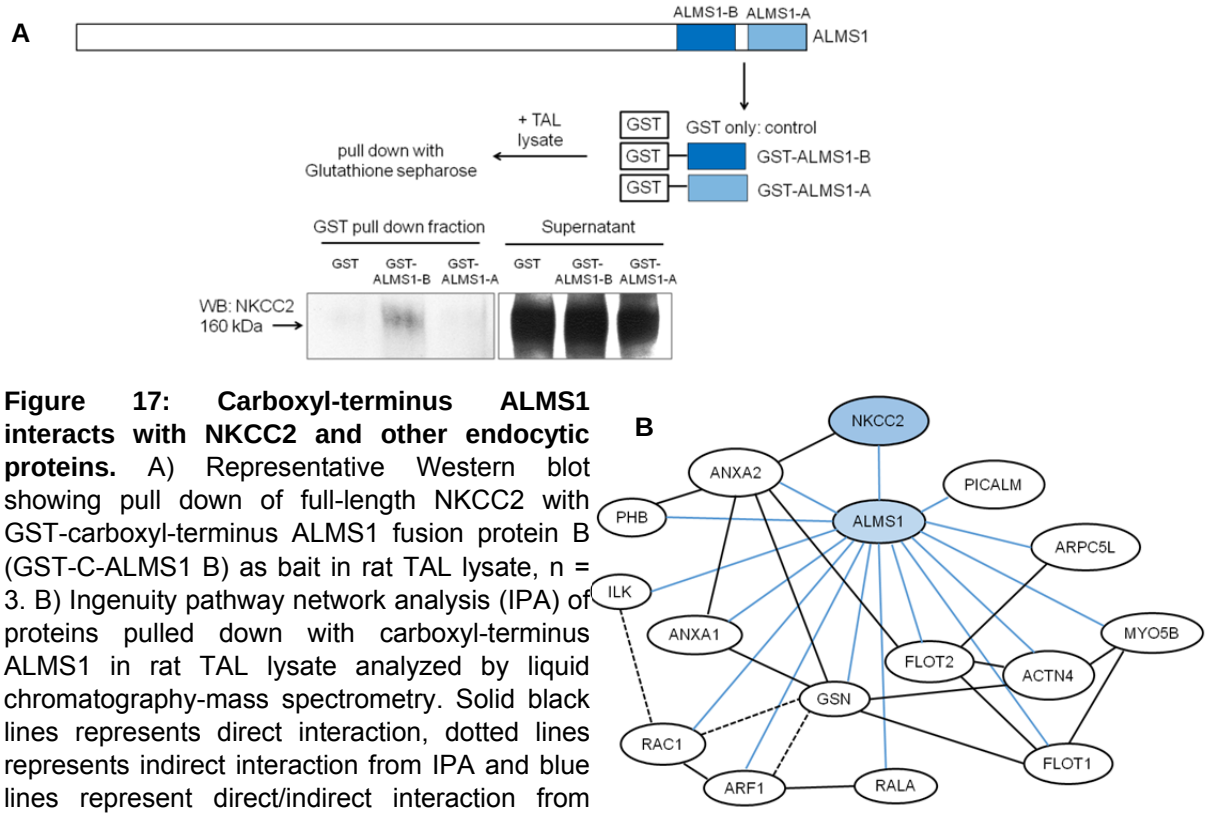

Figure 17: Carboxyl-terminus ALMS1 interacts with NKCC2 and other endocytic proteins. A) Representative Western blot showing pull down of full-length NKCC2 with GST-carboxyl-terminus ALMS1 fusion protein B (GST-C-ALMS1 B) as bait in rat TAL lysate, n = 3. B) Ingenuity pathway network analysis (IPA) of proteins pulled down with carboxyl-terminus ALMS1 in rat TAL lysate analyzed by liquid chromatography-mass spectrometry. Solid black lines represents direct interaction, dotted lines represents indirect interaction from IPA and blue lines represent direct/indirect interaction from GST-C-ALMS1 pull down data

NKCC2 pulled down proteins were phosphatidylinositol binding clathrin assembly protein (PICALM1) and rabaptin (RABEP1; data not shown) respectively, that are known to be involved in early endocytic pathway of other proteins. Ingenuity pathway analysis (Figure 17B) of C-ALMS1 interactome indicated protein-protein interactions among themselves and this suggested that these proteins may form a network of early endocytic machinery of NKCC2 (See Table 2 for details on other pulled down proteins).

ALMS1 co-localizes with NKCC2 in the TAL

In isolated TAL preparations, we observed that ALMS1 was distributed along the apical and sub-apical regions (Figure 18A), similar to the expression pattern of NKCC2 [35].

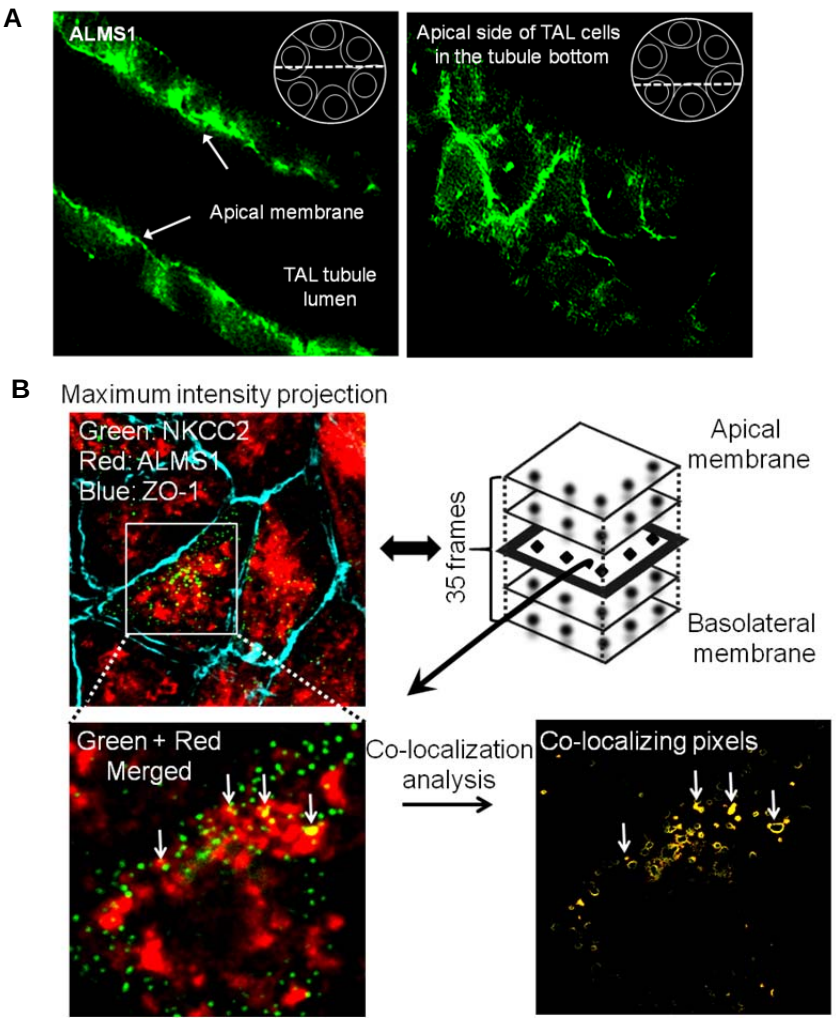

Figure 18: Expression and co-localization of ALMS1 with NKCC2 in apical and sub-apical regions in rat TAL. A) Immunostaining for ALMS1 in isolated perfused rat TAL. B) Co-immunolabeling of ALMS1 and internalized surface NKCC2 in rat TAL primary culture, n = 3. Merged image from sub-apical plane (2 µm from the apical plane) showing co-localization of NKCC2 and ALMS1 in yellow indicated by arrow. Co-localization analysis performed with a Mander's overlap coefficient of > 0.95.

Immuno-labeling of ALMS1 in isolated, perfused rat TAL was performed and imaged across transverse section and apical surface of TAL tubule by confocal microscopy. In rat kidney sections, ALMS1 was seen to co-localize with NKCC2 (Figure 15A). To test whether ALMS1 co-localizes with internalized NKCC2 in cultured rat TALs, we fluorescently labeled surface NKCC2 at 4ºC with an antibody that recognizes an epitope in an extracellular loop [88]. Following a 30 min period of endocytosis at 37ºC, we fixed the cells and labeled ALMS1. We observed that a fraction of ALMS1 co-localized with NKCC2 (Figure 18B). Altogether these data indicate that ALMS1 interacts with C2-NKCC2 at the apical membrane and sub-apical space of TALs where

a fraction of ALMS1 co-localizes with internalized NKCC2.

Generation of ALMS1 genetic deletion rat model and its phenotypic characterization

To test our hypothesis in a stable genetic deletion animal model, we generated *ALMS1* knockout (*ALMS1* KO) rats using zinc finger nuclease gene editing technology in collaboration with the Gene Editing Rat Resource Center (GERRC) at the Medical College of Wisconsin. Deletion of 17 base pairs in exon 1 of the *ALMS1* gene results in a premature stop codon to generate *ALMS1* deletion rat model (Figure 19A). Specific primer amplification followed by restriction digestion show heterozygous and homozygous deletions (Figure 19B). Figure 19C shows a 90% reduction in ALMS1 expression in TALs from *ALMS1* KO rats.

Since ALMS1 is known to be localized to the base of the cilia, a study showed that knockdown of *ALMS1* in mouse inner medullary collecting duct (mIMCD3) cell line resulted in stunted and malformation of cilia [89]. However *ALMS1* mutant mice models show normal cilia length [67]. Thus, there is a controversy whether or not deletion of *ALMS1* caused malformation/stunted appearance of cilia in the kidney. We immuno-labeled cilia in kidney sections from *ALMS1* KO rats and WT rats and we found normal ciliary staining in both groups, indicating normal ciliary development upon *ALMS1* deletion in rats (Figure 20).

Previous reports have shown that transgenic *ALMS1* knockout mice are characterized with age dependent metabolic syndrome and kidney damage. We measured body weight of wild-type (WT) and *ALMS1* KO rats and observed that the body weight of *ALMS1* KO rats is slightly higher than WT only after 10-11 weeks of age. Blood glucose and plasma insulin were not different between the groups by 6-12 weeks

of age. Gross kidney anatomy looked normal in histological sections from 6-12 week old rats (Figure 21). At 6-12 weeks of age, *ALMS1* KO rats had a similar kidney weight and GFR as that of the WT rats (Table 1).

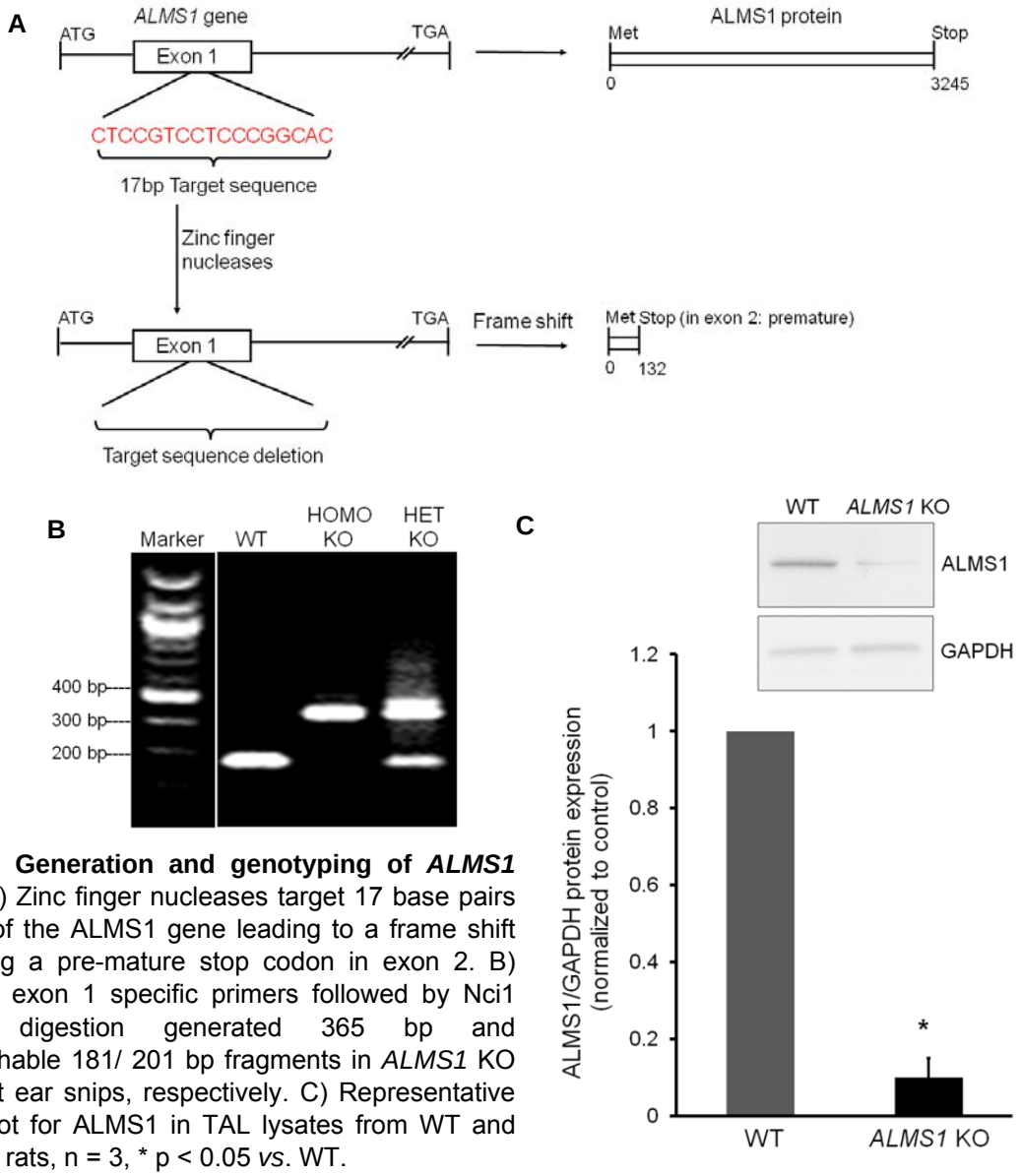

Figure 19: Generation and genotyping of *ALMS1* KO rats. A) Zinc finger nucleases target 17 base pairs in exon 1 of the ALMS1 gene leading to a frame shift and causing a pre-mature stop codon in exon 2. B) PCR using exon 1 specific primers followed by Nci1 restriction digestion generated 365 bp and indistinguishable 181/ 201 bp fragments in *ALMS1* KO and WT rat ear snips, respectively. C) Representative Western blot for ALMS1 in TAL lysates from WT and *ALMS1* KO rats, n = 3, * $p < 0.05$ *vs*. WT.

These data indicate that at this age, *ALMS1* KO rats do not significantly develop metabolic syndrome or kidney damage. To prevent the effect of potentially confounding phenotypes that are expected in older rats, we used rats of age 6-12 weeks for our study.

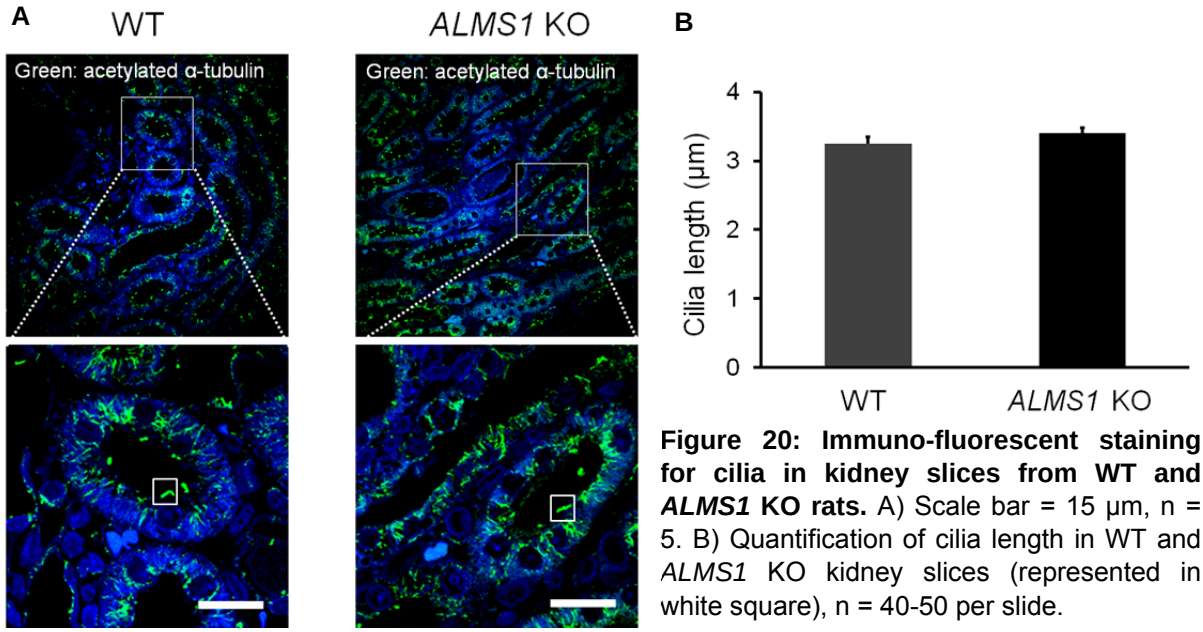

Figure 20: Immuno-fluorescent staining for cilia in kidney slices from WT and *ALMS1* KO rats. A) Scale bar = 15 μm, n = 5. B) Quantification of cilia length in WT and *ALMS1* KO kidney slices (represented in white square), n = 40-50 per slide.

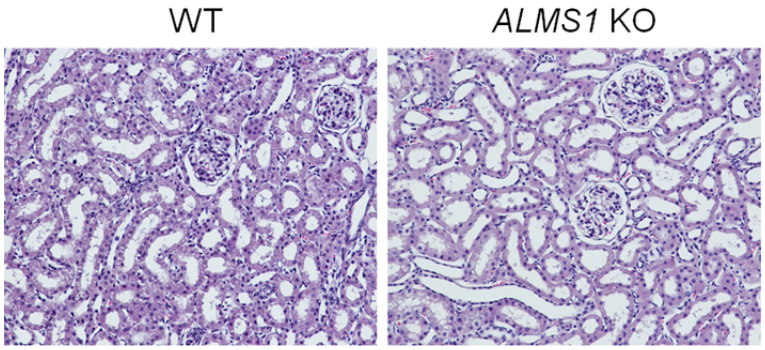

Figure 21: Light micrographs of kidney slices from WT and *ALMS1* KO rats. H&E staining, n = 3.

ALMS1 KO rats have enhanced NKCC2 levels at the apical surface in TAL

To test whether genetic deletion of *ALMS1* in rats leads to enhanced surface NKCC2 in TALs, we performed surface biotinylation in TAL suspension obtained from WT and *ALMS1* KO rats. Western blot for NKCC2 revealed that *ALMS1* KO rats have higher NKCC2 at the surface in TAL compared to WT (*ALMS1* KO: 13.8 ± 1.2% *vs*. WT: 8.1 ± 1.1%, n = 6, $p < 0.05$; Figure 22A). Total NKCC2 expression was not different between the groups (Figure 22B). GAPDH served as a surface biotinylation control.

Table 1: Physiological parameters measured in young (6- 12 week old) WT and *ALMS1* KO rats.

Physiological parameters	WT (6-12 weeks)	*ALMS1* KO (6-12 weeks)
Body weight (g)	309 ± 10	331 ± 11*
Blood glucose (mg/dl)	134 ± 10	138 ± 12
Plasma insulin (ng/ml)	0.45 ± 0.15	0.7 ± 0.1
Kidney weight (g)	2.75 ± 0.1	2.53 ± 0.13
GFR (ml/min/gkw)	0.94 ± 0.16	1.07 ± 0.36

For plasma insulin & blood glucose - n = 3; body weight - n = 5; kidney weight & GFR - WT: n = 6, *ALMS1* KO: n = 5, * $p < 0.05$ *vs*. WT.

Phosphorylation of NKCC2 is unaffected by ALMS1 deletion in rats

To test whether deletion of *ALMS1* leads to changes in NKCC2 phosphorylation, we measured NKCC2 phosphorylation levels with antibodies directed specifically to Threonine (Thr96/101) and Serine (Ser126) residues of NKCC2 and found no significant differences between TALs from WT and *ALMS1* KO rats (Figure 23A and Figure 23B).

Developing ALMS1 shRNA for renal medulla-specific knockdown of ALMS1

We then tested whether the effect of *ALMS1* deletion on surface NKCC2 was due to decreased ALMS1 expression in the renal tubule. For this, we bought a commercially available *ALMS1* shRNA. To test its mRNA knockdown efficacy in a rat cell line, we first studied if *ALMS1* mRNA is expressed in normal rat kidney (NRK-52E) cell line. Upon transfection with *ALMS1* shRNA in this cell line, we observed 78% decreased expression of *ALMS1* mRNA measured by RT-PCR (Figure 24A). We then silenced *ALMS1* in the renal medulla by adenovirus-mediated gene silencing (Figure 24B).

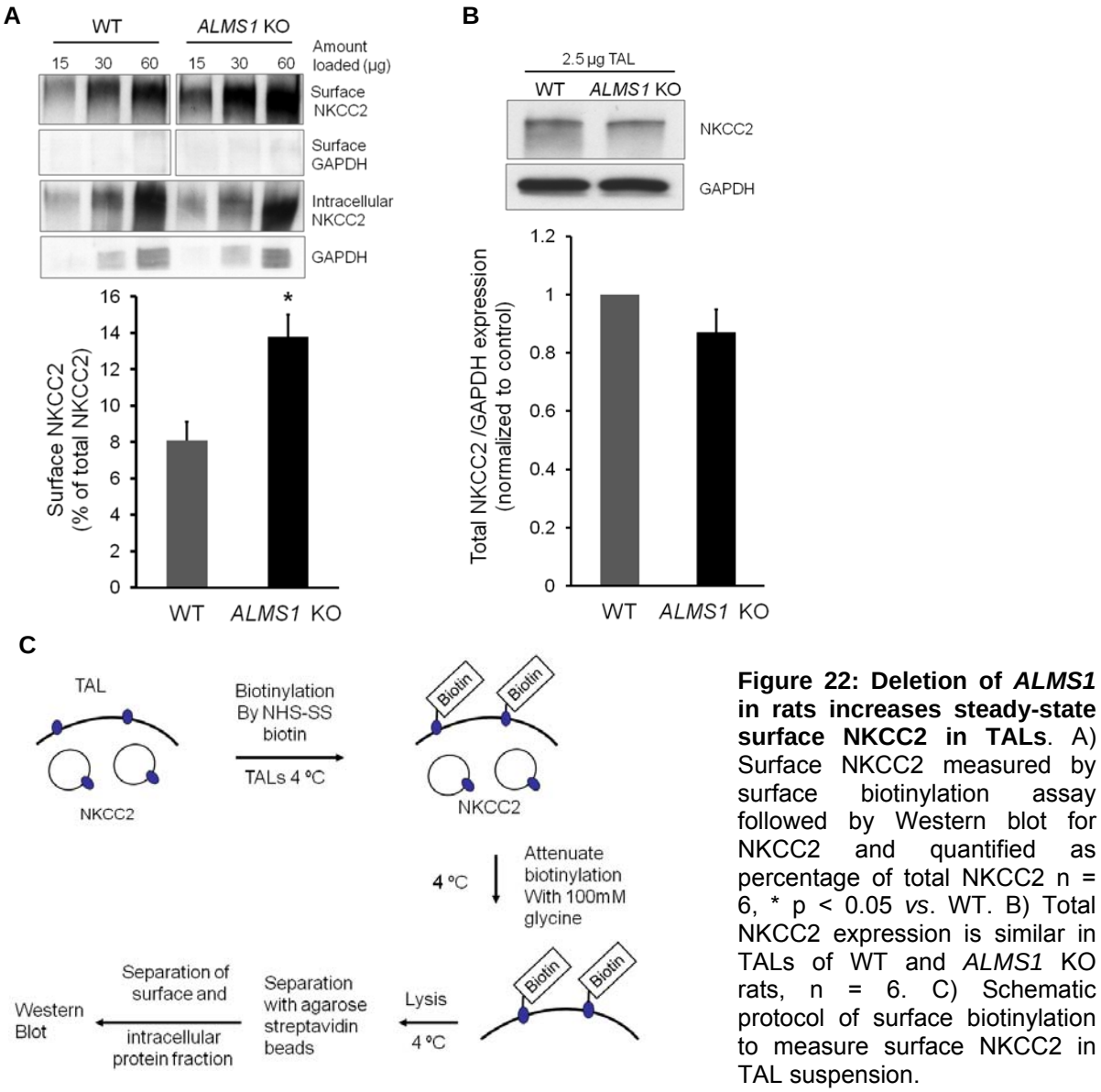

Figure 22: Deletion of *ALMS1* in rats increases steady-state surface NKCC2 in TALs. A) Surface NKCC2 measured by surface biotinylation assay followed by Western blot for NKCC2 and quantified as percentage of total NKCC2 n = 6, * p < 0.05 *vs*. WT. B) Total NKCC2 expression is similar in TALs of WT and *ALMS1* KO rats, n = 6. C) Schematic protocol of surface biotinylation to measure surface NKCC2 in TAL suspension.

For this, we injected adenoviral *ALMS1* shRNA into the outer medulla of the left kidney of normal rats while the right kidney injected with buffer served as the sham control. After 7 days of adenoviral *ALMS1* shRNA injection, we observed 80% decrease in *ALMS1* mRNA (normalized value *ALMS1* shRNA: 0.19 ± 0.04 *vs*. control: 1, n = 3, * p < 0.01) (Figure 24C) and a 60% decrease in ALMS1 protein expression (normalized value *ALMS1* shRNA: 0.39 ± 0.2 *vs*. control: 1, n = 4, * p < 0.05) (Figure 24D) in isolated TALs, together indicating an effective *ALMS1* knockdown.

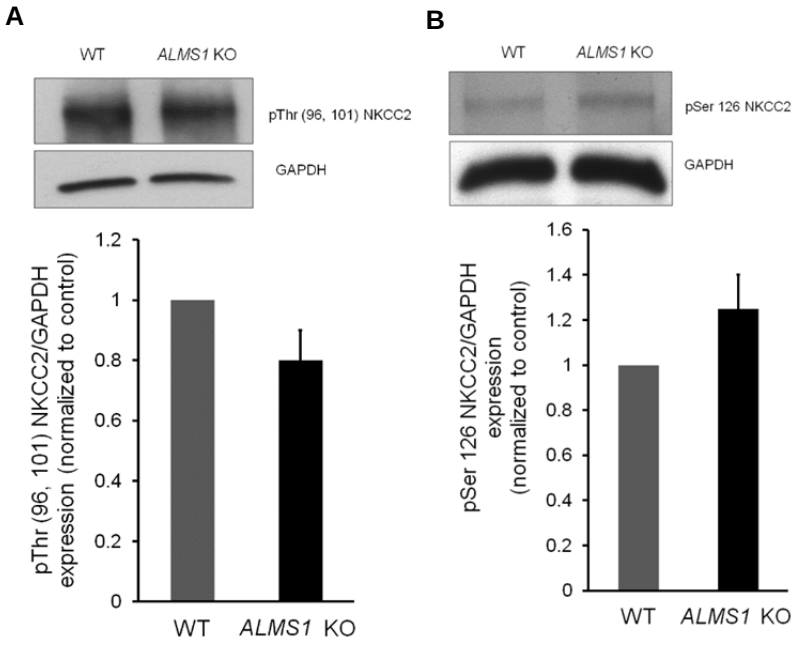

Figure 23: Phosphorylated NKCC2 level is similar in TALs from WT and *ALMS1* KO rats. A) Phosphorylated Thr (96/101) NKCC2 and B) Phosphorylated Ser (126) NKCC2 in TALs from WT and *ALMS1* KO rats, n = 3.

An acute silencing of ALMS1 by ALMS1 shRNA in the TAL leads to higher surface NKCC2

Surface NKCC2 expression was enhanced in TALs from *ALMS1* shRNA injected kidney compared to control injected kidney (*ALMS1* shRNA: 11.1 ± 1.6% *vs*. control: 6.6 ± 0.8%, n = 5, * $p < 0.05$) and there was no change in total NKCC2 expression (normalized value *ALMS1* shRNA: 0.93 ± 0.07 *vs*. control: 1, n = 5, ns) (Figure 25 A, B). GAPDH served as surface biotinylation control. These data indicate that enhanced NKCC2 in the TALs of *ALMS1* KO rats is due to the effect of deletion of *ALMS1* in TALs and not an effect of *ALMS1* deletion in other organs.

Higher surface NKCC2 in TALs of ALMS1 KO rats is due to decreased NKCC2 endocytosis

To test our hypothesis that increased surface NKCC2 in *ALMS1* KO rats is due to decreased NKCC2 endocytosis in the TAL, we performed a modified surface biotinylation protocol to measure NKCC2 internalized fraction at 37ºC (Figure 26C).

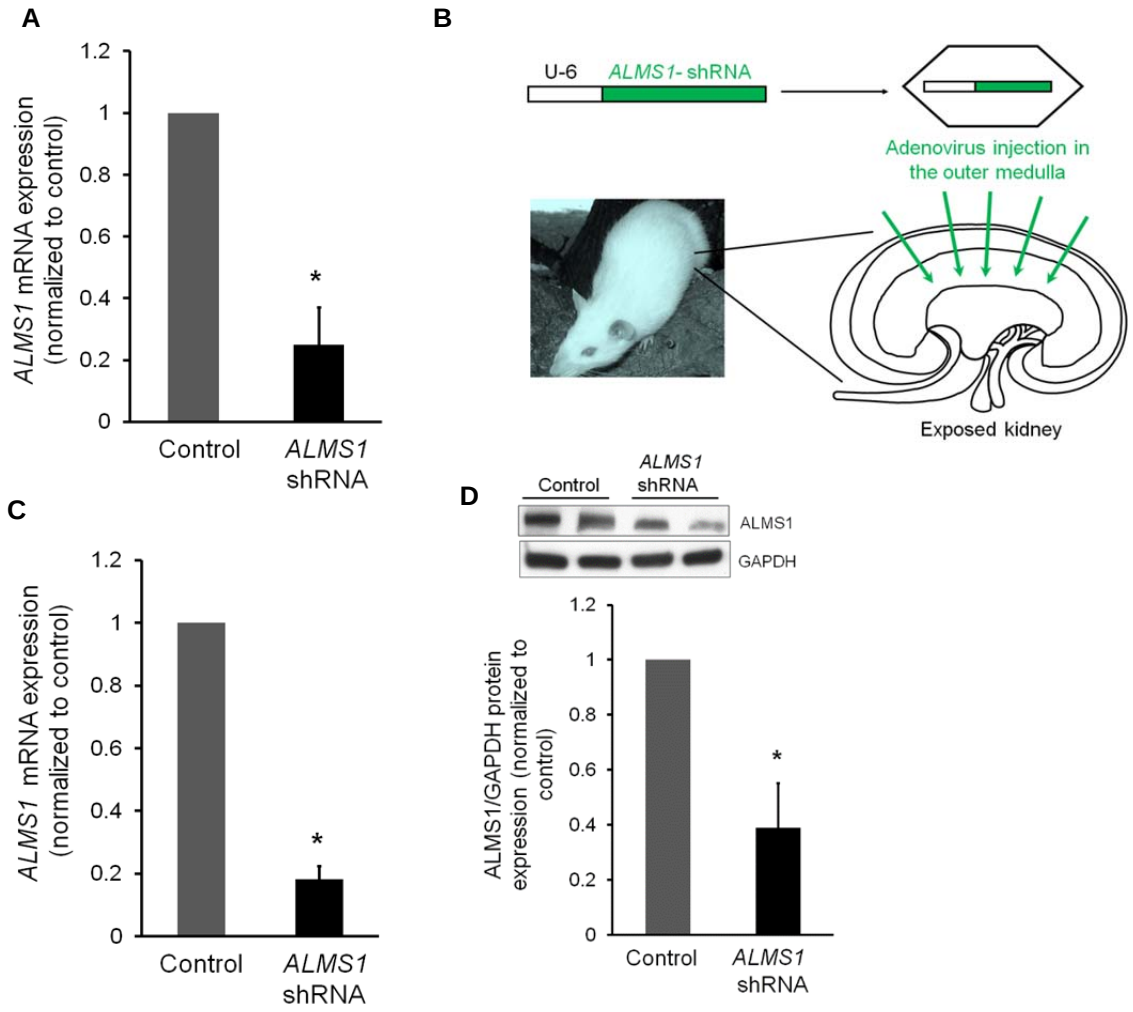

Figure 24: Inhibition of *ALMS1* mRNA and protein expression upon *ALMS1* shRNA transfection. A) *ALMS1* shRNA transfected in NRK-52E cells and mRNA quantified by RT-PCR, n = 3, * $p < 0.01$ *vs*. control. B) *ALMS1* adenoviral shRNA transduced *in vivo* into renal outer medulla of Sprague Dawley rats and *ALMS1* mRNA expression quantified by RT-PCR, n = 3, * $p < 0.01$ *vs*. control. C) *ALMS1* adenoviral shRNA transduction into renal outer medulla of SD rats and ALMS1 protein quantified by Western blot, n = 4, * $p < 0.05$ *vs*. control.

We observed that the internalized fraction of NKCC2 after warming to 37ºC was significantly lower in TALs from *ALMS1* KO rats (Figure 26A). We found that internalized NKCC2 measured as percent of baseline total surface NKCC2 was significantly lower in *ALMS1* KO rats compared to WT (*ALMS1* KO: 13.1 ± 1.4% *vs*. WT: 28.2 ± 2.8% over 20 minutes, n = 5, * $p < 0.05$; Figure 26B), suggesting decreased NKCC2 endocytic rate in TALs from *ALMS1* KO rats (*ALMS1* KO: 0.65 ± 0.07 %/min *vs*.

WT: 1.41 ± 0.14 %/min).

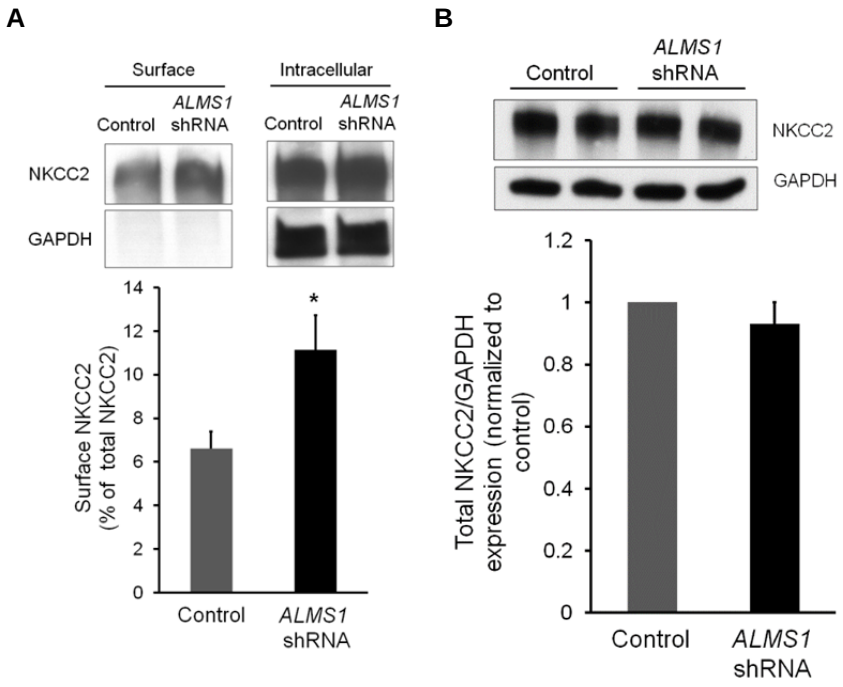

Figure 25: Knockdown of *ALMS1* by *ALMS1* shRNA transduction in renal outer medulla leads to increased steady-state surface NKCC2 in TALs. A) Surface NKCC2 was quantified by surface biotinylation assay and expressed as percentage of total NKCC2. N = 5, * $p < 0.05$ *vs*. control. B) Total NKCC2 expression does not change upon *ALMS1* mRNA knockdown in renal outer medulla of SD rats, n = 5.

Conclusion

We showed that C-ALMS1 interacts with C2-NKCC2 in rat TALs. We also showed that ALMS1 and NKCC2 co-localize in rat TAL primary culture and in rat kidney sections. Ingenuity pathway analysis of ALMS1 interacting proteins suggested that they may together form NKCC2 endocytic machinery. In TALs from *ALMS1* KO, surface NKCC2 measured as a percentage of total NKCC2 at the surface was higher compared to WT. Total NKCC2 expression was not different between strains. We also showed that the effect of enhanced NKCC2 surface abundance is due to *ALMS1* inhibition in the renal tubule and not due to deletion of *ALMS1* in other organs. The increase in surface NKCC2 is due to lower endocytosis because the rate of NKCC2

internalization was lower in TALs from *ALMS1* KO rats. We conclude that ALMS1 interacts with carboxyl-terminus of NKCC2, stimulates NKCC2 endocytosis thereby decreasing steady-state surface NKCC2. The significance and in depth interpretation of all these observations will be addressed in the discussion in Chapter 5.

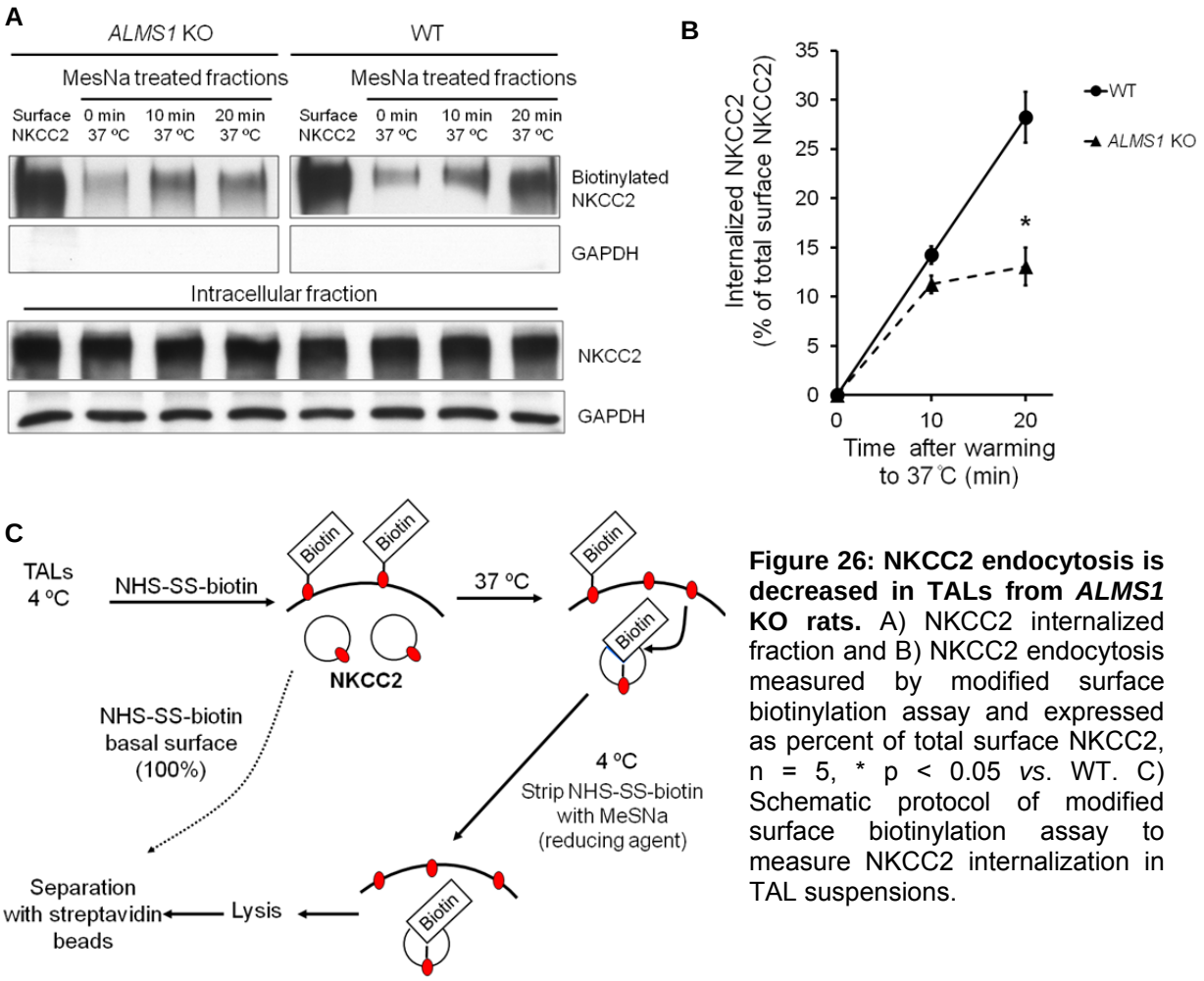

Figure 26: NKCC2 endocytosis is decreased in TALs from *ALMS1* KO rats. A) NKCC2 internalized fraction and B) NKCC2 endocytosis measured by modified surface biotinylation assay and expressed as percent of total surface NKCC2, n = 5, * $p < 0.05$ *vs*. WT. C) Schematic protocol of modified surface biotinylation assay to measure NKCC2 internalization in TAL suspensions.

Aim 4: Hypothesis: ALMS1 decreases NKCC2-mediated NaCl reabsorption by the TAL, thereby plays a role in salt sensitive hypertension

Rationale

Enhanced NKCC2 activity is associated with salt sensitive hypertension but the underlying molecular mechanisms are not very well elucidated [25-31]. Our current understanding of the complex genetic architecture of hypertension and salt sensitivity

relies heavily on identification of several susceptibility loci through population-based association studies. In this regard, genetic loci such as uromodulin (*UMOD)* [90-94] and *ALMS1* [56] among others were identified for genetic risk associated with hypertension. The role of UMOD in regulating NKCC2 activity and salt sensitive hypertension has been well characterized [95]. However, very little is known about the role of ALMS1 or its link with NKCC2. In a targeted proteomics screen, we identified ALMS1 as an interacting partner of NKCC2. We tested the hypothesis that inhibition of *ALMS1* increases NKCC2-mediated NaCl reabsorption, thereby elevates blood pressure and induces salt sensitivity. To specifically address the role of ALMS1, we inhibited ALMS1 expression by genetic deletion of *ALMS1* in rats.

Results

ALMS1 KO rats are hypertensive and salt sensitive

To test our hypothesis that genetic deletion of *ALMS1* in rats leads to increased blood pressure, we used 7-9 week old *ALMS1* KO rats and WT littermates fed on a normal salt diet (0.22% Na) to measure systolic blood pressure by tail cuff plethysmography. We observed that *ALMS1* KO rats have a higher systolic blood pressure and were hypertensive (*ALMS1* KO: 147 ± 3 mmHg *vs*. WT: 135 ± 3.5 mmHg, n = 5, * $p < 0.05$; Figure 27A). Mean arterial pressure (MAP) measured by intra-arterial catheter in anesthetized rats was also found to be higher in *ALMS1* KO rats (*ALMS1* KO: 141 ± 5 mmHg *vs*. WT: 99 ± 6 mmHg, n = 5, * $p < 0.005$; Figure 27B).

To test our hypothesis that genetic deletion of *ALMS1* in rats induces salt sensitivity, we used 8-10 week old *ALMS1* KO rats and WT littermates to measure systolic blood pressure by tail cuff plethysmography in response to increasing salt

(0.4%) in their drinking water after measuring baseline blood pressures as mentioned above. We found that upon the salt challenge, the systolic blood pressure increased significantly higher in *ALMS1* KO rats compared to their WT littermates (ΔSBP *ALMS1* KO: 17 ± 4 mmHg *vs*. ΔSBP WT: 5.1 ± 4.1 mmHg, n = 5, $ p < 0.05; Figure 27A).

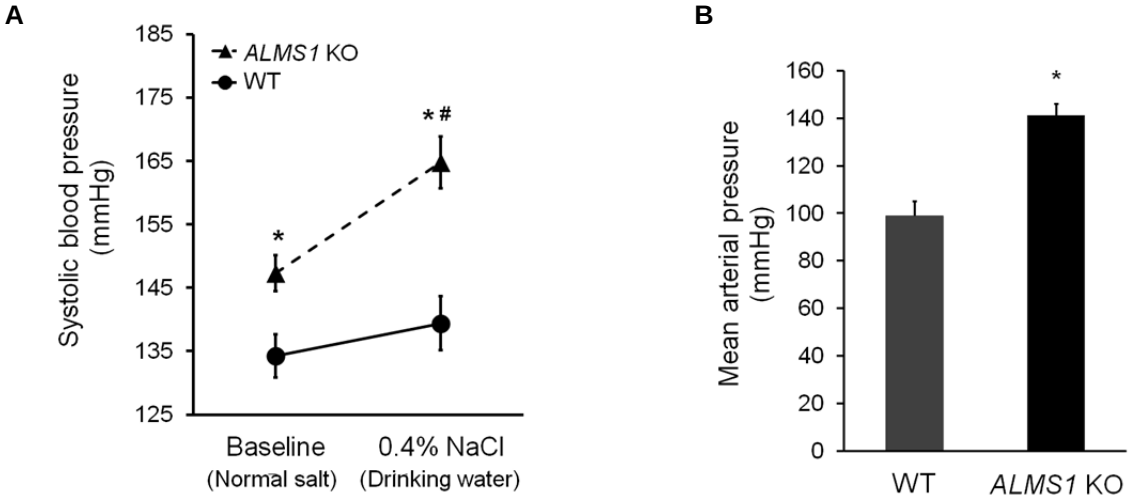

Figure 27: *ALMS1* KO rats are hypertensive and salt sensitive. A) Baseline systolic blood pressure measured on 0.22% salt diet. The rats were then challenged with additional 0.4% NaCl in their drinking water to measure salt sensitivity, n = 5, * p < 0.05 *vs*. WT and # p < 0.01 *vs*. baseline. B) Mean arterial pressure was measured by intra-arterial catheter, n = 5, * p < 0.005 *vs*. WT.

ALMS1 KO rats have lower plasma renin activity

To test whether renin-angiotensin system contributes to the hypertension observed in *ALMS1* KO rats, we measured plasma renin activity (PRA) in *ALMS1* KO rats and we found that PRA was significantly lower in *ALMS1* KO rats compared to WT rats (*ALMS1* KO: 1.28 ± 0.32 ng Ang I/ml/hr, n = 5 *vs*. WT: 2. ± 0.28 ng Ang I/ml/hr, n = 6, * p < 0.05; Figure 28) indicating that hypertension and salt sensitivity in *ALMS1* KO rats is independent of the renin-angiotensin system.

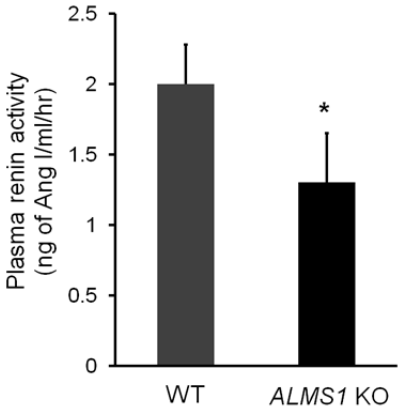

Figure 28: *ALMS1* KO rats have low plasma renin activity. *ALMS1* KO: n = 5, WT: n = 6, * p < 0.05 *vs*. WT.

ALMS1 KO rats have higher NKCC2 activity measured in vivo

To test our hypothesis that deletion of *ALMS1* increases blood pressure due to enhanced NaCl reabsorption in the TAL, we measured NKCC2-mediated NaCl transport *in vivo*. We housed the animals in metabolic cages and collected 24 hour urine. At baseline, we found that the urine volume collected was not significantly different between the groups (*ALMS1* KO: 9.2 ± 0.7 ml/24 hr, n = 5 *vs*. WT: 10 ± 0.8 ml/24 hr, n = 4, ns; Figure 29A). However, the urine osmolality (*ALMS1* KO: 2560 ± 63.4 mOsm/kg water, n = 5 *vs*. WT: 1724 ± 73.1 mOsm/kg water, n = 3, * p < 0.005; Figure 29B) was significantly higher in *ALMS1* KO rats indicating higher urine concentrating capacity which is associated with a higher NKCC2-mediated NaCl reabsorption *via* the generation of high medullary interstitial osmolarity [23]. To measure NKCC2-mediated NaCl reabsorption *in vivo*, we measured acute diuretic and natriuretic effect of NKCC2 inhibitor bumetanide.

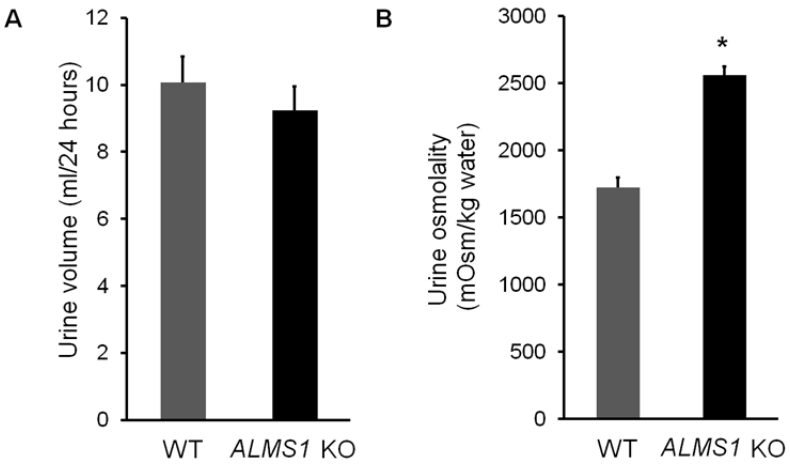

Figure 29: *ALMS1* KO rats have better urine concentrating capacity. A) Urine volume and B) Urine osmolality measured in *ALMS1* KO rats, * p < 0.005 *vs*. WT.

We found that urine flow rate (*ALMS1* KO: 3.1 ± 0.32 ml/8 hours, n = 5 *vs*. WT: 1.6 ± 0.13 ml/8 hours, n = 4, * p < 0.025) and urinary sodium excretion rate (*ALMS1* KO: 485.2 ± 37.1 µmoles/8 hours, n = 5 *vs*. WT: 221.8 ± 32 µmoles/8 hours, n = 4, * p <

0.025) until 8 hours after bumetanide treatment was significantly higher in *ALMS1* KO rats compared to WT rats, indicative of a higher NKCC2 activity in *ALMS1* KO rats (Figure 30A, 30B).

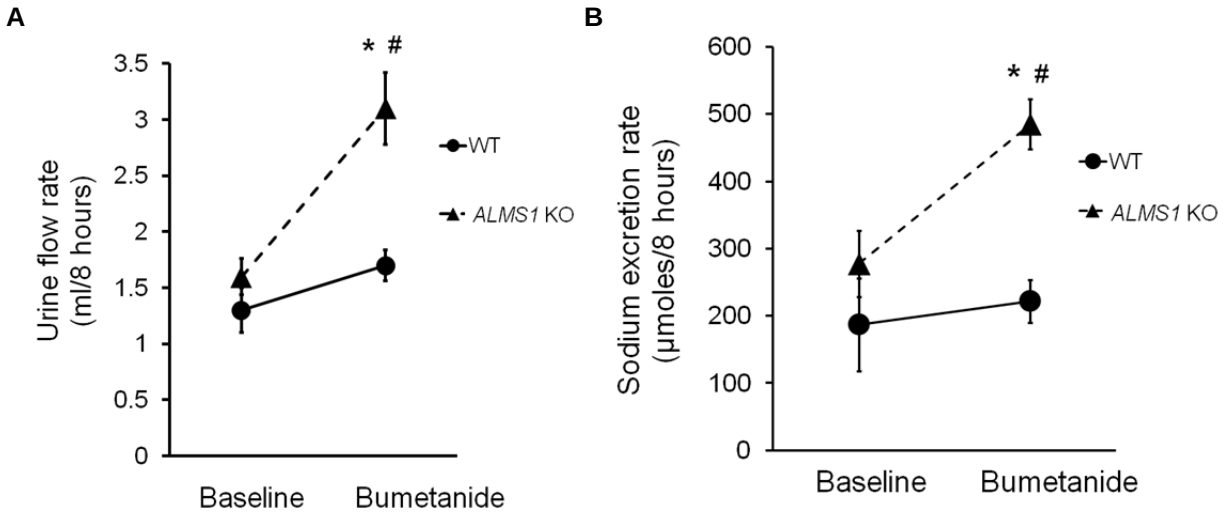

Figure 30: *ALMS1* KO rats have higher bumetanide-induced diuresis and natriuresis. A) Urine flow rate and B) Urinary sodium excretion rate measured until 8 hours after (sub-maximal dose) of 5 mg/ml bumetanide, *ALMS1* KO: n = 5, WT: n = 4, * $p < 0.025$ *vs*. WT, # $p < 0.025$ *vs*. baseline.

We then tested whether higher NKCC2-mediated NaCl reabsorption in the TAL is associated with a decreased ability to excrete a saline/water load. For this, we anesthetized and instrumented rats and performed 3% volume expansion (VE) with respect to their body weight. We collected urine at every 30 min intervals and found that the cumulative urine volume (*ALMS1* KO: 0.7 ± 0.24 ml, n = 8 *vs*. WT: 1.77 ± 0.4 ml, n = 6, * $p < 0.05$) and urinary sodium excretion (*ALMS1* KO: 72.5 ± 37.9 µmoles, n = 8 *vs*. WT: 278.4 ± 64.5 µmoles, n = 6, * $p < 0.05$) after 3% VE (60 to 210 min; corrected to their respective baselines) indicated by shaded regions was significantly lower in *ALMS1* KO rats (Figure 31 A, B).

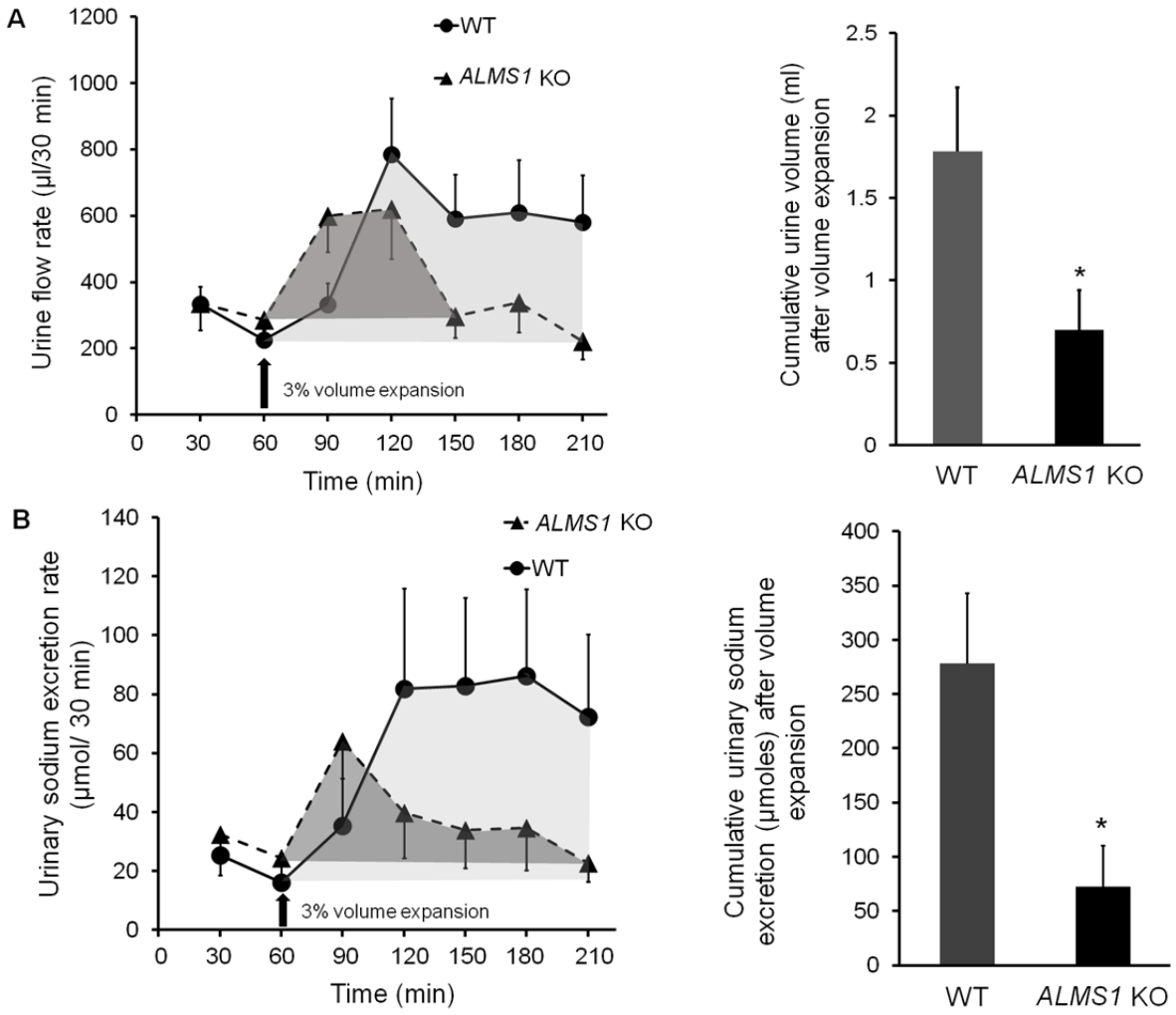

Figure 31: *ALMS1* KO rats have reduced capacity to eliminate volume/salt load. Cumulative A) urine volume B) urinary sodium excreted upon 3% volume expansion, *ALMS1* KO: n = 8, WT: n = 6 * $p < 0.05$.

Conclusion

We show that deletion of *ALMS1* causes higher urine concentrating capacity in rats and higher bumetanide induced diuresis and natriuresis. The excretory capacity upon challenge with salt and water load decreased in *ALMS1* KO rats. We observed that deletion of *ALMS1* in rats increased systolic and mean blood pressure and hypertension develops independent of renin-angiotensin system. Taken together, these data indicate that *ALMS1* KO rats have a higher NKCC2-mediated Na+ absorption and thus a decreased ability to excrete a salt and volume load. These may be in part

responsible for hypertension observed in these rats. The significance and in depth interpretation of these observations will be addressed in Chapter 5.

CHAPTER 4 - ALMS1 IS IMPORTANT FOR MAINTAINING METABOLIC FUNCTION IN RATS

Introduction

In humans, mutations in the *ALMS1* gene causes Alström syndrome which is characterized by obesity, type-2 diabetes in addition to hypertension [50-53]. *ALMS1* transgenic mice model recapitulated age-dependent metabolic syndrome as observed in humans and also exhibited sex-based differences in the development of metabolic syndrome [67,69]. In this chapter we characterized sex-based differences in *ALMS1* KO rats for their metabolic function.

Aim 5: Hypothesis: Deletion of *ALMS1* causes age-dependent metabolic syndrome in rats

Rationale

Mice with *ALMS1* mutations are characterized with sex differences in the development of age dependent metabolic syndrome. In this aim we tested whether *ALMS1* KO rats recapitulated metabolic syndrome as observed in humans and mice with mutation in the *ALMS1* gene.

Results

6-12 week old ALMS1 KO rats do not develop metabolic syndrome

Table 1 clearly shows that 6-12 week old *ALMS1* KO rats have normal plasma leptin, plasma insulin, random blood glucose but only a slightly elevated body weight. This indicates that young *ALMS1* KO rats do not develop metabolic syndrome as indicated previously in *ALMS1* transgenic mice models. Therefore we tested whether 16-18 week old *ALMS1* KO rats develop metabolic syndrome.

Old ALMS1 KO rats develop obesity as they age

We then tested whether older *ALMS1* KO rats are obese. We measured their

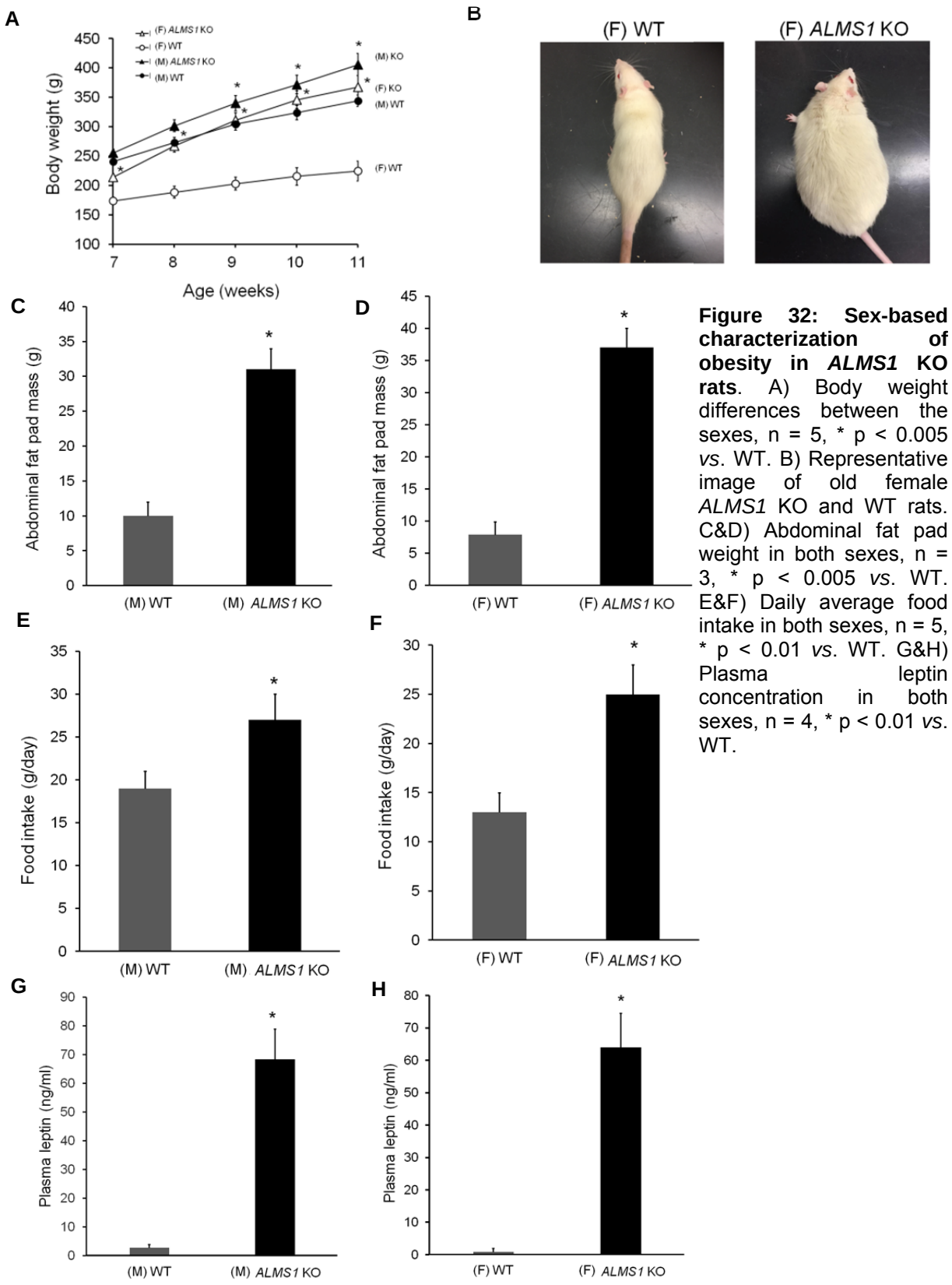

Figure 32: Sex-based characterization of obesity in *ALMS1* KO rats. A) Body weight differences between the sexes, n = 5, * $p < 0.005$ *vs*. WT. B) Representative image of old female *ALMS1* KO and WT rats. C&D) Abdominal fat pad weight in both sexes, n = 3, * $p < 0.005$ *vs*. WT. E&F) Daily average food intake in both sexes, n = 5, * $p < 0.01$ *vs*. WT. G&H) Plasma leptin concentration in both sexes, n = 4, * $p < 0.01$ *vs*. WT.

body weights and found that both male and female *ALMS1* KO rats have a significantly higher body weight compared to their wild type littermates starting at age week 9 in males and week 7 in females (Figure 32A). In 16-18 week old *ALMS1* rats, we measured abdominal fat mass and found that it was higher in both male (*ALMS1* KO: 30.9 ± 3.4 g *vs*. WT: 10.1 ± 2.5 g, n = 3, * $p < 0.005$) and female *ALMS1* KO rats (*ALMS1* KO: 36.9 ± 3.7 g *vs*. WT: 7.9 ± 1.8 g, n = 3, * $p < 0.005$) compared to their wild type littermates (Figure 32 C&D) and appeared obese at 16 weeks of age (representative image of female rats; Figure 32B). We then measured food intake in 16-18 week old *ALMS1* KO rats and found that both male (*ALMS1* KO: 26.9 ± 3.1 g/day *vs*. WT: 19 ± 2.5 g/day, n = 5, * $p < 0.01$) and female *ALMS1* KO rats (*ALMS1* KO: 25.1 ± 2.5 g/day *vs*. WT: 12.9 ± 0.95 g/day, n = 5, * $p < 0.01$) are hyperphagic (Figure 32 E&F), a potential cause for their obesity. We then measured plasma leptin levels in 16-18 week old *ALMS1* KO and found that both male (*ALMS1* KO: 68.3 ± 10.5 ng/ml *vs*. WT: 2.75 ± 1.1 ng/ml, n = 4, * $p < 0.01$) and female *ALMS1* KO rats (ALMS1 KO: 64.1 ± 15.9 ng/ml *vs*. WT: 0.9 ± 0.3 ng/ml, n = 4, * $p < 0.01$) were hyperleptinemic (Figure 32 G&H). These data indicate that older *ALMS1* KO rats may have a deficient leptin signaling leading to its decreased ability to suppress their food intake, indicative of leptin resistance.

Old ALMS1 KO rats exhibit hypertriglyceridemia

We measured plasma lipid profile and we found that only triglyceride levels were significantly elevated in both male (*ALMS1* KO: 633.4 ± 221.2 mg/dl, n = 7 *vs*. WT: 109.4 ± 16.2 mg/dl, n = 4, * $p < 0.01$) and female *ALMS1* KO rats (*ALMS1* KO: 595.9 ± 200.1 mg/dl, n = 7 *vs*. WT: 55.6 ± 12.5 mg/dl, n = 4, * $p < 0.05$). Significant differences

were observed in serum cholesterol (*ALMS1* KO: 151.9 ± 37.8 mg/dl, n = 7 *vs*. WT: 81.9 ± 4.9 mg/dl, n = 4, * p < 0.05) high density lipoprotein (*ALMS1* KO: 41.9 ± 7.9 mg/dl, n = 7 *vs*. WT: 67.8 ± 2.2 mg/dl, n = 4, * p < 0.05) low density lipoprotein levels (*ALMS1* KO: 32.2 ± 6.4 mg/dl, n = 7 *vs*. WT: 15 ± 1.4 mg/dl, n = 4, * p < 0.05) only in female *ALMS1* KO rats but were not different in male *ALMS1* KO rats (Figure 33 A&B).

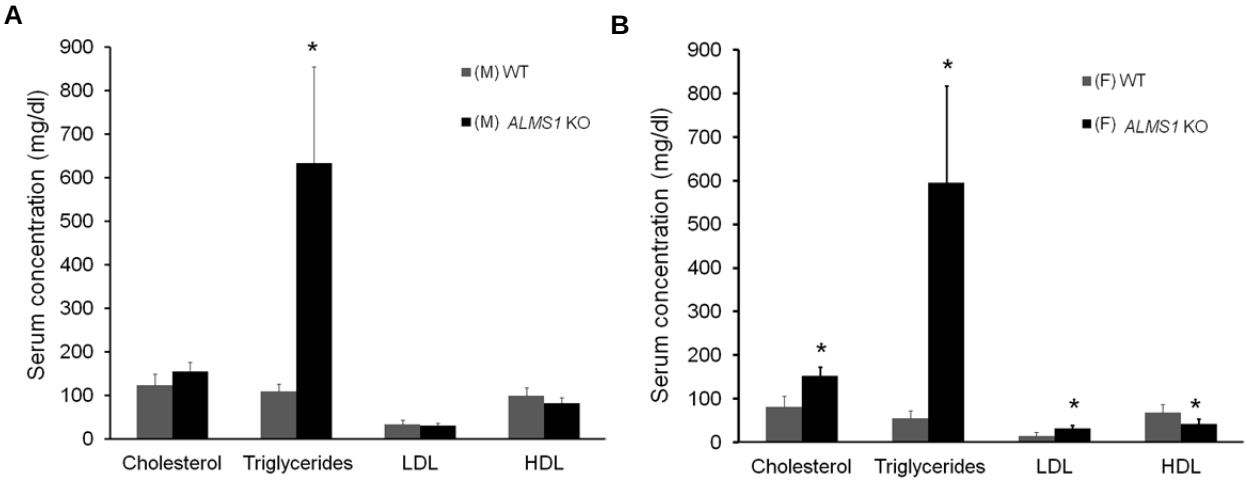

Figure 33: Sex-based differences in serum lipid profiling in *ALMS1* KO rats. A) Males *ALMS1* KO: n = 7, WT: n = 4, * p < 0.01 *vs*. WT and B) Females *ALMS1* KO: n = 7, WT: n = 4, * p < 0.05 *vs*. WT.

Old ALMS1 KO rats are hyperinsulinemic

We tested whether *ALMS1* KO rat model reproduced metabolic dysfunction as seen in the *ALMS1* mutant mice model. We measured random blood glucose by tail snips and we found that it was not different between the groups in either males (*ALMS1* KO: 134.5 ± 9.4 mg/dl *vs*. WT: 132.3 ± 9.9 mg/dl, n = 3) or females (*ALMS1* KO: 126 ± 3.8 mg/dl *vs*. WT: 130.3 ± 3.4 mg/dl, n =3) (Figure 34 A&B). However, the fasting blood glucose was measured to be significantly higher in both male (*ALMS1* KO: 108 ± 4 mg/dl *vs*. WT: 61 ± 17 mg/dl, n = 3, * p < 0.05) and female (*ALMS1* KO: 100 ± 13 mg/dl *vs*. WT: 71 ± 6 mg/dl, n = 3, * p < 0.05) rat groups (Figure 34 C&D). Plasma insulin was measured to be significantly higher in both males (*ALMS1* KO: 8.1 ± 4.3 ng/ml, n = 5 *vs*. WT: 1.38 ± 0.73 ng/ml, n = 3, * p < 0.05) and females (*ALMS1* KO: 8.5 ± 1.9 ng/ml, n =

9 *vs*. WT: 0.93 ± 0.2 ng/ml, n = 6, * p < 0.05) (Figure 34 E&F) indicating *ALMS1* KO rats are hyperinsulinemic.

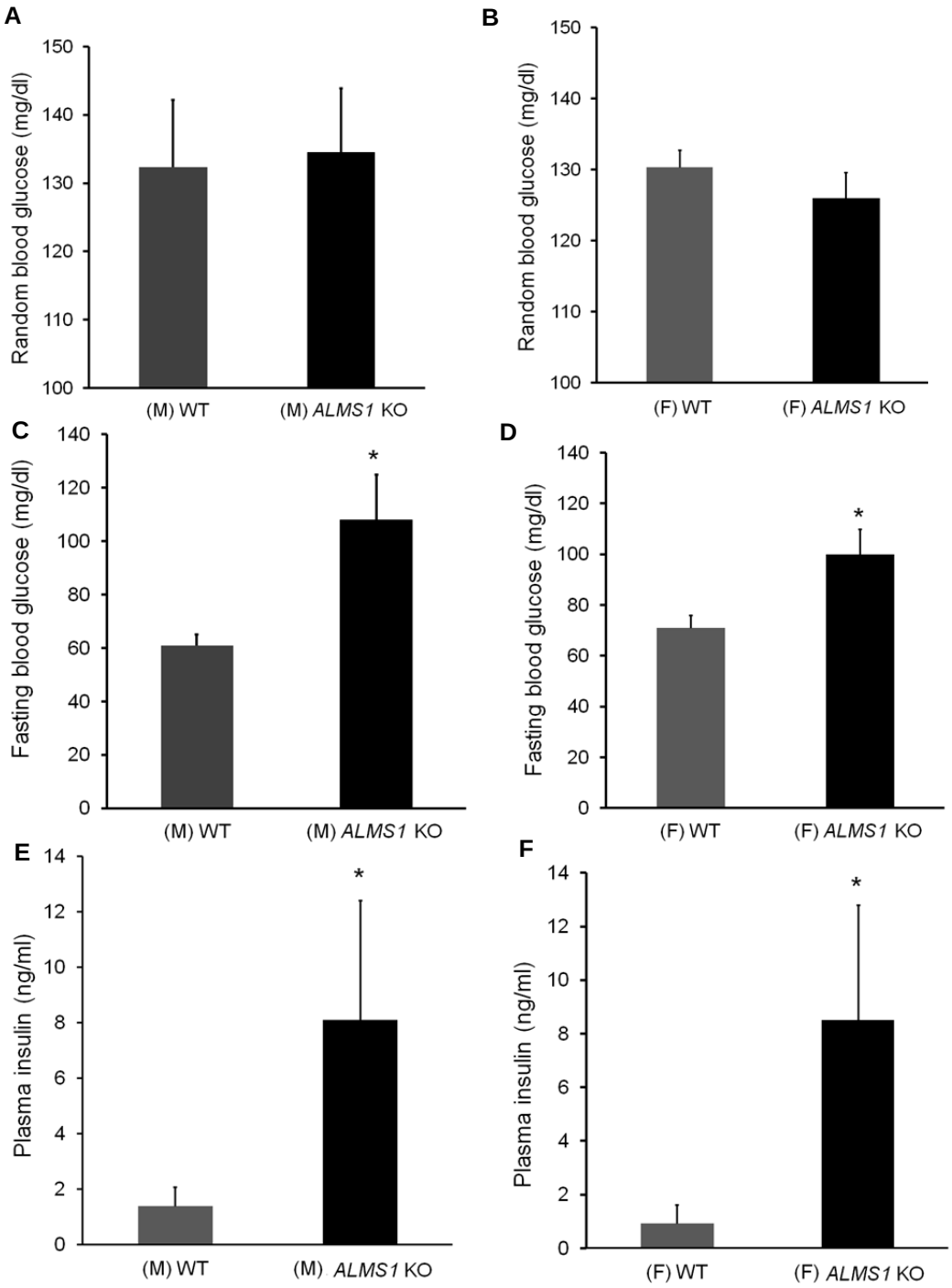

Figure 34: Sex-based characterization of metabolic parameters in *ALMS1* KO rats. A&B) Random blood glucose in both the sexes, n = 3, C&D) Fasted-blood glucose in both sexes, n = 3, * p < 0.05 and E&F) Plasma insulin in both sexes, male *ALMS1* KO: n = 5 & WT: n = 3, female *ALMS1* KO: n = 9 & WT: n = 6, * p < 0.05 *vs*. WT.

Together, these data indicate that both male and female *ALMS1* KO rats may have a deficient insulin signaling leading to its decreased ability to lower fasting blood glucose, indicative of insulin resistance.

Old ALMS1 KO rats are hypertensive

To test whether obese *ALMS1* KO rats are hypertensive, we measured their systolic blood pressure by tail cuff plethysmography and found that both male (*ALMS1* KO: 151 ± 5.1 mmHg *vs*. WT: 125 ± 4.2 mmHg, n = 6, * p < 0.05) and female (*ALMS1* KO: 199 ± 7.1 mmHg *vs*. WT: 134 ± 3.3 mmHg, n = 6, * p < 0.0001) *ALMS1* KO rats are hypertensive (Figure 35A). Systolic blood pressure in female *ALMS1* KO rats was higher than that of their male counterparts (Female *ALMS1* KO: 199 ± 7.1 mmHg *vs*. male *ALMS1* KO: 151 ± 5.1 mmHg, n = 6, $ p < 0.0001) (Figure 35B).

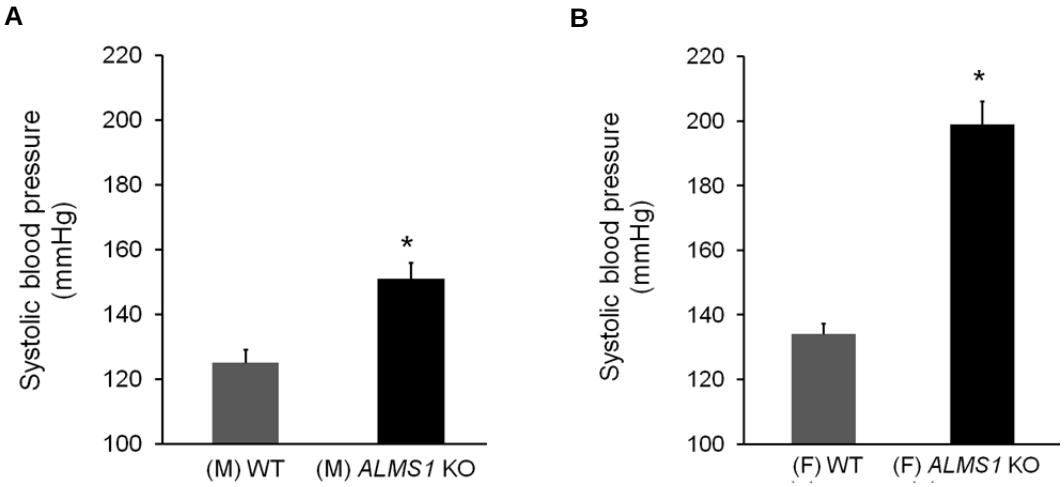

Figure 35: Systolic blood pressure measurement in both sexes of *ALMS1* KO rats.
A) N = 6, * p < 0.05 *vs*. WT. B) N = 6, * p < 0.0001 *vs*. WT

Conclusion

We showed that old male *ALMS1* KO rats are hyperinsulinemic, obese, hyperphagic, hypertriglyceridemic and hyperleptinemic. Insulin and leptin resistance may develop secondarily to obesity since younger non-obese *ALMS1* KO rats are

neither hyperinsulinemic nor hyperleptinemic. We also show that obese *ALMS1* KO rats have a higher systolic blood pressure. Female *ALMS1* KO exhibit all the above phenotypes in addition to having high serum cholesterol, LDL, low HDH levels and higher systolic blood pressure. The significance and in depth interpretation of all these observations will be addressed in the discussion in Chapter 5.

CHAPTER 5 - CONCLUDING REMARKS

Summary of results

In this study we have shown that:

1. TIRF microscopy allows imaging of NKCC2 specific labeled molecules in TAL cells.
2. TIRF microscopy allows real-time monitoring of NKCC2 endocytosis in TAL cells.
3. ALMS1 is expressed apically and sub-apically in the TAL.
4. Carboxyl-terminus NKCC2 domain known to determine its apical targeting interacts with ALMS1.
5. Carboxyl-terminus ALMS1 interacts with NKCC2.
6. ALMS1 and NKCC2 co-localize in kidney sections and in rat TAL.
7. ALMS1 expression is required to maintain normal systolic and mean arterial pressure in rats.
8. ALMS1 expression is required for normal NKCC2-mediated NaCl reabsorption in the rat TAL.
9. ALMS1 expression is required for effective elimination of water/salt load by rats.
10. ALMS1 maintains normal NKCC2 surface expression in rat TAL.
11. ALMS1 stimulates NKCC2 endocytosis in the rat TAL.
12. ALMS1 is required to maintain normal metabolic function in rats.
13. Deletion of *ALMS1* in female rats causes more severe phenotype in terms of lipid profiles, obesity and hypertension.

Discussion

Importance of studying NKCC2 endocytosis

NKCC2 mediates NaCl reabsorption in the thick ascending limb of the loop of Henle [30,31]. NKCC2 activity is shown to be enhanced in salt sensitive hypertension [25-31]. NKCC2 activity is regulated by 1) phosphorylation at threonine (96/101) by STE20- and SPS1-related proline and alanine-rich kinases (SPAK) and oxidative stress-

responsive kinase 1 (OSR1) [49,96-98] and at Ser(126) site by PKA [99], 2) protein-protein interactions [49,100-102] and 3) protein trafficking [37,38]. While the regulation of NKCC2 *via* phosphorylation has been well studied, very little is known about mechanisms and protein-protein interactions which regulate NKCC2 apical trafficking. NKCC2 surface abundance is maintained by a balance between NKCC2 exocytosis, recycling and NKCC2 internalization [36-38]. Our lab has previously shown that constitutive NKCC2 endocytosis is important to maintain baseline NaCl absorption by the TAL because inhibition of endocytosis increased surface NKCC2 abundance and increased chloride absorption by TAL [37,38]. This highlights the importance of understanding the machinery that regulates NKCC2 internalization from the apical membrane in TALs. However, currently available techniques to study NKCC2 endocytosis are unsuccessful in providing time resolution of the dynamic process achieved by live cell imaging. TIRF microscopy is employed for real time visualization of dynamics of molecules at or near the cell surface in real time. This method has yielded detailed dynamic information about clathrin-coated vesicle trafficking at the plasma membrane [41-46].

Traditional surface biotinylation technique which is currently used to study NKCC2 endocytosis has numerous limitations. It uses NHS-SS-biotin that reacts and biotinylates accessible lysine residues in all surface proteins. Thus, it does not differentiate NKCC2 from other surface proteins in the TIRF field. Therefore, we engineered NKCC2-BAD construct which provides the advantage of selective NKCC2 biotinylation by BirA to study real time NKCC2 endocytic events at the plasma membrane of polarized MDCK cells and TALs by TIRF microscopy.

Monitoring real-time NKCC2 endocytosis by TIRF microscopy

To perform live cell imaging for obtaining the rate of NKCC2 endocytosis, the apical surface of MDCK cells and rat TAL primary cells were imaged every second over 20 minutes at 37ºC. On the TIRF field, NKCC2 distribution was observed to be heterogeneous and individual fluorescent entities were observed, referred to as puncta. These puncta on the TIRF field appeared to be clustered and exhibited exponential decrease in intensity within about 1-2 seconds which lead to a progressive decrease in the number of total surface puncta at a rate analogous to constitutive NKCC2 endocytosis as previously measured in TALs [37,38]. The exponential decrease in intensity was confirmed to be due to the internalization of NKCC2 by pre-treating the cells with MβCD that is known to block endocytosis [37,38]. MβCD was previously shown to block NKCC2 endocytosis by depleting membrane cholesterol and not by other mechanisms [37,38]. In contrast, our lab showed that MβCD blocks clathrin-, and lipid raft-mediated endocytosis in thick ascending limbs [38]. Upon pre-treatment with MβCD, we observed that the number of initial puncta remained unchanged over time. This suggested that TIRF microscopy of labeled NKCC2 allows imaging of single endocytic events with a time resolution of 1-2 seconds.

Choice of fluorescent dyes for monitoring real time NKCC2 endocytosis by TIRF microscopy

Imaging during 20 minutes prevents photobleaching of Alexa Fluor dyes during the prolonged duration of image acquisition. It has been reported that a resolution time shorter than 1-2 seconds is possible with usage of fluorescent Quantum Dots because they are brighter and more photo-stable. However, Quantum Dots exhibit fluorescent intermittency or blinking. This is a discontinuous and random emission of light from

fluorescent sources due to random switching between bright fluorescent and non-emissive periods [103]. We observed this phenomenon when using streptavidin-Quantum Dots and due to this phenomenon of blinking, disappearance of fluorescence can be mistaken for an endocytic event. Thus, we used Alexa Fluor dyes covalently linked to streptavidin instead to overcome blinking. However very recently, non-blinking Quantum Dots have been developed to overcome this disadvantage and provide higher quantum yield compared to Alexa Fluor [104,105].

NKCC2 oligomerization

On the TIRF field, we observed that NKCC2 puncta are heterogeneously distributed in the apical surface highly confined to clusters or discrete domains which may suggest homo-oligomerization of NKCC2 [106]. A similar distribution pattern was observed by confocal imaging of TAL cells after labeling apical surface NKCC2 [88]. However, the usage of tetravalent streptavidin-conjugated dyes possibly lead to multimerization of the mono-biotinylated NKCC2-BAD molecules and may be a potential cause of such a heterogenous pattern [41]. Nonetheless, the rate of endocytosis in rat TAL cells by TIRF microscopy was calculated to be 1.09 ± 0.08 % per minute, consistent with that calculated by surface biotinylation methods in native TAL using NHS-SS-biotin [37]. Therefore, it is possible that clustering of NKCC2 may be due to targeting of the co-transporter to specialized membrane domains for efficient and concerted activity as reported for other co-transporters [107-110] and not an artifact due to the method used. Exogenous over-expression seems to be a valid concern since it may cause aggregation of the expressed protein. For this, we measured its impact on rate of NKCC2 endocytosis by changing the concentration of the virus used for

transduction and found no significant effect (data not shown). This suggested that over-expression does not affect NKCC2 endocytosis. While the reason for clustering of surface NKCC2 is unclear, our data clearly point that labeling with tetravalent-streptavidin did not affect the rate of NKCC2 endocytosis in MDCK or TAL cells. Thus, we conclude that site-specific biotinylation allows for specific labeling of NKCC2 at the cell surface to visualize its real-time endocytosis in live cells by TIRF microscopy of apical membranes in polarized MDCK and TAL cells.

Potential application of TIRF microscopy in studying dynamics of NKCC2 endocytosis

Real time imaging by confocal or TIRF microscopy has been very useful in studying how protein-protein interactions [48,111-113], protein motifs/domains [114] and signaling pathways [115,116] regulate trafficking of membrane transporters. Application of novel single molecule tagging technologies coupled with real time tracking has provided information on apical targeting of receptors to highly specialized membrane domains, which can lead to clustering for efficient signal transduction [105,108-110] following stimulation by ligands [117]. Therefore, these potential applications of this method can be used with respect to studying dynamics of NKCC2 endocytosis in further detail and can be extended to other trans-membrane proteins.

Discovering novel proteins involved in NKCC2 endocytosis

Despite the availability of novel technologies and the importance of studying NKCC2 endocytosis, not much is known about the protein-protein interactions that are involved in this process. So far only one protein MALVIP/17 has been characterized and shown to regulate NKCC2 internalization [49] by interacting with a 71 amino acid stretch of carboxyl-terminus domain of NKCC2 (C2-NKCC2). In order to discover new

proteins that may play a role in NKCC2 internalization, we followed a targeted proteomics approach and identified ALMS1 as an interacting partner of C2-NKCC2. The genetic association of obesity, salt-sensitive hypertension with *ALMS1* [50-53,56-61], its cellular role in trafficking of membrane protein [69] and its interaction with proteins in the endocytic pathway [66] is well described. Therefore, we hypothesized that ALMS1 interacts with NKCC2 and stimulates its endocytosis to maintain NKCC2 surface expression and NKCC2-mediated NaCl reabsorption and therefore maintain normal blood pressure.

ALMS1 interacts with NKCC2 and forms a network with endocytic proteins

ALMS1 is involved in trafficking of membrane transporters such as GLUT4. Although it is unclear whether ALMS1 regulates insulin stimulated GLUT4 endocytosis or recycling [69], the carboxyl terminus of ALMS1 interacts with proteins that form the endocytic machinery (α-actinin 4, Myosin Vb, RINT1 etc.) [66,70-73]. C2-NKCC2 is a 71 amino acid domain in carboxyl-terminus of NKCC2 which is shown to be important for apical targeting of NKCC2 [81]. Liquid chromatography and mass spectrometric analysis of C2-NKCC2 interactome revealed the presence of unique peptides corresponding to ALMS1. We found that ALMS1 is expressed along the nephron but appears to be enriched in the TAL where it interacts with the carboxyl terminus of the apical $Na^+/K^+/2Cl^-$ co-transporter, NKCC2. We found that ALMS1 co-localizes with NKCC2 in sub-apical regions of TAL while Ingenuity pathway network analysis of C-ALMS1 and C2-NKCC2 interacting proteins show that ALMS1 may form a network with RABEP1 and other Ras-related proteins (RAB5A, RAB22A; data not shown) in the TAL and thus may be involved in the early endocytic pathway of NKCC2 [118,119]. We

propose that ALMS1 may act as a scaffolding protein to recruit proteins involved in NKCC2 early endocytic pathway. It is important to note that ALMS1 may not directly interact with NKCC2 but form a complex network with other endocytic proteins, pulled down with C-ALMS1 (Table 2).

Table 2: C-ALMS1 interacting proteins and their role in the regulation of endocytosis

C-ALMS1 interacting proteins	Role in regulating endocytosis
RAC1: Ras-related C3 botulinum toxin substrate 1	See Ref (160)
FLOT 1: Flotillin 1	See Ref (161)
FLOT 2: Flotillin 2	See Ref (162)
ANXA 2: Annexin A2	See Ref (163)
ANXA 1: Annexin A1	See Ref (164)
PICALM: Phosphatidyl inositol binding clathrin assembly protein	See Ref (165)
ARPC5L: Actin related protein 2/3 complex, subunit 5-like	See Ref (166)
RALA: Ras like proto-oncogene A	See Ref (167)
ARF 1: ADP ribosylation factor 1	See Ref (168)
ILK: Integrin linked kinase	See Ref (169)
PHB: Prohibitin	See Ref (170)
ACTN 4: α-actinin 4	See Ref (171)
MYO5B: Myosin 5b	See Ref (172)

NKCC2 is known to undergo endocytosis in a clathrin and lipid-raft dependent manner to maintain NKCC2 surface levels [38]. In this study, we show that ALMS1 mediates NKCC2 endocytosis and also identified some proteins that may form NKCC2 endocytic protein network. With carboxyl-terminus of ALMS1 (C-ALMS1), we pulled down flotillin-2 (FLOT2) which is a lipid raft marker protein. We also pulled down Annexin A2 (ANXA2) which has been shown to be important for lipid raft-associated

apical trafficking of NKCC2 [120]. This suggested that ALMS1 may be involved in lipid raft-dependent NKCC2 endocytosis. We also pulled down phosphatidylinositol binding clathrin assembly protein (PICALM) with C-ALMS1, which has been shown to mediate clathrin-dependent endocytosis and targeting of clathrin-coated vesicles to early and late endosomes of other proteins [121]. This suggests the role of ALMS1 as a common scaffold to recruit various proteins involved in determining lipid raft and/or clathrin dependent NKCC2 endocytosis. While this question remains to be answered, ingenuity pathway network analysis of C-ALMS1 interacting proteins, suggest a role for ALMS1 in mediating membrane protein endocytosis.

ALMS1 stimulates NKCC2 endocytosis, a mechanism to maintain NKCC2 surface levels in the TAL

In this study, we show that ALMS1 interacts with C2-NKCC2 and stimulates NKCC2 internalization in the TAL such that genetic deletion of *ALMS1* decreases NKCC2 internalization only after 20 min of warming TALs at 37ºC to facilitate constitutive NKCC2 endocytosis but not at 10 min time point. Since NKCC2 is known to undergo endocytosis *via* clathrin-dependent and lipid-raft dependent pathways [38], it is possible that these pathways differentially participate at distinct time points during constitutive NKCC2 internalization in TALs. While it is still debatable as to which one of these pathways does ALMS1 play a role in, inhibition of ALMS1 expression may significantly retard either one of these pathways that appears to be active during the latter 10 minutes. This may result in a significant difference in NKCC2 internalization in TALs from WT and *ALMS1* KO rats only after 20 minutes of allowing NKCC2 endocytosis. In addition, we demonstrated that a decrease in NKCC2 endocytosis correlated with higher surface NKCC2 in TALs from *ALMS1* KO rats.

A previous study had shown that another protein MAL/VIP17 interacts with this domain in NKCC2 in LLC-PK1 cell lines and decreases NKCC2 internalization *via* NKCC2 retention at the surface. This suggests that C2-NKCC2 may be an important regulatory domain involved in modulating NKCC2 surface expression mediated *via* specific protein-protein interactions. *MAL/VIP17*-overexpressing transgenic mice presented only with an increase in NKCC2 phosphorylation and NKCC2 glycosylation indicative of stable surface expression. This observation was not accompanied by any report on renal ion transport phenotype in these mice [49]. In the present study, we show that deletion of NKCC2 interacting protein *ALMS1* in rats presents with high NKCC2 surface expression accompanied with a phenotype related to higher renal tubular Na^+ reabsorption. Since NKCC2 activity is also known to be stimulated by phosphorylation [29], we measured this using specific antibodies against pThr(96,101) or pSer(126) NKCC2 and found no difference in NKCC2 phosphorylation between the groups. This shows that ALMS1 is not involved in regulating NKCC2 phosphorylation but primarily involved in regulating NKCC2 endocytosis.

ALMS1 regulates NKCC2-mediated NaCl reabsorption and therefore blood pressure

The thick ascending limb (TAL) of the loop of Henle plays an important role in maintenance of NaCl homeostasis and blood pressure regulation [30,31]. NaCl reabsorption by this nephron segment is dependent on the apical $Na^+/K^+/2Cl^-$ co-transporter NKCC2. In spontaneously hypertensive rats, progression from pre-hypertensive to hypertensive state is accompanied by an increased surface NKCC2 expression compared with control rats [122]. Dahl salt-sensitive rats exhibited higher surface NKCC2 expression and NKCC2 activity in TALs compared to Dahl salt-resistant

rats [123]. This indicates that a higher NaCl reabsorption in the TAL is associated with elevated arterial pressure and salt sensitivity. Our data suggest that knockout of *ALMS1* in rats leads to elevated blood pressure and salt sensitivity possibly *via* this mechanism since diuretic and natriuretic response to bumetanide was increased in *ALMS1* KO rats. Bumetanide inhibits NKCC2 activity which leads to a decreased interstitial osmolarity and thus decreased water reabsorption in the collecting duct [124]. A sub-maximal dose of bumetanide (5 mg/kg) was used to detect subtle differences in bumetanide sensitivity between the groups. Increased urinary concentrating ability of *ALMS1* KO rats may be in part due to higher NKCC2-mediated NaCl reabsorption leading to increased medullary interstitial osmolarity and secondarily causing enhanced water reabsorption in the cortical collecting duct *via* aquaporins. However, it is possible that ALMS1 may also be primarily involved in apical trafficking of aquaporins and thereby regulating water reabsorption in collecting duct principal cells. Together, these data indicate that a higher NKCC2-mediated NaCl reabsorption in the TAL contributes at least in part to the hypertension and salt-sensitivity in *ALMS1* KO rats. In addition, plasma renin activity (PRA) is lower in *ALMS1* KO rats despite the collection method used which has been reported to cause abnormal increase in PRA by anesthesia or by renal baroreflex [125], suggesting that hypertension is independent of renin-angiotensin system. These data together suggest that salt sensitive hypertension in *ALMS1* KO rats is predominantly due to a higher renal tubular NaCl reabsorption which probably causes a rightward shift in the pressure natriuresis curve in order to maintain sodium balance [27,122,132].

It is worth nothing that baseline GFR in hypertensive *ALMS1* KO rats is similar to

WT rats however baseline renal blood flow (RBF) in *ALMS1* KO rats tended to be slightly lower although not significantly different from WT rats (*ALMS1* KO: 7.6 ± 0.65 ml/min/gkw, n = 5 *vs*. WT: 6.55 ± 0.63 ml/min/gkw, n = 6). This GFR auto-regulation as seen in other models [128-131] has been implicated to be predominantly due to enhanced myogenic response of preglomerular arterioles [126,127] and tubulo-glomerular feedback (TGF) [133-136]. We observed an increased renal vascular resistance (RVR) in *ALMS1* KO rats (*ALMS1* KO: 28.7 ± 2.3 mmHg/ml/min/gkw *vs*. WT: 16.5 ± 0.9 mmHg/ml/min/gkw, n = 5, * $p < 0.05$) and this may be a mechanism to protect the kidney from elevations in arterial pressures to be transmitted to the glomerular capillaries and cause injury. While the underlying mechanism of GFR autoregulation in *ALMS1* KO rats is unknown, understanding the contributing role of TGF is important. Decreased Cl^- delivery to the macula densa in *ALMS1* KO rats due to higher TAL NaCl reabsorption may tend to decrease TGF activity [133-136]. While increased NKCC2-mediated NaCl reabsorption at the macula densa in *ALMS1* KO rats may tend to increase TGF activity [133-136]. Thus, under mutually opposing conditions, examining baseline TGF responses in *ALMS1* KO rats may offer new insights into understanding its mechanism. Upon 3% volume expansion, GFR in WT rats increased whereas it remained relatively unchanged in *ALMS1* KO rats (data not shown). This may indicate TGF resetting in WT rats which seems to be absent in *ALMS1* KO rats to facilitate elimination of salt/water load [133-136]. This phenomenon of TGF resetting may in part explain faster volume/salt load excretion in WT rats compared to *ALMS1* KO rats.

Association of ALMS1 gene locus to renal function and hypertension

Single nucleotide polymorphisms in the *ALMS1* gene have been associated with

hypertension, pulse pressure and pulse rate in a multipoint linkage analysis in primary sibling samples of African American, Caucasian and Mexican populations [56]. Several quantitative trait loci for salt sensitivity are associated with the *ALMS1* gene locus [57-61]. Two independent GWAS [62,63] found genetic variants in *ALMS1* associated with kidney function and one study associated SNPs in the *ALMS1* locus to hypertension and increased pulse pressure [4]. The same GWAS [62] along with studies by other independent consortia [90-94] found susceptibility variants in uromodulin (*UMOD*, Tamm-Horsfall protein), a protein expressed in the TAL, to be associated with decreased renal function and hypertension. A functional link between NKCC2 and UMOD was established showing that UMOD plays a role in blood pressure regulation and salt sensitivity *via* regulating NKCC2 activity [95]. While the molecular function of UMOD has been well studied, it is not known whether ALMS1 and UMOD interact. We did not pull down UMOD with GST-C-ALMS1 A/B, suggesting that UMOD may interact with some other region of ALMS1 or may be independently linked to renal function through regulation of NKCC2 activity rather than interacting with each other. Nonetheless, mutations in *ALMS1*, similar to *UMOD* contribute to hypertension and may serve as a biomarker or a therapeutic target for lowering blood pressure and preserving renal function.

Hypertension is a complex polygenic disease in which multiple genes contribute to alter multiple organ function to elevate blood pressure. Our current understanding of the complex genetic architecture of hypertension relies heavily on the identification of mutations causing rare inherited disorders and of several susceptibility loci through population-based association studies. Such studies have allowed us to identify genetic

regions associated with hypertension, its complications like renal dysfunction, chronic kidney disease (CKD) [137,138] among others. Given the existing GWAS data linking SNPs in *ALMS1* with decreased renal function, and the severe phenotype observed in Alström syndrome patients [50-53], our data provides the first evidence that ALMS1 is involved in the regulation of renal sodium transport and therefore blood pressure regulation such that *ALMS1* KO rats are hypertensive and have decreased ability to excrete a volume load. The mechanism for this defect involves decreased NKCC2 endocytosis, which causes accumulation of NKCC2 at the apical surface and higher TAL NaCl transport. ALMS1 was not exclusively located in the TAL, suggesting that it may also regulate endocytosis of other renal sodium transporters. Our data is the first to suggest that enhanced tubular NaCl reabsorption and hypertension may be involved in progressively decreasing renal function in patients with decreased ALMS1 function/expression.

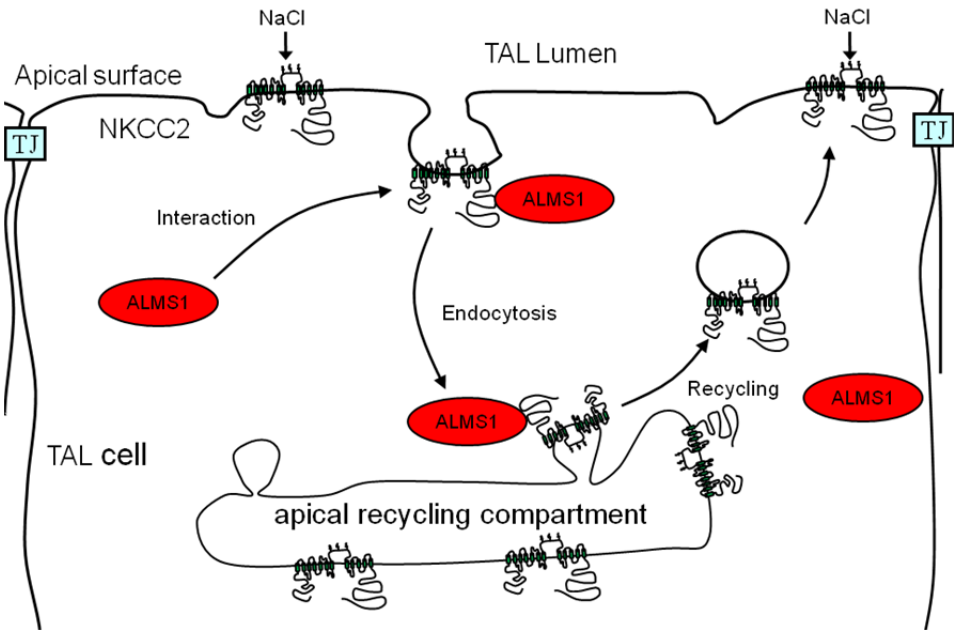

Figure 36: Working model for cellular role of ALMS1 in the regulation of NKCC2 endocytosis in the thick ascending limb.

Based on our observations, we propose the model depicted in Figure 36. ALMS1 interacts with NKCC2 in the sub-apical regions in the TAL and may be involved in its early endocytic pathway as a scaffold protein to recruit other endocytic proteins to facilitate NKCC2 endocytosis. Regulation of NKCC2 endocytosis is important for maintaining normal NKCC2 surface expression and NKCC2-mediated NaCl reabsorption which contributes to maintenance of normal blood pressure.

Splice variants and isoforms of NKCC2 and their interaction with ALMS1

Although NKCC2 is encoded by a single gene (Slc12a1), differential splicing of NKCC2 mRNA results in three splice variants - NKCC2 A, B and F due to the variable exon 4. These isoforms differ in their localization along the TAL, macula densa and in their affinity for Cl^- ion [158]. Since the amino acid changes in these variants are located in one of the intracellular transmembrane loop closer to the N-terminus, it is very likely that the interaction of ALMS1 with C2-NKCC2 is conserved across the isoforms. Additionally, NKCC2 B isoform is primarily expressed in the macula densa and thus, ALMS1 *via* its interaction with NKCC2, may potentially play a role in regulating TGF.

NKCC1 is a very closely related member to NKCC2, belonging to the cation-chloride co-transporter family. Despite sharing 60% homology with NKCC2, C2-NKCC2 region that interacts with ALMS1 is not conserved between the isoforms as depicted by highlighted residues in Figure 37. Additionally, phenylephrine which is known to stimulate vascular contractility by enhanced NKCC1 phosphorylation and activity [159], induced similar vasoconstrictor response in abdominal and thoracic aorta from 6-10 week old WT and *ALMS1* KO rats (Figure 38). These data together

suggest that ALMS1 is likely not an interacting partner of NKCC1 and therefore may not regulate its membrane trafficking and activity.

```
NKCC2  802   FEIGVVIVRISQGFDISPVLQVQDELEKLEQERLALEAAIKDNDCEEGKGGIRGLFKKAG  861
              + GVV++R+ +G DIS  LQ Q+EL   +++    +  + + D    K   +  FK +G
NKCC1  904   IQYGVVVIRLKEGLDISH-LQGQEELLSSQEKSPGTKDVVVNVDYS--KKSDQDAFKASG  960

NKCC2  862   KLNITKPAPKKDSNIST----------IQSMHVGEFNQKLVEASAQFKKKQGKGTIDVW  910
              +  IT+   ++D   ST          +  ++V +  QKL+EAS QF+KKQGK TIDVW
NKCC1  961   EKPITQKDEEEDGKTSTQPLLKKESKGPVAPLNVAD--QKLLEASTQFQKKQGKNTIDVW  1018
```

Figure 37: Alignment of C2-NKCC2 and corresponding protein sequence in NKCC1.

ALMS1 KO rats have normal cilia

In some cells, ALMS1 is known to be involved in ciliary function. A study demonstrated that knockdown of *ALMS1* in mouse inner medullary collecting duct (mIMCD3) cell line caused defective ciliogenesis [89], indicating a role for ALMS1 in the maintenance of ciliary function. In contrast, cilia appeared to assemble normally in renal collecting tubules from *ALMS1* transgenic mice [67]. Similarly, fibroblasts from human Alström syndrome patients were shown to have normal cilia but had defects in membrane trafficking [66], indicating that the pathology observed in these patients may be due to defects in intracellular trafficking. While the role of ALMS1 in ciliary function is debatable, our data suggest that *ALMS1* KO rats seem to have normal ciliary development in the renal tubules indicating that the renal phenotype observed in *ALMS1* KO may be independent of cilia. However, it has to be noted that we only measured cilia length but not ciliary function in WT and *ALMS1* KO rats. Despite cilia appearing normal in length and number, it is possible that ciliary function such as flow-induced nitric oxide synthesis etc. may be affected in *ALMS1* KO rats. However, it is unlikely that other cilia-mediated signaling in response to flow stimulus that are associated with development of cysts are affected because the kidneys (n = 9) from 7

month old (oldest surviving) *ALMS1* KO rats do not appear polycystic.

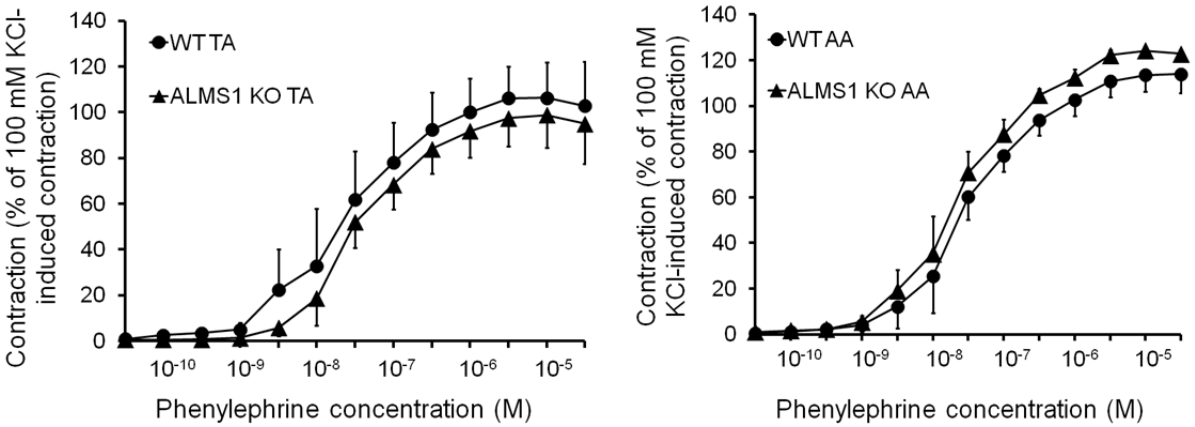

Figure 38: Phenylephrine-induced vasoconstriction is similar in abdominal (AA) and thoracic (TA) aorta from *ALMS1* KO and WT rats, N = 3.

ALMS1 and metabolic syndrome

Little is known about the function of ALMS1 in other organs. ALMS1 seems to be involved in the development of obesity, since Alström syndrome patients develop early onset obesity and *ALMS1* targeted mutations in mice leads to the development of age dependent obesity, insulin resistance, diabetes and hepatic steatosis between the ages of 18 to 21 weeks [67]. In our study to measure renal function and blood pressure, we used young adult rats between the age of 6 to 12 weeks to avoid the potential effect of other confounding factors on the measurement of blood pressure and renal function. At this age, body weight was slightly higher in *ALMS1* KO but metabolic parameters were normal (Table 1). ALMS1 may be involved in the development of insulin resistance through the regulation of insulin-stimulated GLUT4 trafficking. At the age we studied our rats (6 to 12 weeks), they had normal plasma glucose and insulin. However, we hypothesized that *ALMS1* KO rats will develop metabolic syndrome as they age.

ALMS1 is required to maintain normal metabolic function in rats

Metabolic syndrome is known as a clustering of cardiovascular risk factors

associated with hypertension, insulin resistance, glucose intolerance, hypertriglyceridemia and low levels of high-density lipoprotein (HDL). Several genetic loci have been discovered that are individually associated with a few of the above mentioned risk factors. In humans, inactivating mutations in the *ALMS1* gene causes Alström syndrome which is characterized by cardiomyopathy, diabetes mellitus, obesity and hypertension. Both sexes of the *ALMS1* mutant mice recapitulated metabolic syndrome as seen in Alström patients while some sex-differences were observed [67]. However, loss of *ALMS1* in mice was not characterized for hypertension or renal function. To understand the underlying integrated mechanism of hypertension and associated etiologies in both sexes, we generated an *ALMS1* KO rat model by zinc finger nuclease gene targeting of exon 1 of the *ALMS1* gene. In this study we show that *ALMS1* KO rats are a model of metabolic syndrome including hypertension. Elevated blood pressure preceded other characteristics of metabolic dysfunction in these rats. Additionally, female *ALMS1* KO rats exhibited a more severe form of metabolic syndrome compared to their male counterparts. The underlying cause of sex-differences is unknown. However, we found that C-ALMS1 interacts with proteins involved in estrogen receptor signaling such as prohibitin 2 and KRAS protooncogene (data not shown) and this may be a potential hypothesis that requires further testing.

Role of ALMS1 in development of insulin resistance

ALMS1 mutant mice displayed altered intracellular localization of GLUT4 and decreased insulin-stimulated trafficking of GLUT4 to the plasma membrane in adipocytes [69]. Thus, ALMS1 may be involved in the development of insulin resistance through the regulation of insulin-stimulated GLUT4 trafficking. However, caloric

restriction in an Alström patient prevented hyperinsulinemia [139] indicating hyperinsulinemia may develop secondary to obesity. In foz/foz, a mouse strain carrying mutation in *ALMS1*, it was found that along with hyperphagia, impaired brown adipose tissue (BAT) diet-induced thermogenesis is an important factor driving diet-induced obesity and glucose intolerance [140]. Additionally, stable knockdown of *ALMS1* in 3T3-L1 preadipocytes was associated with impairment of lipid accumulation and a twofold reduction in adipocyte gene expression following hormonal induction of adipogenesis [141], suggesting that partial impairment of early phase adipogenesis in Alström syndrome may contribute to the severity of the associated metabolic phenotype [141,142]. In contrast, pre-adipocytes isolated from *ALMS1* mutant mice demonstrated normal adipogenic differentiation but gave rise to mature adipocytes with reduced insulin-stimulated glucose uptake. Reduced insulin-stimulated GLUT4 translocation to the plasma membrane in adipose depots may serve as a potential explanation for glucose intolerance and the compensatory hyperinsulinemia. Thus adipose tissue with a reduced glucose uptake can expand by *de novo* lipogenesis to an obese state [69].

Role of ALMS1 in development of obesity

In hypothalamic neurons, ALMS1 is known to be present in the base of the cilia, known to play a role in the control of satiety. In foz/ foz mice, loss of ALMS1 from this location coincided with a reduction in adenylyl cyclase 3 (AC3), a signaling protein implicated in obesity, suggesting the role of ALMS1 in neuronal ciliary function [143]. However, we found that *ALMS1* KO rats have normal circulating leptin before any difference in body weight was be detected (data not shown). Thus it is debatable whether hyperleptinemia develops secondary to obesity due to a role of ALMS1 in

neuronal cilia or primarily due to a role of ALMS1 in leptin receptor signaling and this requires further examination.

In summary, *ALMS1* KO rat model provide an appropriate tool to elucidate the associated pathophysiological mechanisms of metabolic dysfunction and cardiovascular risk factors.

Strengths and limitations of the study

Strengths: We performed most of our work in native TALs or in primary culture of TALs which retain native cellular characteristics compared to commercial cell lines. We utilized *in vivo* silencing techniques *via ALMS1* shRNA adenoviral transduction into outer renal medulla in rats. We also took advantage of global knockout animal models for testing our hypothesis. We consider that these approaches enhance the significance of our findings and increase the translational relevance of the mechanisms elucidated to human physiology.

Limitations: Despite well conserved basic principles of cellular and renal physiology between rodents and humans, some limitations do exist. However, the kind of research we conducted here would have been impossible to perform in human subjects.

Following are some specific limitations related to our study:

1. Despite only labeling surface NKCC2 for live-cell imaging and monitoring its endocytosis by TIRF, visualization of other NKCC2 trafficking events such as recycling is possible. However, these events will be extremely rare over 20 minutes of live cell imaging because constitutive NKCC2 recycling in rat TALs becomes significant only about 40 minutes after warming the TAL at 37 ºC to allow internalization.

2. Our experiments were performed in medullary TAL suspensions that are enriched from whole outer renal medullary suspensions and thus are not completely pure. Despite this limitation, the fact that NKCC2 is only expressed in TALs makes the contamination of other nephron segments in medullary TAL suspensions less relevant. However, this is not applicable to ALMS1 which is expressed in other outer renal medullary tubules and thus >90% TALs in the enriched suspension or a standardized TAL enrichment protocol across all sample groups is an acceptable representative sample for comparing protein expression.

3. The studies performed in TAL primary cell culture are not best representative of native cellular physiology as they grow under controlled laboratory conditions which do not mimic native conditions and is devoid of complex confounding environment found *in vivo*

4. The GST pull down studies enabled us to identify that ALMS1 interacts with NKCC2 but does not help us determine whether this interaction is direct or *via* intermediate proteins, since these proteins could precipitate as part of a larger protein complex.

5. ALMS1 is very likely involved in trafficking of other plasma membrane proteins which could have an indirect effect on NKCC2 endocytosis in TAL and thereby affect blood pressure. However, we found a direct evidence of interaction and co-localization between ALMS1 and NKCC2 in TAL, suggesting they are very likely to play a direct role. By no means is this an indication that such a role is exclusive for NKCC2 and certainly not a way we formulated our hypothesis and interpreted our results. It is very likely that ALMS1 is involved in trafficking of other renal transporters like NHE3, ROMK,

NCC, ENaC etc. which may possibly explain the mechanism underlying higher blood pressure in *ALMS1* KO rats but testing this hypothesis goes beyond the scope of this study.

We consider testing whether ALMS1 mediates trafficking of other proteins in the TAL, a mechanism which could in turn affect NKCC2 endocytosis indirectly. However, this is a separate hypothesis and requires a different experimental design.

6. We measured renal function and blood pressure in global *ALMS1* knockout rats. In order to address whether ALMS1 expressed specifically in the TAL mediates the effects we observed, a different model of TAL or renal tubule (Pax8)- targeted *ALMS1* deletion is necessary. Although we believe our studies provide the first observation that ALMS1 is important for renal function and blood pressure regulation, this does not mean ALMS1 in the TAL is exclusively responsible for the effects we found.

7. The *ALMS1* KO rats were obtained from MCW and were generated on a Dahl salt sensitive (SS) background. Since Dahl SS rats are known to be salt sensitive, we can only measure whether genetic deletion of *ALMS1* in these rats exacerbates salt sensitivity. However, a previously characterized *ALMS1 mutant* mouse model bred on a C57/Bl6J background were not available for our research and studying trafficking with murine tissue would be very cumbersome.

8. Zinc finger nuclease gene editing technology has been known to have several off-target effects. With the exception of blood pressure and renal phenotype, some of the metabolic characteristics observed in the *ALMS1* KO rats have been previously reported in a different *ALMS1* transgenic mouse model indicating these effects may be due to *ALMS1* specific deletion in the current rat model and not due to off-target effects.

Perspectives

About 35% of Americans are hypertensive [144] which incur huge healthcare costs and lost productivity thereby affecting the economy [145]. Hypertension is associated with an increased risk of left ventricular hypertrophy, a risk factor for cardiovascular death. Coexistence of hypertension and diabetes mellitus triples the risk for cardiovascular disease as indicated in Framingham Heart study [146] and MRFIT trials [147]. Obesity-related hypertension is also known to predispose to coronary heart disease, renal dysfunction, left ventricular hypertrophy and congestive heart failure [148-151]. Presence of hypertension in the setting of obesity and diabetes create a viscious feed-forward loop that also increases the occurrence of end-stage kidney failure [152].

The kidneys reduce extracellular fluid volume by enhancing sodium and water excretion in response to increased arterial pressure [153], thus playing a crucial role in maintaining blood pressure. In this dissertation we have described a molecular mechanism that regulates NKCC2 endocytosis, a key pathway that maintains normal surface NKCC2 expression and activity in the TAL, a nephron segment that has a substantial influence over blood pressure regulation.

Here we propose a mechanism that regulates NKCC2 surface expression *via* interaction with ALMS1. According to Rat Genome Database, *ALMS1* (chromosome 4) genetically overlaps with several quantitative trait loci (QTL) in hypertensive strains and has been associated with hypertension and renal function in several genome wide association studies. Our study is the first to show the role of ALMS1 in regulating NKCC2-mediated NaCl reabsorption and thereby blood pressure and propose that this

mechanism may be involved in progressively decreasing renal function in patients with decreased ALMS1 expression and/or function. Furthermore, *ALMS1* mutations in humans causes Alström syndrome characterized by age-dependent metabolic dysfunction. Elucidation of new genes that are involved in regulation of NKCC2 activity and metabolic function could lead the way to identifying potential biomarkers and understanding the interacting mechanisms of hypertension and metabolic syndrome which are known to increase the risk for cardiovascular and renal disease.

CHAPTER 6 - GENERAL METHODS

Animals

In vivo transduction of *ALMS1* shRNA in the outer medulla was performed in 90-110g male Sprague Dawley rats (Charles River Breeding Laboratories, Wilmington, MA) as reported previously [88]. *ALMS1* KO rats were generated in Dahl salt-sensitive background and were males of 6-12, males and females of 16-18 weeks of age. Age matched littermate controls were male and female Dahl salt-sensitive rats respectively. Animals were fed a standard diet (0.22% Na, 1% K) from Envigo (Indianapolis, IN). All procedures involving live animals were approved by the Institutional Animal Care and Use committee (IACUC) of the Henry Ford Hospital and conducted following guidelines.

Generation of *ALMS1* KO rats

Frame shift deletion of 17 bp in exon 1 (containing a Nci1 restriction site) of *ALMS1* gene was facilitated by injecting zinc Finger nucleases targeting the sequence CCCGCCTCCGACTCCGCCtccgtcCTCCCGGCACCAGTA into Dahl SS/JrHsdMcwi rat embryos. This deletion caused a fame shift leading to a pre-mature stop codon in exon 2. Confirmation of deletion was done by PCR using exon 1 specific primers:

Forward primer- AGAGGAAGAGTTGGAAGGGG,

Reverse primer- ATACATAGGCAGAGCGACCC

followed by Nci1 restriction digestion.

Antibody and reagents

The anti-NKCC2 antibody was generated in rabbit against a carboxy-terminal sequence as described before [35,37]. pThr (96/101) NKCC2 and pSer (126) NKCC2 antibodies were used as previously described [29,88]. Antibodies against carboxyl-terminus ALMS1 was generated in rabbit and was obtained from Dr. Jürgen Naggert

[66). Another ALMS1 antibody was generated against a short peptide epitope in the C-terminus of ALMS1: CEARLEEDSDVTSSSEEKAKE (similar to antibody obtained from Dr. Naggert) [66]. Another ALMS1 antibody was generated against amino acids (2174-2296) of mouse ALMS1 (Genscript Inc., Piscataway, NJ). Reagents for surface biotinylation were from Thermo Fisher scientific (Waltham, MA) and for GST-pull down were from GE Life Sciences. Bumetanide was purchased from Sigma Aldrich.

Constructs and plasmids

The eGFP-NKCC2 (mouse) construct was provided by Dr. Gerardo Gamba, Universidad Nacional Autonoma de Mexico, Mexico [154]. eGFP-NKCC2 was sub-cloned from pSPORT1 into VQAd5CMV adenovirus plasmid vector (ViraQuest, North Liberty, IA) between ApeI and NotI restriction sites. cMyc-NKCC2 (rat) sequence (accession number U10096.1) was commercially synthesized by Genscript (Piscataway, NJ) and was sub-cloned into VQAd5CMV adenovirus vector between KpnI and NotI restriction sites. XbaI restriction site was introduced by site directed mutagenesis in the extracellular loop between the 5^{th} and 6^{th} trans-membrane domains of NKCC2. The XbaI site was used to introduce the Biotin Acceptor Domain (BAD) derived from *Propionibacterium shermanii* [74,75,79] to generate VQAd5CMV-cMyc-NKCC2-BAD adenoviral construct. The ss-BirA (secretory sequence- BirA)-IRES-mCherry construct consists of a biotin ligase fused to yolk sac secretory sequence which targets proteins for secretory pathway [75,79]. It was sub-cloned from CSCW lentiviral vector to VQAd5CMV between BamHI and XbaI restriction sites resulting in the VQAd5CMV-ssBirA adenoviral construct. All clones were fully sequenced and adenoviral particles were assembled and purified by ViraQuest Inc (North Liberty, IA).

MDCK cell culture

Mardin- Darby Canine Kidney (MDCK) Type-2 cell were obtained from American Type Culture Collection (ATCC, Rockville, MD). Cells were cultured in Dulbecco's modified Eagle's medium (DMEM-high glucose, HEPES, no phenol red) (Life Technologies, Grand Island, NY) supplemented with 5 % heat inactivated fetal bovine serum (FBS) (Life Technologies), and Penicillin- Streptomycin mix (Life Technologies). Cells were seeded in collagen-coated Trans-well permeable support (Corning, Tewksbury, MA) and incubated for 3 days at 37ºC and 5% CO_2 until 90% confluent.

Primary culture of rat TALs

Primary culture of rat TAL was done as previously described [88] following institutional and national guidelines for the care and use of laboratory animals. All protocols involving animals were approved by the IACUC at the Henry Ford Hospital. Sprague-Dawley rats weighing 100-120 g were used. Kidneys were perfused with 0.1% collagenase (Sigma, St. Louis, MO) and the outer medulla was dissected. Individual TAL cells were obtained from TAL suspensions after digesting the tubules with 0.1% collagenase, 0.25% trypsin (Sigma) and 0.0021% DNase (Sigma). Single TAL cells were isolated by density gradient centrifugation in 35% Percoll (Sigma) washed and seeded in permeable supports (Corning, Tewksbury, MA) coated with basement membrane extract (Trevigen, Gaithersburg, MD). Cells were grown for 4 days in DMEM (Low glucose, no phenol red, no glutamine) supplemented with 1% FBS, Penicillin-Streptomycin mix and Insulin-Transferrin-Selenium (Life Technologies) at 37ºC and 5% CO_2 until 90% confluent.

Transduction of polarized cells

Cells were transduced by adding adenoviruses at $1x10^8$ Plaque Forming Units (PFU) per ml suspended in serum-free DMEM and added to the basolateral compartment of the transwells. 2 hours after viral transduction, serum was added to inactivate viruses and the cells were incubated at 37ºC for 20 -24 hours.

Suspensions of medullary TALs

TAL suspensions were obtained as described previously. Animals were anesthetized with ketamine and xylazine mixture i.p. and kidneys perfused *via* the descending aorta with 0.001% collagenase. Kidneys were harvested, the outer medulla was dissected and digested in 0.1% collagenase at 37ºC for 30 minutes with oxygenation every 5 minutes followed by mechanical stirring on ice for 30 minutes. The suspension was then filtered through a 250 um nylon mesh.

Steady-state surface biotinylation

Steady-state surface NKCC2 was measured in suspensions of TALs as described previously [37]. TALs were biotinylated at 4ºC with NHS-SS-biotin (0.9 mg/ml) and then washed and lysed. Extracted proteins were incubated with steptavidin-agarose beads (Pierce Biotechnology) at 4ºC overnight to separate the biotinylated protein fraction (surface protein fraction) from the non-biotinylated protein fraction (intracellular protein fraction). Beads were washed and proteins were extracted from beads by warming at 37ºC. Proteins were resolved by SDS-PAGE (6% gels). NKCC2 and GAPDH were detected by Western blot. Surface NKCC2 was calculated as a percentage of total NKCC2 (sum of surface and intracellular NKCC2 fraction).

For surface biotinylation in MDCK cells, it was performed using NHS-SS-biotin by

a method that we described previously in primary cultures of rat TAL suspension [88]. In order to confirm correct targeting of eGFP-NKCC2 construct to apical surface and absence of targeting to the basolateral surface, we performed apical and basolateral surface biotinylation. Cells were biotinylated at 4ºC with NHS-SS-biotin (0.9 mg/ml) added either in the apical or basolateral compartment of the transwells. To prevent access of NHS-SS-biotin to the apical surface from the basolateral compartment during basolateral surface biotinylation or vice versa, MDCK cells were pre-treated with NHS-acetate (2 mg/ml) for 1 hour at 4ºC added to either the apical or basolateral compartment of the transwell to mask lysine biotinylation sites [36] prior to the addition of NHS-SS-biotin. Cells were washed and lysed in buffer containing 150 mM NaCl, 50 mM HEPES (pH 7.5), 5 mM EDTA, 1% Triton X-100, 0.2% SDS and protease inhibitors. Extracted proteins were incubated with streptavidin-agarose beads (Pierce Biotechnology) at 4ºC overnight. Beads were washed and biotinylated proteins were extracted by boiling in 60 µl SDS-loading buffer containing 100 mM dithiothreitol and 5% β-mercaptoethanol. Proteins extracted from the beads (surface) and supernatant (intracellular) were resolved by SDS-PAGE (6% gels). NKCC2 and GAPDH were detected by Western blot.

Site-specific NKCC2 biotinylation and streptavidin Alexa Fluor-488 labeling

Cells transduced to express NKCC2-BAD were serum starved for 2 hours at 37ºC and then treated with or without 5 mM Methyl-β-cyclodextrin (MβCD) (Sigma) in serum-free DMEM for 20 minutes. Cells were then washed with PBS containing 0.1 mM $CaCl_2$ and 4 mM $MgCl_2$ (PBS-Ca-Mg) pH 7.6. Cells were incubated with 5% BSA in PBS-Ca-Mg (pH 7.6) for 20 minutes to block non-specific binding reactions in the

following steps. To allow biochemical biotinylation of BAD-NKCC2, a solution containing 10 μM d-biotin (Avidity, Aurora, CO), 2 mM ATP and 0.53 μM biotin ligase (BirA) (Avidity, Aurora, CO) in PBS-Ca-Mg was added to the extracellular apical bath and incubated for 20 minutes at room temperature. VQAd5CMV-ssBirA adenovirus construct was co-transduced with NKCC2-BAD to facilitate metabolic biotinylation. Unreacted biotin was removed by cooling the cells to 4ºC and briefly washing with chilled PBS-Ca-Mg (pH 7.6) and then with PBS-Ca-Mg (pH 3.0). Alexa Fluor 488-conjugated streptavidin (Life Technologies) was added to the apical bath at 1:400 dilution in 5% BSA/ PBS-Ca-Mg (pH 7.6, 4ºC). Finally, multiple washes were done to remove unbound streptavidin with PBS-Ca-Mg at pH-7.6 and 3.0.

Apical total internal reflection fluorescence (TIRF) microscopy

The membranes in the Trans-well were carefully cut and separated from the inserts, and placed in a temperature-controlled chamber at 37ºC facing down, such that the apical surface faced the objective lens. Cells were covered with a 0.13-0.17 mm thick glass coverslip (Fisher Scientific, Waltham, MA) and transferred to an inverted scope (Nikon TE2000U), equipped with “through the lens” TIRF module, 100x 1.45 NA TIRF lens (Nikon), in a way that the apical membranes faced the objective lens. A blunt glass pipette mounted on micromanipulators was lowered on the membrane from the basolateral side to push the apical membranes down and closer to the glass coverslip. Prior to imaging, serum-free DMEM was added to the basolateral side of the chamber and cells were allowed to equilibrate at 37ºC for 10 min. A region of interest was selected and the 488 nm excitation laser was angled until reflection was observed on the glass coverslip. To observe and measure real-time endocytosis, images were

acquired continuously once per second. Images were captured and acquired once per minute at 1000 millisecond frame rate for twenty minutes. Images were acquired at 1024x1024 pixel resolution with an EM-enhanced cooled CCD (Photometrics Cascade II 1024 EMCCD). Each image was deconvolved using AutoQuant software (Media Cybernetics, Rockville, MD) and analyzed with Metamorph® software (Molecular Devices, Sunnyvale, CA). The Granularity module of Metamorph was used to automatically count the number of puncta (singular- punctum) present on the TIRF field over time. Background fluorescence intensity was measured from a region on TIRF field with no punctum.

Endocytosis assay of NKCC2 in TALs

NKCC2 endocytosis was measured as described previously [37,38]. TALs were biotinylated at 4ºC. Suspension was split in four and the last 3 fractions were warmed to 37ºC for 0, 10 and 20 minutes to allow endocytosis. The TALs were rapidly cooled to halt protein trafficking. TALs were then treated for 30 minutes at 4ºC with the membrane-impermeant reducing agent MesNa (50 mM) to strip biotin from surface proteins while protecting biotinylated proteins that internalized. TALs from all four fractions were then lysed and equal amounts of proteins were incubated with agarose-streptavidin to separate biotinylated proteins that internalized while the first fraction served as baseline surface NKCC2. Proteins were then resolved by SDS-PAGE and NKCC2 was detected by Western blot. Internalized NKCC2 was measured as a percentage of total (100%) biotinylated surface NKCC2 fraction.

GST pull down

A GST fusion protein consisting of GST fused to the 71 amino acid domain in

NKCC2 that is shown to be important for apical targeting of NKCC2 (GST-C2-NKCC2) was engineered by subcloning the corresponding nucleotides in the sequence of rat NKCC2 downstream of GST in the pGEX-6P-1 vector (GE healthcare). GST alone construct served as the negative control. The constructs were separately transformed by heat shock into competent E. coli and induced to express the construct by incubation with 0.18 mM IPTG at 28ºC for 10 hours. Bacterial proteins were extracted and incubated with glutathione-conjugated sepharose beads (GE healthcare) to purify the induced protein. 100 µg of rat TAL protein lysate was incubated with purified GST-C2-NKCC2 and GST alone overnight at 4ºC after pre-clearing the lysate with GST alone for 1 hour. The beads were washed next day and submitted to the Proteomics Core of Michigan State University (East Lansing, MI) for liquid chromatography and mass spectrometry to identify C-NKCC2 interacting proteins. The resulting protein candidates were analyzed and screened based on criteria mentioned in the results section. To determine if C-ALMS1 binds to NKCC2, two truncated carboxyl-terminus ALMS1 constructs were obtained from Dr Jürgen Naggert. These truncated constructs correspond to amino acids 2683 to 2932 (referred to as C-ALMS1-B) and 2988 to 3251 (referred as C-ALMS1-A) in mouse ALMS1. These constructs were cloned downstream of GST in pGEX-6P-1 vector while GST alone served as a negative control. Purification of the induced proteins and GST pull down assay was performed as mentioned above. The pull-down proteins were eluted from glutathione-conjugated sepharose beads with 6x loading buffer containing DTT and β-mercaptoethanol and resolved by SDS-PAGE. NKCC2 was detected by Western blot.

Histology and immunohistochemistry

Kidneys were fixed by perfusing the rats with 4% paraformaldehyde through the abdominal aorta. The kidneys were then stored in 10% formalin for at least a day before embedding and processing the tissue by the Biobank and Correlative Science Core at Wayne State University (Detroit, MI). 5 µm thick sections of the kidney were obtained for hematoxylin-eosin (H&E) and immuno-staining. For co-labeling of NKCC2 and ALMS1 in kidney sections, paraffin-embedded slices were first deparaffinized with xylene and then hydrated gradually through 100% ethanol to distilled water. Heat-induced epitope retrieval was used to unmask the antigens followed by incubation with 1% BSA for 30 min to block nonspecific binding. Slides were incubated with 1:50 dilution of NKCC2 primary antibody for 1 hour at RT. This was followed by 1:100 of Alexa-Fluor 488 Goat anti-Rabbit IgG (Molecular probes, Eugene, OR) for 1 hours at RT. To facilitate labeling of ALMS1, biotinylated ALMS1 antibody was prepared using the antibody biotinylation kit (Pierce, Thermo Fisher Scientific, Waltham, MA). The slides were incubated with 1:50 dilution of streptavidin prior to incubating them with ALMS1 biotinylated antibody at 1:20 dilution overnight at RT for 1 hour to block nonspecific binding. This was followed by incubating with 1:100 of streptavidin Alexa-Fluor 647 for 1 hour at RT. Finally the slides were counter-stained with DAPI at 1:2000 for 5 min at RT. For staining cilia in kidney sections, slides were incubated with 1:250 dilution of mouse anti-acetylated α-tubulin antibody (Abcam) followed by 1:200 dilution of Alexa Fluor 488 goat anti-mouse IgG (Thermofisher) for 1 hr at RT. Slides were mounted and imaged by Leica multi-photon microscope TCS SP8 MP (Leica Microsystems, Germany).

Immuno-labeling of surface NKCC2 in MDCK cells

Cells were fixed with 4% paraformaldehyde for 30 minutes at 4ºC. Fixed cells were blocked with 5% BSA (Equitech-Bio, Kerrville, TX) in PBS (Life Technologies) for 20 minutes at RT. Anti-zonula occludens-1 (ZO-1) (1: 100 dilution) were added to the cells for 1 hour at RT followed by (1: 100 dilution) of Alexa Fluor 568- conjugated secondary anti-mouse antibody for 1 hour. For surface NKCC2 labeling, antibodies to extracellular epitope of NKCC2 (1:100 dilution) [36] were added to both apical and basolateral compartments of live cells cooled to 4ºC for 2 hours, then washed and incubated with Alexa-Fluor 488- conjugated secondary anti-rabbit antibody for 1 hour at 4ºC in both compartments of the transwell. Cells were then fixed and labeled for ZO-1 as mentioned above. Membranes were cut and mounted on a glass slide. Glass slides were imaged by laser scanning confocal microscopy system (Visitech International, Sutherland, England). For z-section confocal imaging, we used an Olympus FV1200 confocal system at 60X, 1.4 NA. Z sections were obtained at 0.25µm step for 10 µm total z-distance.

Co-immunostaining in TAL primary culture

TAL primary cells that achieved 90% confluence on permeable supports were cooled to 4ºC. Live cells were incubated with 5 % BSA (Equitech-Bio, Kerrville, TX) in PBS (Life Technologies) for 20 minutes at 4ºC. Surface NKCC2 was labeled with an antibody (1:100) directed towards extracellular epitope of NKCC2 added to the apical compartment of the live cells for 2 hours [36]. The cells were then washed and incubated with an Alexa Fluor 488-conjugated anti-rabbit antibody for 1 hour at 4ºC in the apical compartment of the transwell. The cells were washed and warmed to 37ºC

for allowing internalization of the surface labeled NKCC2. The cells were then fixed with 4% paraformaldehyde for 30 min at 4ºC. Fixed cells were washed and incubated with 5% BSA in PBS for 20 min at RT. To facilitate labeling of ALMS1, biotinylated ALMS1 antibody was prepared using the antibody biotinylation kit (Pierce, Thermo Fisher Scientific, Waltham, MA) and was then subsequently added to the apical compartment for 1 hour at RT. The cells were washed and then incubated with streptavidin Alexa Fluor- 647 for 1 hour at RT. The cells were then washed and a mouse primary antibody against zonula occludens-1 (ZO-1) was added to the cells, which were incubated for 1 hour at room temperature followed by the addition of an Alexa Fluor 568-conjugated secondary anti-mouse antibody for 1 hour. The membranes were then washed, cut and mounted on a glass slide. Glass slides were imaged by Leica multi-photon microscope TCS SP8 MP (Leica Microsystems, Germany). For Z-section confocal imaging, we used this confocal system at X60, 1.4 NA. Z-sections were obtained at 0.25 µm steps for 8.5 µm total Z-distance (35 slices). The co-localization pixels were identified by using a Mander's overlap coefficient ≥ 0.95.

Labeling of ALMS1 in isolated perfused rat TAL

Isolated perfused rat TALs were fixed with 4% formaldehyde and then blocked with 2.5% BSA. We then labeled TALs with anti-ALMS1 antibody in 2.5% BSA followed by Alexa Fluor 488 anti-rabbit IgG highly adsorbed at 1:100 in 2.5 % BSA. Images were acquired using a laser scanning confocal microscopy system (Visitech, Sutherland, England). Images were acquired at 100X (1.3 NA).

Blood pressure measurements

Systolic blood pressure was also measured in awake rats by tail-cuff

plethysmography. Mean arterial pressure was measured by implanting an intra-arterial catheter connected to a pressure transducer, into the femoral artery of rats anesthetized with inactin i.p.

Urine and ion excretion measurements

Rats were placed in metabolic cages with free access to food and water. The rats were allowed to get adjusted to the new cage for 3 days after which urine samples were collected while recording body weights to ensure it remains relatively unchanged due to any stress to the animal. Urine volume was recorded and urine osmolality was measured by freezing point depression with Advanced Model 3300 Micro Osmometer (Advanced Instruments Inc. Norwood, MA). Urine Na was measured in Nova 1+ Analyzer (Nova Biomedical, Waltham, MA). For bumetanide response experiments, a different group of rats were trained to eat all of their food between 6 P.M and 9 A.M the next day. At 10 A.M, rats were given 1g chocolate and were trained to eat chocolate within 10 minutes for 5 days. On day 5, urine was collected until 8 hours after the rats were given chocolate frosting to record baseline urine volume and Na^+ excretion. On day 6, 5 mg/kg bumetanide was mixed with the chocolate pudding and urine was collected until 8 hours after the rats were given chocolate and urine volume and Na^+ excretion was measured.

Glomerular filtration rate (GFR) and renal blood flow (RBF) measurement

Rats were fasted overnight and on the following day, they were anesthetized and their femoral vein was cannulated for bolus administration (3 µl/g body weight) of 1 mg/ml FITC-inulin followed by its constant infusion at a rate of 0.15 µl/min/g body weight for measurement of GFR by measuring clearance of FITC-inulin. A mid line incision

was made to expose the left kidney and the bladder. A flow probe was placed on the renal artery to measure renal blood flow (RBF). The bladder was catheterized to collect urine. Plasma and urine inulin fluorescence was assessed with a Synergy H1 Microplate Reader (BioTek, Winooski, VT) to measure plasma and urine inulin concentrations as described previously [155].

Volume expansion (VE)

Rats were anesthetized with inactin and a femoral artery and vein were cannulated with PE-50 tubing. Femoral arterial pressure was measured with a pressure transducer. The bladder was exposed through a suprapubic incision and was cannulated with a needle attached to PE-50 tubing. Isotonic saline was infused intravenously to administer 3 ml/100 g body weight in 30 minutes (3% volume expansion), after which volume expansion was maintained by infusing at a rate averaging 0.15 µl/min/g body weight. Following a 30 minute recovery period after surgery, urine was collected at two consecutive 30-minute intervals ((time points: 30 min and 60 min) for baseline measurements of urine volume and urinary sodium excretion and then at five consecutive 30-minute intervals (time points: 90 min – 210 min) following 3% volume expansion. The data points plotted represent values for total urine volume and urinary sodium excretion measured over 30 min starting from the preceding data point. These physiological parameters measured after 3% volume expansion, were first normalized to their respective baseline values at 60 min. Then, their cumulative values between time points 60 min and 210 min (represented by light and dark grey shaded regions; Figure 31A and B) were calculated and plotted in the corresponding bar graph.

***In vivo* gene silencing**

The target sequence for *ALMS1* silencing was a 29-nucleotide sequence from the rat *ALMS1* gene: 5'-TCCTGAATCAGGTGACCAGAAGACTCATT-3'. The sense and antisense sequences are spaced by a loop sequence (TCAAGAG). This shRNA sequence was tested by transfection in NRK-52E cells. Expression of *ALMS1* and GAPDH was monitored by RT-PCR. After the efficacy of the shRNA was tested, the shRNA was subcloned between the 5' AscI and 3' HindIII sites in the adenovector-pMIGHTY (Viraquest, North Liberty, IA) for production of adenoviral particles as recently described [36]. The adenoviral *ALMS1* shRNA was injected with 3 mm calibrated needles into the outer medulla of left rat kidney while the right kidney was injected with the control buffer acting as a sham operated kidney as described before for other genes [156]. The kidneys were harvested 7 days later to obtain TAL suspensions which were lysed and resolved by SDS-PAGE in 4% gels or 6% gels for the detection of ALMS1 and NKCC2 by Western blot, respectively. Surface NKCC2 was calculated as a percentage of total NKCC2 (sum of surface and intracellular NKCC2 fraction).

Plasma insulin and leptin measurement

Whole blood was collected from the jugular vein of rats and was immediately mixed with appropriate volume of EDTA (5:1 ratio) to prevent blood coagulation. Blood was then spun at 200g for 20 minutes to collect plasma. Plasma samples were used to measure insulin and leptin concentration using Enzyme immunoassay kit from Cayman (Ann Arbor, MI).

Plasma renin activity

Plasma renin activity was analyzed by generation of angiotensin (Ang) I (ng Ang

l/ml/hr) using a Gamma Coat RIA kit (DiaSorin, Stillwater, MN) as previously described and according to the manufacturer's instructions [157].

Ingenuity pathway analysis

TAL proteins pulled down either with GST-C-ALMS1 A/B were identified by liquid chromatography-mass spectrometry. These proteins were found to be involved with key biological processes such as "Cellular assembly and organization", "Molecular transport", "Protein trafficking", "Renal disease" and "clathrin and caveolar-mediated endocytosis signaling" with an enrichment probability value less than 0.05, considered statistically significant by Ingenuity pathway network analysis (IPA: Ingenuity systems, Inc; Qiagen, Inc.). These proteins were further curated with IPA knowledgebase by Ingenuity pathway network analysis to determine direct or indirect interactions among themselves.

Blood glucose and serum lipid profiling

Random and fasting blood glucose was measured using Wavesense Presto Blood Glucose meter (AgaMatrix, Salem, NH). Lipid profiling using rat serum samples was done using Siemen's healthcare diagnostic analyzer (Siemens, Malvern, PA) according to the manufacturer's instructions.

Vascular reactivity

Briefly, rats were anesthetized with pentobarbital (50 mg/kg). Abdominal and thoracic aorta was removed while maintaining endothelium intact and suspended in water baths containing perfusion solution to measure phenylephrine-induced vascular reactivity. Phenylephrine- induced vasoconstriction was measured as a percentage of 100 mM KCl-induced vascular contraction.

Statistical analysis

Results are expressed as mean ± standard error. Single intergroup comparisons between two groups were performed with a Student's *t*-test and paired *t*-test for paired samples. For Figure 27A and 30 A&B, two way analysis of variance (ANOVA) was used to determine differences between means in two treatments and groups. For Figure 35, one way ANOVA was used to determine differences in means in treatments with more than two groups. Post hoc analysis was performed when differences between means was found using the Bonferroni correction for multiple comparisons. $p<0.05$ was considered statistically significant.

APPENDIX A

List of acronyms

ACTN 1/4: α-actinin 1/4

ALMS1: Alström syndrome 1 protein (Italicized version correspond to its gene or RNA)

ANOVA: Analysis of Variance

ANXA2: Annexin A2

AC3: Adenylyl cyclase 3

ARF1: ADP-ribosylation factor 1

ARPC5L: Actin related protein 2/3 complex subunit 5 like

βAR: β adrenergic receptor

BAD: Biotin acceptor domain

BAT: Brown adipose tissue

BirA: *Escherichia coli* biotin ligase

C2-NKCC2: A region in the carboxyl-terminus of NKCC2

CKD: Chronic kidney disease

DTT: Dithiothreitol

E. coli: *Escherichia coli*

ENaC: Epithelial Na channel

eGFP: Enhanced green fluorescent protein

ER: Endoplasmic reticulum

FLOT2: Flotillin-2

GAPDH: Glyceraldehyde 3-phosphate dehydrogenase

GEERC: Gene editing rat resource center

GFR: Glomerular filtration rate

GLUT4: Glucose transporter-4

GSN: Gelsolin

GST: Glutathione S-transferase

GWAS: Genome-wide association studies

HDL: High density lipoproteins

IACUC: Institutional Animal Care and Use Committee

ILK: Integrin-linked protein kinase

IPA: Ingenuity pathway analysis

IPTG: Isopropyl β-D-1 thiogalactopyranoside

KO: Knockout

LC: Liquid chromatography

LDL: Low density lipoproteins

mRNA: messenger RNA

MAL/VIP17: Myelin and lymphocytes-associated protein

MAP: Mean arterial pressure

MDCK: Mardin Darby Canine Kidney

mIMCD3: Mouse inner medullary collecting duct

MRFIT: Multiple Risk Factor Intervention Trial

MS: Mass spectrometry

MYO5B: Myosin Vb

Na^+/K^+/ATPase: Sodium-potassium pump

NHE: Na/H exchanger

NHGRI: National human genome research institute

NHS: N-Hydroxysulfosuccinimide

NIH: National Institutes of Health

NKCC2: $Na^+/K^+/2Cl^-$ co-transporter

NRK: Normal rat kidney

PFU: Plaque-forming unit

PHB: Prohibitin

PICALM: Phosphatidylinositol binding clathrin assembly protein

PKA: Protein kinase A

QTL: Quantitative trait loci

RAC1: Ras-related C3 botulinum toxin substrate 1

RBF: Renal blood flow

RGD: Rat genome database

RAB: Ras-related protein

RABEP1: Rabaptin

RALA: Ras-related protein Ral-A precursor

RBP: Renal blood flow

RINT1: Rad 50 interactor -1

ROMK: Renal outer medullary K^+ channel

RT-PCR: Reverse transcriptase- Polymerase chain reaction

RVR: Renal vascular resistance

SBP: Systolic blood pressure

shRNA: Short hairpin RNA

SD: Sprague-Dawley

SNP: Single nucleotide polymorphism

ss: Secretory signal

TAL: Thick ascending limb

TGF: Tubulo-glomerular feedback

TGN: Trans-golgi network

TIRF: Total internal reflection fluorescence

UMOD: Uromodulin

V2R: Vasopressin-2 receptor

WT: Wild-type

ZO-1: Zonula occludens 1

APPENDIX B

IACUC Approval Letters

WAYNE STATE UNIVERSITY

INSTITUTIONAL ANIMAL
CARE AND USE COMMITTEE
87 E. Canfield, Second Floor
Detroit, MI 48201-2011
Telephone: (313) 577-1629
Fax Number: (313) 577-1941

ANIMAL WELFARE ASSURANCE # A3310-01

PROTOCOL # A 04-12-15

Protocol Effective Period: May 28, 2015 – April 30, 2018

TO: Ms. Ankita Jaykumar
Physiology
2799 West Grand Blvd
E&R building, Room- 7038
Detroit, MI 48202

FROM: Lisa Anne Polin, Ph.D.
Chairperson
Institutional Animal Care and Use Committee

SUBJECT: Approval of Protocol # A 04-12-15

"Role of ALMS1 on NKCC2 endocytosis and NaCl reabsorption in the TAL (ADMIN - HFHS)"

DATE: May 28, 2015

Your animal research protocol has been reviewed by the Wayne State University Institutional Animal Care and Use Committee, and given final approval for the period effective **May 28, 2015** through **April 30, 2018**. The listed source of funding for the protocol is **HFHS Internal**. Be advised that this protocol must be reviewed by the IACUC on an annual basis to remain active.

The work on the project will not involve the use of live animals conducted within Wayne State University or John D. Dingell VAMC facilities. The principal investigator conducting this work requires an approved IACUC protocol for the live animal work conducted in that facility. However, be aware that the grantee always retains the primary responsibility for ensuring compliance with PHS Policy.

The Guide for the Care and Use of Laboratory Animals is the primary reference used for standards of animal care at Wayne State University. The University has submitted an appropriate assurance statement to the Office for Laboratory Animal Welfare (OLAW) of the National Institutes of Health. The animal care program at Wayne State University is accredited by the Association for Assessment and Accreditation of Laboratory Animal Care International (AAALAC).

Henry Ford Health System

Research Administration
CFP-Basement 046
2799 West Grand Boulevard
Detroit, MI 48202-2689
(313) 916-2024 Office
(313) 916-2018 Fax

February 28, 2014

To: Pablo A. Ortiz, Ph.D.
Hypertension

Fm: Frederick Valeriote, Ph.D., Chair
Robert Knight, Ph.D., Vice Chair
Institutional Animal Care and Use Committee

Re: **"THE ROLE OF ALMS1 AND PREX1 IN RENAL FUNCTION AND BLOOD PRESSURE"** (IACUC No. 1303)

Period of IACUC Approval: **February 28, 2014 through February 27, 2017**

Number of Animals Approved: Rats and Mice

Strain	Number of Animals
Sprague Dawley rats	1245
Alms1 KO rats	521
PREX1 KO rats	281
Dahl Salt-Sensitive rats	553
C57 bL6J	295
ALMs1 floxed	23
TAL-specific ALMs1 KO	46
NKCC2-Cre	23

Dear Dr. Ortiz:

Thank you for responding to IACUC concerns. All concerns have been adequately addressed and full approval has been granted.

The expiration date for this study is February 28, 2017. In order to remain compliant with federal regulations, a new, complete IACUC Protocol must be submitted for full board review if you intend to proceed with this line of work beyond the above indicated expiration date. A Final Report must be submitted at the completion of the 3-year approval period or upon early termination of the project.

Any adverse effects on animals must be reported to the IACUC as soon as possible.

A copy of the signed and stamped protocol indicating approval of the Institutional Animal Care and Use Committee is enclosed for your files. Please feel free to contact the Research Administration Office at 916.2024 if you have any questions regarding this matter.

Enc.
cc: Bioresources

APPENDIX C

License Terms and Conditions-American Journal of Physiology

Home | Create Account | Help

Title: Real-time monitoring of NKCC2 endocytosis by total internal reflection fluorescence (TIRF) microscopy

Author: Ankita Bachhawat Jaykumar,Paulo S. Caceres,Ibrahim Sablaban,Bakhos A. Tannous,Pablo A. Ortiz

Publication: Am J Physiol-Renal Physiology

Publisher: The American Physiological Society

Date: Jan 15, 2016

LOGIN

If you're a copyright.com user, you can login to RightsLink using your copyright.com credentials. Already a RightsLink user or want to learn more?

Permission Not Required

Permission is not required for this type of use.

BACK | CLOSE WINDOW

REFERENCES

1. Good DW. Sodium-dependent bicarbonate absorption by cortical thick ascending limb of rat kidney. *Am J Physiol. Renal Physiol.* 248:F821-F829, 1985.
2. Good DW and Watts BA III. Functional roles of apical membrane Na^+/H^+ exchange in rat medullary thick ascending limb. *Am J Physiol. Renal Physiol.* 270:F691-F699, 1996.
3. Kaplan MR, Plotkin MD, Lee WS, Xu ZC, Lytton J and Hebert SC. Apical localization of the Na-K-Cl cotransporter, rBSC1, on rat thick ascending limbs. *Kidney Int.* 49:40-47, 1996.
4. Obermuller N, Kunchaparty S, Ellison DH and Bachmann S. Expression of the Na-K-2Cl cotransporter by macula densa and thick ascending limb cells of rat and rabbit nephron. *J Clin Invest.* 98:635-640, 1996.
5. Molony DA, Reeves WB, and Andreoli TE. $Na^+K^+2Cl^-$ cotransport and the thick ascending limb. *Kidney Int.* 36:418-426, 1989.
6. Hebert SC and Andreoli TE. Control of NaCl transport in the thick ascending limb. *Am J Physiol.* 246:F745-F756, 1984
7. Greger R. Ion transport mechanisms in thick ascending limb of Henle's loop of mammalian nephron. *Physiol Rev.* 65:760-797, 1985.
8. Greger R, Bleich M and Schlatter E. Ion channels in the thick ascending limb of Henle's loop. *Renal Physiology & Biochemistry.* 13:37-50, 1990.
9. Di Stefano A, Jounier S and Wittner M. Evidence supporting a role for KCl cotransporter in the thick ascending limb of Henle's loop. *Kidney Int.* 60:1809-1823, 2001.
10. Bleich M, Schlatter E and Greger R. The luminal K+ channel of the thick ascending

limb of Henle's loop. *Pflugers Archiv - European Journal of Physiology.* 415:449-460, 1990.

11. Greger R. Cation selectivity of the isolated perfused cortical thick ascending limb of Henle's loop of rabbit kidney. *Pflugers Archiv - European Journal of Physiology.* 390:30-37, 1981.
12. Mandon B, Siga E, Roinel N and de Rouffignac C. Ca2+, Mg2+ and K+ transport in the cortical and medullary thick ascending limb of the rat nephron: influence of transepithelial voltage. *Pflugers Arch.* 424:558-560, 1993.
13. Simon DB, Karet FE, Hamdan JM, DiPietro A, Sanjad SA and Lifton RP. Bartter's syndrome, hypokalemic alkalosis with hypercalciuria, is caused by mutations in the Na-K-2Cl cotransporter NKCC2. *Nat Genet*. 13:183-188, 1996.
14. Starremans PG, Kersten FF, Knoers NV, van den Heuvel LP and Bindels RJ. Mutations in the human Na-K-2Cl cotransporter (NKCC2) identified in Bartter syndrome type I consistently result in nonfunctional transporters. *J Am Soc Nephrol.* 14:1419-1426, 2003.
15. Bettinelli A, Ciarmatori S, Cesareo L, Tedeschi S, Ruffa G, Appiani AC, Rosini A, Grumieri G, Mercuri B, Sacco M. *et al*. Phenotypic variability in Bartter syndrome type I. *Pediatr Nephrol*. 14:940-945, 2000.
16. Fukuyama S, Okudaira S, Yamazato S, Yamazato M and Ohta T. Analysis of renal tubular electrolyte transporter genes in seven patients with hypokalemic metabolic alkalosis. *Kidney Int.* 64:808-816, 2003.
17. Kurtz CL, Karolyi L, Seyberth HW, Koch MC, Vargas R, Feldmann D, Vollmer MM, Knoers NV, Madrigal G and Guay-Woodford LM. A common NKCC2 mutation

in Costa Rican Bartter's syndrome patients: evidence for a founder effect. *J Am Soc Nephrol.* 8:1706-1711, 1997.

18. Vargas-Poussou R, Feldmann D, Vollmer M, Konrad M, Kelly L van den Heuvel LP, Tebourbi L, Brandis M, Karolyi L, Hebert SC. *et al*. Novel molecular variants of the Na-K-2Cl cotransporter gene are responsible for antenatal Bartter syndrome. *Am J Hum Genet*. 62:1332-1340, 1998.
19. Adachi M, Asakura Y, SatoY, Tajima T, Nakajima T, Yamamoto T, and Fujieda K. Novel SLC12A1 (NKCC2) mutations in two families with Bartter syndrome type 1. *Endocr J*. 54:1003-1007, 2007.
20. Ellison DH. Divalent cation transport by the distal nephron: insights from Bartter's and Gitelman's syndromes. *Am J Physiol. Renal Physiol.* 279:F616-F625, 2000.
21. Bartter FC, Pronove P, Gill JR Jr, and MacCardle RC. Hyperplasia of the juxtaglomerular complex with hyperaldosteronism and hypokalemic alkalosis. A new syndrome. 1962. *J Am Soc Nephrol.* 9:516-528, 1998.
22. Shaer AJ. Inherited primary renal tubular hypokalemic alkalosis: a review of Gitelman and Bartter syndromes. *Am J Med Sci*. 322:316-332, 2001.
23. Takahashi N, Chernavvsky DR, Gomez RA, Igarashi P, Gitelman HJ, and Smithies O. Uncompensated polyuria in a mouse model of Bartter's syndrome. *Proc Natl Aacd Sci USA.* 97:5434-5439, 2000.
24. Acuna R, Martinez-de-la-Maza L, Ponce-Coria J, Vazquez N, Ortal-Vite P, Pacheco- Alvarez D, Bobadilla NA, and Gamba G. Rare mutations in SLC12A1 and SLC12A3 protect against hypertension by reducing the activity of renal salt cotransporters. *J Hypertens*. 29:475-483, 2011.

25. Monette MY, Rinehart J, Lifton RP and Forbush B. Rare mutations in the human Na-K-Cl cotransporter (NKCC2) associated with lower blood pressure exhibit impaired processing and transport function. *Am J Physiol. Renal Physiol.* 300:F840- F847, 2011.

26. Kirchner KA, Crosby BA, Patel AR and Granger JP. Segmental chloride transport in the Dahl-S rat kidney during L-arginine administration. *J Am Soc Nephrol.* 5:1567-1572, 1995.

27. Kirchner KA. Greater loop chloride uptake contributes to blunted pressure natriuresis in Dahl salt sensitive rats. *J Am Soc Nephrol.* 1:180-186, 1990.

28. Kirchner KA. Increased loop chloride uptake precedes hypertension in Dahl salt-sensitive rats. *Am J Physiol.* 262:R263-R268, 1992.

29. Haque MZ, Ares GR, Caceres PS and Ortiz PA. High Salt Differentially regulates Surface NKCC2 Expression in Thick Ascending Limbs of Dahl Salt sensitive and Salt Resistant Rats. *Am J Physiol. Renal Physiol.* 300:F1096-1104, 2011.

30. Glorioso N, Filigheddu F, Troffa C, Soro A, Parpaglia PP, Tsikoudakis A, Myers RH, Herrera VL and Ruiz-Opazo N. Interaction of alpha(1)-Na,K- ATPase and Na,K,2Cl-cotransporter genes in human essential hypertension. *Hypertension*. 38:204-209, 2001.

31. Jung J, Basile DP and Pratt JH. Sodium reabsorption in the thick ascending limb in relation to blood pressure: a clinical perspective. *Hypertension.* 57(5):873-879, 2011.

32. Hong NJ and Garvin JL. Angiotensin II type 2 receptor-mediated inhibition of NaCl absorption is blunted in thick ascending limbs from Dahl salt-sensitive rats.

Hypertension. 60:765-769, 2012.

33. Meade P, Hoover RS, Plata C, Vazquez N, Bobadilla NA, Gamba G, Hebert SC. cAMP-dependent activation of the renal-specific Na^+-K^+-$2Cl^-$ cotransporter is mediated by regulation of cotransporter trafficking. *Am J Physiol Renal Physiol*. 284(6):F1145-F1154, 2003.

34. Nielsen S, Maunsbach AB, Ecelbarger CA, and Knepper MA. Ultrastructural localization of Na-K-2Cl cotransporter in thick ascending limb and macula densa of rat kidney. *Am J Physiol.* 275:F885-F893, 1998.

35. Ortiz PA. cAMP increases surface expression of NKCC2 in rat thick ascending limbs: role of VAMP. *Am J Physiol. Renal Physiol.* 290:F608-F616, 2006.

36. Caceres PS, Ares GR, and Ortiz PA. cAMP stimulates apical exocytosis of the renal Na(+)-K(+)-2Cl(-) cotransporter NKCC2 in the thick ascending limb: role of protein kinase A. *J Biol Chem.* 284:24965-24971, 2009.

37. Ares GR and Ortiz PA. Constitutive endocytosis and recycling of NKCC2 in rat thick ascending limbs. *Am J Physiol. Renal Physiol.* 299:F1193-F1202, 2010.

38. Ares GR and Ortiz PA. Dynamin2, clathrin, and lipid rafts mediate endocytosis of the apical Na/K/2Cl cotransporter NKCC2 in thick ascending limbs. *J Biol Chem.* 287:37824-37834, 2012.

39. Grimsey NL, Narayan PJ, Dragunow M, Glass M. A novel high-thoughput assay for the quantitative assessment of receptor trafficking. *Clin Exp Pharmacol Physiol.* 35:1377-1382, 2008.

40. Aaron JS and Timlin JA. Advanced optical imaging of endocytosis. In: *Molecular regulation of endocytosis*, 2012.

41. Liu A, aguet F, Danuser G, Schmid SL. Local clustering of transferrin receptors promotes clathrin-coated pit initiation. *J Cell Biol.* 191:1381-1393, 2010.

42. Merrifield CJ, Feldman M.E, Wan L, Almers W. Imaging actin and dynamin recruitment during invagination of single clathrin-coated pits. *Nat Cell Biol* 4: 691-698, 2002.

43. Merrifield CJ, Perrais D, Zenisek, D. Coupling between clathrin-coated-pit invagination, cortactin recruitment and membrane scission observed in live cells. *Cell.* 121:593-606, 2005.

44. Einarson MB, Pugacheva EN, Orlinick JR. GST pull-down. *CSH Protoc*. 2007.

45. Rappoport JZ, Kemal S, Benmerah A, Simon SM. Dynamics of clathrin and adaptor proteins during endocytosis. *Am J Physiol Cell Physiol.* 291:C1072-C1081, 2006.

46. Schneider D, Greb C, Koch A, Straube T, elli A, Delacour D, Jacob R. Trafficking of galectin-3 through endosomal organelles of polarized and non-polarised cells. *Eur J of Cell Biol.* 89:788-798, 2010.

47. Mathur AB, Truskey GA, Reichert WM. Atomic force and total internal reflection fluorescence microscopy for the study of force transmission in endothelial cells. *Biophys J.* 78:1725-1735, 2000.

48. Blaine J, Okamura K, Giral H, Breusegem S, Caldas Y, Millard A, Barry N, Levi M. PTH-induced internalization of apical membrane NaPi2a: role of actin and myosin VI. *Am J Physiol Cell Physiol.* 297:C1339-C1346, 2009.

49. Carmosino M, Rizzo F, Procino G, Basco D, Valenti G, Forbush B, Schaeren-Wiemers N, Caplan M J, Svelto M. MAL/VIP17, a new player in the regulation of

NKCC2 in the kidney. *Mol Biol Cell*. 21(22):3985–3997, 2010.

50. Marshall JD, Hinmam EG, Collin GB, Beck S, Cerqueira R, Maffei P, Milan G, Zhang W, Wilson DI, Hearn T, Tavares P, Vettor R, […], So WV, Nishina PM, Naggert JK. Spectrum of *ALMS1* variants and evaluation of genotype-phenotype correlations in Alström syndrome. *Hum Mutat*. 28:1114-1123, 2007.

51. Marshall JD, Bronson RT, Collin GB, Nordstrom AD, Maffei P, Paisey RB, Carey C, MacDermott S, Russell-Eggitt I, Shea SE, Davis J, Beck S, Sicolo N, Naggert JK, Nishina PM. New Aström Syndrome phenotypes based on the evaluation of 182 cases. *Arch Intern Med*. 165:675-683, 2005.

52. Marshall JD, Maffei P, Collin GB, Naggert JK. Alström syndrome: Genetics and clinical overview. *Curr Genomics.* 12:225-235, 2011.

53. Joy T, Cao H, Black G, Malik R, Charlton-Menys V, Hegele RA, Durrington PN. Alström syndrome (OMIM 203800): a case report and literature review. *Orphanet J Rare Diseases.* 2:49, 2007.

54. Go AS, Chertow GM, Fan d, McCulloch CE, Hsu CY. Chronic kidney disease and the risks of death, cardiovascular events and hospitalization. *N Engl J Med*. 351:1296-305, 2004.

55. Kastarinen M, Juutilainen A, Kastarinen H, Salomaa V, Karhapaa P. Risk factors for end-stage renal disease in a community-based population: 26-year follow-up of 25,821 men and women in eastern Finland. *J Intern Med*. 267:612–20, 2010.

56. Barkley RA, Chakravarti A, Cooper RS, Ellison C, Hunt SC, Province MA, Turner ST, Weder AB, Boerwinkle E. Positional Identification of hypertension

susceptibility genes on chromosome 2. *Hypertension.* 43:477-482, 2004.

57. Schulz A, Litfin A, Kossmehl P, Kreutz R. Genetic dissection of increased urinary albumin excretion in the munich wistar fromter rat. *J Am Soc Nephrol*. 13:2706-2714, 2002.

58. Atwood LD, Samollow PB, Hixson JE, Stern MP, MacCluer JW. Genome-wide linkage analysis of blood pressure in Mexican Americans. *Genet. Epidemiol*. 20:373-382, 2001.

59. Aneas I, Rodrigues MV, Pauletti BA, Silva GJJ, Carmona R, Cardoso L, Kwitek AE, Jacob HJ, Soler JMP, Krieger JE. Congenic strains provide evidence that four mapped loci in chromosomes 2, 4, and 16 influence hypertension in the SHR. *Physiol Genomics.* 37:52-57, 2009.

60. Sugiyama F, Churchill GA, Higgins DC, Johns C, Makaritsis KP, Gavras H, Paigen B. Concordance of murine quantitative trait loci for salt-induced hypertension with rat and human loci. *Genomics.* 71:70-77, 2001.

61. Takami S, Higaki J, Rakugi H, Miki T, Katsuya T, Nakata Y, Serikawa T, Ogihara T. Analysis and comparison of new candidate loci for hypertension between genetic hypertensive rat strains. *Hypertens Res*.19:51-56, 1996.

62. Köttgen A, Pattaro C, Boger CA, Fuchsberger C, Olden M, Glazer NL, Parsa A, Gao X, Yang Q, Smith AV, O'Connell JR, Li M, [...], Kao WH, Heid IM and Fox CS. Multiple new loci associated with kidney function and chronic kidney disease: The CKDGen consortium. *Nature Genet.* 42:376-384, 2010.

63. Chambers JC, Zhang W, Lord GM. Genetic loci influencing kidney function and chronic kidney disease. *Nature Genetics.* 42:373-75, 2010.

64. Boger CA, Heid IM. Chronic kidney disease: novel insights from genome-wide association studies. *Kidney Blood Press Res*. 34:225-234, 2011.

65. Boger CA *et al*. Association of eGFR-related loci identified by GWAS with incident CKD and ESRD. *PLoS Genet*. 7(9):e1002292, 2011.

66. Collin GB, Marshall JD, King BL, Milan G, Maffei P, Jagger DJ, Naggert JK. The Alström syndrome protein, ALMS1, interacts with α-Actinin and components of the endosome recycling pathway. *PLoS One.* 7:e37925, 2012.

67. Collin GB, Cyr E, Bronson R, Marshall JD, Gifford W, Hicks W, Murray SA, Zheng QY, Smith RS, Nishina PM, Naggert JK. *Alms1*-disrupted mice recapitulate human Alström syndrome. *Hum Mol Genet*. 14:2323-2333, 2005.

68. Leitch CC, Lodh S, Prieto-Echague V, Badano JL, Zaghloul NA. Basal body proteins regulate Notch signaling through endosomal trafficking. *J Cell Sci*. 127:2407-2419, 2014.

69. Favaretto F, Milan G, Collin GB, Marshall JD, Stasi F, Maffei P, Vettor R, Naggert JK. GLUT4 defects in adipose tissue are early signs of metabolic altercations in *Alms1*$^{GT/GT}$, a mouse model for obesity and insulin resistance. *PLoS One.* 9:e109540, 2014.

70. Schulz TW, Nakagawa T, Licznerski P, Pawlak V, Kolleker A, Rozov A, Kim J, Dittgen T, Kohr G, Sheng M, Seeburg PH, Osten P. Actin/-Actinin-dependent transport of AMPS receptors in dendritic spines: Role of the PDZ-LIM protein RIL. *J Neur*. 24:8584-8594, 2004.

71. Provance WD, Addison EJ, Wood Pr, Chen DZ, Silan CM, Merce JA. Myosin-Vb functions as a dynamic tether for peripheral endocytic compartments during

transferrin trafficking. *BMC Cell Biol.* 9:44, 2008.

72. Piirainen H, Taura J, Kursula P, Ciruela F, Jaakola VP. Calcium modulates calmodulin/α-actinin 1 interaction with and agonist-dependent internalization of adenosine A2A receptor. *Biochim Biophys Acta*. 1864(4):674-686, 2017.

73. Arasaki K, Takagi D, Furuno A, Sohda M, Misumi Y, Wakana Y, Inoue H, Tagaya M. A new role for RINT-1 in SNARE complex assembly at the *trans*-golgi network in coordination with the COG complex. *Mol Biol Cell*. 24(18):2907-2917, 2013.

74. Barat B, Wu AM. Metabolic biotinylation of recombinant antibody by biotin ligase retained in the endoplasmic reticulum. *Biomol Eng.* 24:283-291, 2007.

75. Niers JM, Chen JW, Weissleder R, Tannous BA. Enhanced *in vivo* imaging of metabolically biotinylated cell surface reporters. *Anal Chem.* 83:994-999, 2011.

76. Parrott MB, Adams KE, Mercier GT, Mok H, Campos SK, Barry MA. Metabolically biotinylated adenovirus for cell targeting, ligand screening, and vector purification. *Mol Ther.* 8:688–700, 2003.

77. Wood HG, Barden RE. Biotin enzymes. *Annu Rev Biochem* 46:385-413, 1997.

78. Howarth M, Ting AY. Imaging proteins in live mammalian cells with biotin ligase and monovalent streptavidin. *Nat Protoc.* 3:534-545, 2008.

79. Tannous BA, Grimm J, Perry KF, Chen JW, Weissleder R, Breakefield XO. Metabolic biotinylation of cell surface receptors for *in vivo* imaging. *Nat methods.* 3:391-396, 2006.

80. Zaarour N, Demaretz S, Defontaine N, Mordasini D, Laghmani K. A highly conserved motif at the COOH terminus dictates endoplasmic reticulum exit and

cell surface expression of NKCC2. *J Biol Chem*. 284:21752-21764, 2009.

81. Carmosino M, Gimenez I, Caplan M, Forbush B. Exon loss accounts for differential sorting of Na-K-Cl co-transporters in polarized epithelial cells. *Mol Biol Cell*. 19:4341-4351, 2008.

82. Mattheyses AL, Simon SM, Rappoport JZ. Imaging with total internal reflection fluorescence microscopy for the cell biologist. *J Cell Sci*. 123:3621-3628, 2010.

83. Vizcay-Barrena G, Webb SED, Martin-Fernandez ML, Wilson ZA. Subcellular and single-molecule imaging of plant fluorescent proteins using total internal reflection fluorescence microscopy (TIRFM). *J Exp Botany.* 62:5419, 2011.

84. Burnstock G. Purine and pyrimidine receptors. *Cell Mol Life Sci.* 64:1471-1483, 2007.

85. Howarth M, Takao K, Hayashi Y, Ting AY. Targeting quantum dots to surface proteins in living cells with biotin ligase. *Proc Natl Acad Sci USA.* 102:7583-7588, 2005.

86. Parrott MB, Barry MA. Metabolic biotinylation of secreted and cell surface proteins from mammalian cells. *Biochem Biophys Res Commun.* 281:993–1000, 2001.

87. Predonzani A, Arnoldi F, Lopez-Requena A, Burrone OR. In vitro site-specific biotinylation of proteins within the secretory pathway using a single vector system. BMC *Biotechnol.* 8:41, 2008.

88. Caceres PA, Mendez M, Ortiz PA. Vesicle-associated membrane protein 2 (VAMP2) but not VAMP3 mediates cAMP-stimulated trafficking of the renal NKCC2 co-transporter in thick ascending limbs. *J Biol Chem.* 289:23951-23962,

2014.

89. Li G, Vega R, Nelms K, Gekakis N, Goodnow C, McNamara P, Wu H, Hong NA, Glynne R. A role for Alström syndrome protein, Alms1, in kidney ciliogenesis and cellular quiescence. *PLoS Genet*. 3(1):e8, 2007.

90. Padmanabhan S *et al*. Genome-wide association study of blood pressure extremes identifies variant near *UMOD* associated with hypertension. *PLoS Genet*. 6(10):e1001177, 2010.

91. Pattaro C *et al*. A meta-analysis of genome-wide data from five European isolates reveals an association of COL22A1, SYT1, and GABRR2 with serum creatinine level. *BMC Med. Genet*. 11:41, 2010.

92. Gudbjartsson, DF *et al*. Association of variants at UMOD with chronic kidney disease and kidney stones-role of age and comorbid diseases. *PLoS Genet*. 6(7):e1001039, 2010.

93. Köttgen A *et al*. Multiple loci associated with indices of renal function and chronic kidney disease. *Nat Genet*. 41(6):712-717, 2009.

94. Pattaro C *et al*. Genome-wide association and functional follow-up reveals new loci for kidney function. *PLoS Genet*. 8(3):e1002584, 2012.

95. Trudu M *et al*. Common noncoding *UMOD* gene variants induce salt-sensitive hypertension and kidney damage by increasing uromodulin expression. *Nat Medicine.* 19(12):1655-1660, 2013.

96. Richardson C, Sakamoto K, de los Heros P, Deak M, Campbell DG, Prescott AR, Alessi DR. Regulation of the NKCC2 ion cotransporter by SPAK-OSR1-dependent and –independent pathways. *J Cell Sci.* 124(pt 5):789-800, 2011.

97. Piechotta K, Lu J, Delpire E. Cation chloride cotransporters interact with the stress-related kinases Ste20-related proline-alanine-rich kinase (SPAK) and oxidative stress response 1 (OSR1). *J Biol Chem*. 277:50812-50819, 2002.

98. Gagnon KB, Delpire E. On the substrate recognition and negative regulation of SPAK, a kinase modulating Na^+-K^+-$2Cl^-$ cotransport activity. *Am J Physiol Cell Physiol*. 299:C614-C620, 2010.

99. Gunaratne R, Braucht DW, Rinschen MM, Chou CL, Hoffert JD, Pisitkun T, Knepper MA. Quantitative phosphoproteomic analysis reveals cAMP/vasopressin-dependent signaling pathways in native renal thick ascending limb cells. *Proc Natl Acad Sci USA*. 107:15653-15658, 2010.

100. Carmosino M, Rizzo F, Procino G, Zolla L, Timperio AM, Basco D, Barbieri C, Torretta S, Svelto M. Identification of moesin as NKCC2-interacting protein and analysis of its functional role in the NKCC2 apical trafficking. *Biol Cell.* 104:658-676, 2012.

101. Benziane B, Demaretz S, Defontaine N, Zaarour N, Cheval L, Bourgeois S, Klein C, Froissart M, Blanchard A, Paillard M. NKCC2 surface expression in mammalian cells: down-regulation by novel interaction with aldolase B. *J Biol Chem.* 282:33817-33830, 2007.

102. Zaarour N, Defontaine N, Demaretz S, Azroyan A, Cheval L, Laghmani K. Secretory carrier membrane protein 2 regulates exocytic insertion of NKCC2 into cell membrane. *J Biol Chem.* 286:9489-9502, 2011.

103. Krauss TD, Peterson JJ. Quantum Dots: A charge for blinking. *Nat mater* 11:14-16, 2012.

104. Marchuk K, Guo Y, Sun W, Vela J, Fang N. High precision tracking with non blinking quantum dots resolves nanoscale vertical displacement. *J Am Chem Soc*. 134(14):6108-6111, 2012.

105. Lane LA, Smith AM, Lian T, Nie S. Compact and blinking suppressed quantum dots for single particle tracking in live cells. *J Phys Chem B*. 118(49):14140-14147, 2014.

106. Brunet GM, Gagnon E, Simard CF, Daigle ND, Caron L, Noel M, Lefoll M-H, Bergeron MJ and Isenring P. Novel insights regarding the operational characteristics and teleological purpose of the renal NKCC2 co-transporter splice variants. *J Gen Physiol* 126:325-337, 2005.

107. Brinkerhoff CJ, Woolf PJ, Linderman JJ. Monte Carlo simulations of receptor dynamics: insights into cell signaling. *J Mol Histol.* 35:667-677, 2004.

108. Costa MN, Radhakrishnan K, Edwards JS. Monte Carlo simulations of plasma membrane corral-induced EGFR clustering. *J Biotechnol* 151:261-270, 2011.

109. Fallahi-Sichani M, Linderman JJ. Lipid raft-mediated regulation of G-protein coupled receptor signaling by ligands which influence receptor dimerization: a computational study. *PLoS One* 4:e6604, 2009.

110. Gonnard P, Blouin CM, Lamaze C. Membrane trafficking and signaling: two sides of the same coin. *Semin Cell Dev Biol* 23:154-164, 2012.

111. Dobrinskikh E, Lanzano L, Rachelson J, Cranston D, Moldovan R, Lei T, Gratton E, Doctor RB. Shank2 contributes to the apical retention and intracellular redistribution of NaPiIIa in OK cells. *Am J Physiol Cell Physiol* 304:C561-C573, 2013.

112. Ketchem CJ, Khundmiri SJ, Gaweda AE, Murray R, Clark BJ, Weinman EJ, Lederer ED. Role of Na+/H+ exchanger regulatory factor 1 in forward trafficking of the type IIa Na+-Pi cotransporter. *Am J Physiol Renal Physiol* 309:F109-F119, 2015.

113. Reed AA, Loh NY, Terryn S, Lippiat JD, Partridge C, Galvanovskis J, Williams SE, Jouret F, Wu FT, Courtoy PJ, Nesbit MA, Rorsman P, Devuyst O, Ashcroft FM, Thakker RV. CLC-5 and KIF3B interact to facilitate CLC-5 plasma membrane expression, endocytosis, and microtubular transport: relevance to pathophysiology of Dent's disease. *Am J Physiol Renal Physiol* 298:F365-F380, 2010.

114. Subramanian VS, Marchant JS, Boulware MJ, Said HM. A C-terminal region dictates the apical plasma membrane targeting of the human sodium-dependent vitamin C transporter-1 in polarized epithelia. *J Biol Chem* 279:27719-27728, 2004.

115. Blanchard MG, Kittikulsuth W, Nair AV, de Baaii JH, Latta F, Genzen JR, Kohan DE, Bindels RJ, Hoenderop JG. Regulation of Mg 2+ reabsorption and transient receptor potential melastatin type 6 activity by cAMP signaling. *J Am Soc Nephrol* 27:804-813, 2016.

116. Cohen M, Kitsberg D, Tsytkin S, Shulman M, Aroeti B, Nahmias Y. Live imaging of GLUT2 glucose-dependent trafficking and its inhibition in polarized epithelial its inhibition in polarized epithelial cysts. *Open Biol* 4:140091, 2014.

117. Bouley R, Hawthorn G, Russo LM, Lin HY, Ausiello DA, Brown D. Aquaporin 2 (AQP2) and vasopressin type 2 receptor (V2R) endocytosis in kidney epithelial

cells: AQP2 is located in 'endocytosis-resistant' membrane domains after vasopressin treatment. *Biol Cell* 98:215-232, 2006.

118. Zhang Z, Zhang T, Wang S, Gong Z, Tang C, Chen J, Ding J. Molecular mechanism for Rabex-5 GEF activation by Rabaptin-5. *Elife*. 3, 2014

119. Zhu H, Qian H, Li G. Delayed onset of positive feedback activation of Rab5 and Rabaptin-5 in endocytosis. *PLoS One*. 5(2):e9226, 2010.

120. Dathe C, Daigeler AL, Seifert W, Jankowski V, Mrowka R, Kalis R, Wanker E, Mutig K, Bachmann S, Paliege A. Annexin A2 mediates apical trafficking of renal Na^+-K^+-$2Cl^-$ cotransporter. *J Biol Chem*. 289(14):9983-9997, 2014.

121. Rai S, Tanaka H, Suzuki M, Ogoh H, Taniguchi Y, Morita Y, Shimada T, Tanimura A, Matsui K, Yokota T, Oritani K, Tanabe K, Watanabe T, Kanakura Y, Matsumura I. Clathrin assembly protein CALM plays a critical role in KIT signaling by regulating its cellular transport from early to late endosomes in hematopoietic cells. *PLoS One*. 9(10):e109441, 2014.

122. Roman RJ, Cowley AW., Jr. Abnormal pressure-diuresis-natriuresis response in spontaneously hypertensive rats. *Am J Physiol Renal Fluid Electrolyte Physiol* 248:F199–F205, 1985.

123. Sonalker PA, Tofovic SP, Jackson EK. Cellular distribution of the renal bumetanide-sensitive Na-K-2Cl cotransporter BSC-1 in the inner stripe of the outer medulla during the development of hypertension in the spontaneously hypertensive rat. *Clin Exp Pharmacol Physiol* 34:1307–1312, 2007.

124. Koeppen BM. Stanton BA. Physiology of diuretic action. Renal Physiology (Fifth edition), 2013.

125. Pettinger WA. Anesthesia and the renin-angiotensin-aldosterone axis. Anesthesiology 48:393-396, 1978.

126. Arendshorst WJ, Beierwaltes WH. Renal and nephron hemodynamics in spontaneously hypertensive rats. *Am J Physiol*. 236:F246-F251, 1979.

127. Griffin KA, Churchill PC, Picken M, Webb RC, Kurtz TW, Bidani AK. Differential salt-sensitivity in the pathogenesis of renal damage in SHR and stroke prone SHR. *Am J Hypertens*. 14:311–320, 2001.

128. Kimbrough HM, Vaughan ED, Cavey RM, Ayers CR. Effect of intrarenal angiotensin II blockade on renal function in conscious dog. *Circ Res*. 40:174-178, 1977.

129. Arendshorst WJ, Finn WF. Renal hemodynamics in the rat before and during inhibition of angiotensin II. *Am J Physiol*. 233:F290-297, 1977.

130. Johnston PA, Bernard DB, Perrin NS, Arbeit L, Lieberthal W, Levinsky NG. Control of rat renal vascular resistance during alterations in sodium balance. *Circ Res*. 48:728-733, 1981.

131. Davis JM, Haberle DA, Kawata T. The control of glomerular filtration rate and renal blood flow in chronically volume-expanded rats. *J Physiol*. 402:473-495, 1988.

132. Hall JE, Mizelle HL, Hildebrandt DA, Brands MW. Abnormal pressure natriuresis. A cause or a consequence of hypertension? *Hypertension*. 15(6 Pt 1):547-559, 1990.

133. Thomson SC, Blantz RC. Glomerulotubular balance, tubuloglomerular feedback and salt homeostasis. *J Am Soc Nephrol*. 19(12):2272-2275, 2008.

134. Thomson SC, Vallon V, Blantz RC. Resetting protects efficiency of tubuloglomerular feedback. *Kidney Int*. 54(67):S65-S70, 1998.

135. Brannstrom K, Arendshorst WJ. Resetting of exaggerated tubuloglomerular feedback activity in acutely volume-expanded young SHR. *Am J Physiol Renal Physiol*. 276:F409-F416, 1999.

136. Brown R, Ollerstam A, Persson AE. Neuronal nitric oxide synthase inhibition sensitizes the tubuloglomerular feedback mechanism after volume expansion. *Kidney Int*. 65:1349-1356, 2004.

137. Palmer BF. Impaired renal autoregulation implications for the genesis of hypertension and hypertension-induced renal injury. *Am J Med Sci*. 21:388-400, 2001.

138. Burke M, Pabbidi MR, Farley J, Roman RJ. Molecular mechanisms of renal blood flow. *Curr Vasc Pharmacol*. 12(6):845-858, 2014.

139. Lee NC, Marshall JD, Collin GB, Naggert JK, Chien YH, Tsai WY, Hwu WL. Caloric restriction in Alström syndrome prevents hyperinsulinemia. *Am J Med Genet A*. 149A(4):666, 2009.

140. Festuccia WT. Turning up the heat against metabolic syndrome and non-alcoholic fatty liver disease. *Clin Sci (Lond)*. 131(4):327-328, 2017.

141. Huang-Doran I, Semple RK. Knockdown of Alström syndrome-associated gene *Alms1* in 3T3-L1 predipocytes impairs adipodenesis but has no effect on cell autonomous insulin action. *Int J Obes (Lond).* 34(10):1554-8, 2010.

142. Romano S, Milan G, Veronese C, Collin GB, Marshall JD, Centobene C, Favaretto F, Dal Pra C, Scarda A, Leandri S, Naggert JK, Maffei P, Vettor R. Regulation of Alström syndrome gene expression during adipogenesis and its relationship with fat cell insulin sensitivity. *Int J Mol Med.* 21(6):731-736, 2008.

143. Heydet D, Chen LX, Larter CZ, Inglis C, Silverman MA, Farrell GC, Leroux MR. A truncating mutation of *Alms1* reduces the number of hypothalamic neuronal cilia in obese mice. *Dev Neurobiol*. 73(1):1-13, 2013.

144. Yoon SS, Carroll MD, Fryar CD. Hypertension prevalence and control among adults: United States, 2011-2014. *NCHS Data Brief*. 220:1-8, 2015.

145. Heidenreich PA, Trogdon JG, Khavjou OA, Butler J, Dracup K, Ezekowitz MD, Finkelstein EA, Hong Y, Johnston SC, Khera A et al. Forecasting the future of cardiovascular disease in the united states: a policy statement from the American Heart Association. *Circulation*. 123:933-944, 2011.

146. Kannel WB. McGee DL. Diabetes and cardiovascular risk factors: the Framingham study. *Circulation*. 59:8-13, 1979.

147. Stamler J, Vaccaro O, Neaton JD, Wentworth D. Diabetes, other risk factors and 12-yr cardiovascular mortality for men screened in the Multiple Risk Factor Intervention Trial. *Diabetes Care* 16:434-444, 1993.

148. Frohlich ED. Clinical management of the obese hypertensive patient. *Cardiol Rev*. 10(3):127–138, 2002.

149. Hall JE. Pathophysiology of obesity hypertension. *Curr Hypertens Rep*. 2(2):139–147, 2000.

150. Hall JE, Crook ED, Jones DW, Wofford MR, Dubbert PM. Mechanisms of obesity-associated cardiovascular and renal disease. *Am J Med Sci*. 324(3):127–137, 2002.

151. Wofford MR, Hall JE. Pathophysiology and treatment of obesity hypertension. *Curr Pharm Des*. 10(29):3621–3637, 2004.

152. Bakris GL, Weir MR, Sowers JR. Therapeutic challenges in the obese diabetic patient with hypertension. *Am J Med*. 101:33S-46S, 1996.

153. Guyton AC, Coleman TG, Cowley AV Jr, Scheel KW, Manning RD Jr, Norman RA Jr. Arterial pressure regulation: overriding dominance of the kidneys in long-term regulation and in hypertension. *Am J Med*. 52:584-594, 1972.

154. Parades A, Plata C, Rivera M, Moreno E, Vazquez N, Munoz-Clares R, Hebert SC, Gamba G. Activity of renal NKCC2 cotransporter is reduced by mutagenesis of N-glycosylation sites: role for protein surface charge in Cl^- transport. *Am J Physiol Renal Physiol*. 290:F1094-F1102, 2006.

155. Sigmon DH, Beierwaltes WH. Influence of nitric oxide derived from neuronal nitric oxide synthase on glomerular filtration. *Gen Pharmacol*. 34(2):95-100, 2000

156. Ortiz PA, Hong NJ, Plato CF, Varela M, Garvin JL. An *in vivo* method for adenovirus-mediated transduction of thick ascending limbs. *Kidney Int*. 63(3):1141-1149, 2003.

157. Atchinson DK, Harding H, Beierwaltes WH. Vitamin D increases plasma renin activity independently of plasma Ca^{2+} *via* hypovolemia and β-adrenergic activity. *Am J Physiol Renal Physiol*. 305(8):F1109-F1117, 2013.

158. Ares GR, Caceres PS, Ortiz PA. Molecular regulation of NKCC2 in the thick ascending limb. *Am J Physiol Renal Physiol*. 301(6):F1143-F1159, 2011.

159. Akar F, Skinner E, Klein JD, Jena M, Paul RJ, O'Neill WC. Vasoconstrictors and nitrovasodilators reciprocally regulate the Na+/K+/2Cl- cotransporter in rat aorta. *Am J Physiol*. 276:C1383-C1390, 1999.

160. Akhtar N, Hotchin NA. RAC1 regulates adherens junctions through endocytosis of E-cadherin. *Mol Biol Cell*. 2001;12(4):847-862.

161. Cremona ML, Matthies HJ, Pau K, Bowton E, Speed N, Lute BJ, Anderson M, Sen N, Robertson SD, Vaughan RA. Flotillin-1 is essential for PKC-triggered endocytosis and membrane microdomain localization of DAT. *Nat Neurosci*. 2011;14:469-477.

162. Schneider A, Rajendran L, Honsho M, Gralle M, Donnert G, Wouters F, Hell SW, Simons M. Flotillin-dependent clustering of the amyloid precursor protein regulates its endocytosis and amyloidogenic processing in neurons. *J Neurosci*. 2008;28(11):2874-2882.

163. de Graauw M, Cao L, Winkel L, van Miltenburg MH, le Devedec SE, Klop M, Yan K, Pont C, Rogkoti VM, Tijsma A, Chaudhuri A, Lalai R, Price L, Verbeek F, van de Water B. Annexin A2 depletion delays EGFR endocytic trafficking *via* cofilin activation and enhances EGFR signaling and metastasis formation. *Oncogene*. 2014;33(20):2610-2619.

164. Rescher U, Zobiack N, Gerke V. Intact Ca^{2+} binding sites are required for targeting of annexin 1 to endosomal membranes in living HeLa cells. *J Cell Sci*. 2000;113(Pt 22):3931-3938.

165. Thomas RS, Henson A, Gerrish A, Jones L, Williams J, Kidd EJ. Decreasing the expression of PICALM reduces endocytosis and the activity of β-secretase: implications for Alzheimer's disease. BMC Neurosci. 2016;17(1):50.

166. Hussain KM, Leong KL, Ng MM, Chu JJ. The essential role of clathrin-mediated endocytosis in the infectious entry of human enterovirus 71. *J Biol Chem*.

2011;286(1):309-321.

167. Han K, Kim MH, Seeburg D, Seo J, Verpelli C, Han S, Chung HS, Ko J, Lee HW, Kim K, Heo WD, Meyer T, Kim H, Sala C, Choi SY, Sheng M, Kim E. Regulated RalBP1 binding to RalA and PSD-95 controls AMPA receptor endocytosis and LTD. *PLoS Biol*. 2009;7(9):e1000187.

168. Kumari S, Mayor S. ARF1 is directly involved in dynamin-independent endocytosis. *Nat Cell Biol*. 2008;10:30-41.

169. Akhtar N, Streuli CH. An integrin-ILK-microtubule network orients cell polarity and lumen formation in glandular epithelium. *Nat Cell Biol*. 2013;15(1):17-27.

170. Wang YJ, Guo XL, Li SA, Zhao YQ, Liu ZC, Lee WH, Xiang Y, Zhang Y. Prohibitin is involved in the activated internalization and degradation of protease-activated receptor 1. *Biochim Biophys Acta*. 2014;1843(7):1393-1401.

171. Kim JH, Lee-Kwon W, Park JB, Ryu SH, Yun CH, Donowitz M. Ca^{2+} dependent inhibition of Na^{+}/H^{+} exchanger 3 (NHE3) requires an NHE3-E3KARP-alpha-actinin-4 complex for oligomerization and endocytosis. *J Biol Chem*. 2002;277(26):23714-23724.

172. Provance DW Jr, Addison EJ, Wood PR, Chen DZ, Silan CM, Mercer JA. Myosin-Vb functions as a dynamic tether for peripheral endocytic compartments during transferrin trafficking. *BMC Cell Biol*. 2008;9:44.

ABSTRACT

ROLE OF ALSTRÖM SYNDROME (ALMS1) IN NKCC2 ENDOCYTOSIS, THICK ASCENDING LIMB FUNCTION, BLOOD PRESSURE REGULATION AND METABOLIC FUNCTION

by

ANKITA BACHHAWAT JAYKUMAR

August 2017

Advisor: Dr. Pablo A. Ortiz

Major: Physiology

Degree: Doctor of Philosophy

NaCl absorption by the Thick Ascending Limb (TAL) is mediated by the apical $Na^+/K^+/2Cl^-$ co-transporter, NKCC2. Increased NKCC2 activity and apical trafficking are associated to salt sensitive hypertension in rodents and humans. NKCC2 endocytosis is important for maintaining surface NKCC2 such that blocking NKCC2 endocytosis increased NKCC2 surface abundance and NKCC2-mediated NaCl reabsorption. Despite its importance, NKCC2 endocytosis has been poorly studied and a part of the reason may be attributed to the lack of availability of methods with good time resolution. Hence, we developed a method to image apical NKCC2 to monitor its endocytosis in real-time by Total Internal Reflection Fluorescence (TIRF) microscopy. NKCC2 endocytosis is regulated by protein-protein interactions but only one protein has been characterized and shown to regulate NKCC2 endocytosis by interacting with a 71 amino acid region in the carboxyl terminus of NKCC2 (C2-NKCC2). To identify new TAL proteins that may mediate NKCC2 endocytosis, we performed a proteomics-based screening of TAL proteins that interacted with glutathione-S-transferase-C2-NKCC2 as bait, and identified Alström syndrome 1 (ALMS1) as an interacting partner. *ALMS1* has

been linked to human hypertension and renal function in genome-wide association studies, QTL in rats with salt sensitivity and mutations in the *ALMS1* gene in humans causes obesity, cardiomyopathy, type-2 diabetes, hypertension and kidney disease. The role of ALMS1 in regulating blood pressure or renal Na^+ handling is unknown. GST pull down with C-terminus of ALMS1 (C-ALMS1) pulled down full length NKCC2 along with several proteins known to be involved in endocytosis of other proteins. Thus, we hypothesized that ALMS1 is involved in NKCC2 endocytosis in the TAL, NaCl reabsorption and blood pressure regulation and generated *ALMS1* knockout rat model in collaboration with Medical College of Wisconsin. We found that in (6-12 week old) *ALMS1* KO rats, NKCC2 endocytosis was decreased and this correlated with higher NKCC2 surface abundance in TALs. *ALMS1* KO rats also exhibited higher urine concentrating capacity, higher bumetanide sensitivity, a decreased ability to eliminate a volume/salt load, hypertension and salt sensitivity in these rats. Altogether, this phenotype is consistent with increased TAL function. Thus, ALMS1 interacts with NKCC2 in the TAL, mediates its endocytosis to regulate NKCC2 surface expression and activity in the TAL and thereby maintains normal blood pressure. In addition, *ALMS1* KO rats develop metabolic syndrome as they age (16-18 week old) and females exhibit more severe form of metabolic dysfunction compared to their male counterparts. The mechanism causing salt-sensitive hypertension in *ALMS1* KO rats may be in part due to higher TAL NaCl reabsorption and higher NKCC2 activity. However, it is possible that insulin resistance and obesity that develops in these *ALMS1* KO rats may play a role in salt sensitivity. Thus, ALMS1 is not only important for renal function but may also be involved in the regulation of glucose homeostasis and metabolism in rats.

AUTOBIOGRAPHICAL STATEMENT

ANKITA BACHHAWAT JAYKUMAR

EDUCATION

Ph.D. Candidate in Physiology (Minor: Cell and Molecular biology), Wayne State University (WSU) School of Medicine (SoM).
Master of Science in Biotechnology, VIT University, India, 2011.
Bachelor of Science, in Biology, Chemistry & Microbiology, Bangalore University, 2009.

FELLOWSHIPS AND SCHOLARHIPS

AHA Pre-doctoral fellowship 01/2016- 12/2017, American Heart Association., Wayne State University Graduate school scholarship 2016- 2017, WSU
Interdepartmental Biomedical Science Pre-doctoral Scholarship 09/2012- 09/2015, WSU SoM
Frank and Jane Warchol Foundation Scholarship 07/2011- 05/2012, WSU

HONORS AND AWARDS (selected)

Pre-doctoral renal research excellence award- APS Renal section, 2017.
Caroline tum suden/Frances Hellebrandt Professional Opportunity award- APS 2016.
Recognition for excellence in renal research- APS Renal section, 2016.
Pre-doctoral renal research excellence award- APS Renal section, 2016 (Finalist).
Experimental biology conference Travel award- APS, 2016.
Kidney Council New Investigator Travel award- AHA council on Hypertension, 2016.
Outstanding Oral Presentation award- Michigan Physiological Society, 2016
Marion I. Barnhart Graduate student award- Department of Physiology, WSU SoM, 2016.
Wayne State University graduate research excellence award- WSU graduate school, 2015.
New Investigator Travel Award - AHA Council on Hypertension, 2015.
Experimental biology conference Travel award- APS, 2014.

PUBLICATIONS (selected)

1. **Bachhawat A**, Mohamed SS, Thirumurugan T. Screening of fifteen ayurvedic plants for alpha-glucosidase inhibitory activity and enzyme kinetics. International J of Pharmacy & Pharmaceutical Sciences. 3: 267-274, 2011.
2. Bao J, Bielski E, **Bachhawat A**, Taha D, Gunther LK. R1 motif is the major actin-binding domain of TRIOBP-4. J Biochem. 6: 5256-5264, 2013.
3. **Jaykumar AB**, Caceres PS, Sablaban I, Bakhos TA, Ortiz PA. Real time monitoring of NKCC2 endocytosis by total internal reflection fluorescence microscopy. Am. J Physiol. Renal Physiol. 310: F183-F191, 2016.
4. **Jaykumar AB**, Caceres PS, Ortiz PA. Mini review: Single molecule tagging to study renal transporter trafficking. Am J Physiol Renal Physiol. 2017 (Invited; under review)
5. **Jaykumar AB**, Caceres PS, King-Medina K, Beierwaltes WH, Ortiz PA. Novel role of ALMS1 (Alström syndrome 1) in blood pressure regulation. J Clin Invest. 2017. (Manuscript ready for submission)
6. **Jaykumar AB**, Ortiz PA. Sex differences in *ALMS1* (Alström syndrome 1) KO rat: a model of age dependent metabolic syndrome and renal damage. Am J Physiol Endocrinol Metab. 2017. (manuscript in preparation)
7. King-Medina K, **Jaykumar AB**, Ortiz PA. Deletion of *ALMS1* (Alström syndrome 1) in rats causes salt sensitive hypertension. Hypertension. 2017. (manuscript in preparation)
8. King-Medina K, **Jaykumar AB**, Ortiz PA. Caloric restriction reverses insulin resistance but not hypertension in *ALMS1* KO rats. Am J Physiol Endocrinol Metab. 2017. (in preparation)
9. **Jaykumar AB**, Ortiz PA. Mini review: Alström syndrome. Am J Physiol Renal Physiol. 2017. (Invited)